

Designing structures with tree forks: Mechanical characterization and generalized computational design approach

by
Ishani Desai

B.S. in Civil and Environmental Engineering, Rice University, 2019
Massachusetts Institute of Technology, 2020

Submitted to the Department of Civil and Environmental Engineering
in Partial Fulfillment of the Requirements for the degree of

MASTER OF ENGINEERING IN CIVIL AND ENVIRONMENTAL ENGINEERING

at the

MASSACHUSETTS INSTITUTE OF TECHNOLOGY

May 2020

©2020 Ishani A. Desai. All rights reserved.

The author hereby grants to MIT permission to reproduce and to distribute publicly paper and electronic copies of this thesis document in whole or in part in any medium now known or hereafter created.

Signature of Author:

Ishani Desai
Department of Civil and Environmental Engineering
May 8, 2020

Certified by:

Caitlin Mueller
Associate Professor, Civil and Environmental Engineering and Architecture
Thesis Supervisor

Accepted by:

Colette L. Heald
Professor of Civil and Environmental Engineering
Chair, Graduate Program Committee

Designing structures with tree forks: Mechanical characterization and generalized computational design approach

by

Ishani Desai

Submitted to the Department of Civil and Environmental Engineering on May 8, 2020 in Partial Fulfillment of the Requirements for the Degree of Master of Engineering in Civil and Environment Engineering

ABSTRACT

Timber structures have seen a resurgence in structural design in recent years due to a desire to reduce embodied carbon in the built environment. While many of these structures use standardized or regular elements, the recent revolution in digital fabrication has resulted in a variety of more complex and irregular timber forms, usually achieved through milling or other machine-driven production processes. However, the organic nature of wood has also inspired architects and engineers to harness naturally occurring formal variation, for example, in the geometries of tree forks and branches, to produce designs that are more directly responsive to their constitutive materials. Compared to conventional fabrication processes for timber, in which the material is often processed several times to achieve characteristics that are present in the original material, this approach embodies little waste in material and effort.

Naturally occurring branching tree forks seem to exhibit outstanding strength and material efficiency as a natural moment connection, which underpins previous research investigating their use in design. This thesis advances the use of tree forks as a natural connection in structures through two specific contributions. First, the paper establishes a flexible matching-based methodology for designing structures with a pre-existing library of tree fork nodes (based on actual available materials from salvaged trees, for example), balancing an initial target design, node matching quality, and structural performance. The methodology uses a combination of Iterative Closest Point and Hungarian Algorithms as a real-time computational approach for matching nodes in the library to nodes in the design. The thesis presents results that systematically test this methodology by studying how matching quality varies depending on the number and species of tree forks available in the library and relates this back to the mechanical properties of tree branches found through physical testing.

Second, mechanical laboratory testing of tree fork nodes of various tree species (available locally in the area) is presented to quantify the structural capacity of these connections and observe the behavior under tree fork load transfers. A structural score is developed to characterize the tolerance of tree fork nodes to imperfect matches in terms of structural capacity; these resulting geometries are compared to the previous matching-based scoring system. The resulting approach is projected forward as a framework for a more general computational approach for designing with existing material systems and geometries that can also be expanded beyond tree forks.

Thesis Supervisor: Caitlin Mueller

Title: Associate Professor, Civil and Environmental Engineering and Architecture

ACKNOWLEDGMENTS

I would first like to thank my thesis advisor and professor, Caitlin Mueller, for her invaluable support throughout this academic year. I am continuously inspired by the work she leads within the Digital Structures group and always leave inspired about the progress and future of structural engineering after any meeting, discussion, or class.

I wish to acknowledge Felix Amtsberg, Kevin Moreno Gata, and Yijiang Huang for their previous work on this project as well. Their contributions instigated this project and provided much of the initial framework for the matching-based design algorithm.

I would also like to thank Christopher Dewart and Stephen Rudolph for their expertise and support in executing the structural capacity testing within the N51 Wood Shop and Pierce Laboratory.

I am forever thankful to my friends of the Master of Engineering program that made this year an unforgettable experience that went above and beyond my expectation.

Finally, I would like to thank my parents and my partner for their unconditional love and support during this year.

TABLE OF CONTENTS

ABSTRACT	2
ACKNOWLEDGMENTS	4
TABLE OF CONTENTS	5
LIST OF FIGURES	7
LIST OF TABLES	11
1 Introduction & Literature Review	13
1.1 Background	13
1.2 Motivation	13
1.3 Literature review	14
1.3.1 Shipbuilding with “compass” timbers.....	15
1.3.2 Biomechanics of tree forks	16
1.3.3 Tree fork geometry case study precedents.....	18
1.3.3.1 Hooke Park.....	18
1.3.3.2 IASS 2018	19
1.3.4 Designing with existing materials.....	21
1.4 Research objective	24
2 Matching-based design methods and results	26
2.1 Conceptual overview of design process	26
2.1.1 Previous work	26
2.1.2 General methodology.....	28
2.1.2.1 Tree species	29
2.1.2.2 Branch angles	29
2.1.2.3 Tree branch diameters	30
2.1.2.4 Methodology for simulating random tree fork library	31
2.1.2.5 Target structures	32
2.1.2.6 Matching score	32
2.1.2.7 Optimization.....	34
2.2 Simulated inventories and case studies	35
2.2.1 Pavilion geometry with 2 control curves (4 variables)	36
2.2.2 Hexagonal geometry with 5 Control Points (5 variables)	37
2.2.3 Hexagonal geometry with 1 Control Curve (3 variables)	38
2.3 Results	41
2.3.1 Pavilion geometry with 2 control curves (4 variables) results	41
2.3.2 Hexagonal geometry with 5 control points (5 variables) results	43
2.3.3 Hexagonal geometry with 1 control curve (3 variables) results.....	44

2.4	Discussion and conclusion.....	50
3	Structural performance of tree branch nodes.....	53
3.1	Background on tree mechanics and previous testing	53
3.1.1	Tree fork structural mechanics.....	53
3.1.2	Previous work	54
3.1.3	Breaking modes and characteristics.....	54
3.2	Physical load tests	56
3.2.1	Pre-processing of tree forks	56
3.2.2	Testing	59
3.2.3	Results	61
3.2.4	Computational model of behavior	67
3.3	Structural performance computational model	69
3.3.1	Design framework	69
3.3.2	Structural analysis setup	72
3.3.3	Results	73
3.4	Discussion and conclusion.....	74
4	Conclusion	76
4.1	Summary of contributions	76
4.2	Potential impact.....	77
4.3	Future work	77
4.4	Concluding remarks.....	78
5	References.....	80
6	Appendix.....	85
	Appendix A: Hexagonal geometry with 5 control points, matching score results	85
	Appendix B: Hexagonal geometry with 1 control curve, matching score results	85
	Appendix C: Hexagonal geometry with 1 control curve, matching score vs. ratio graphs.....	85
	Appendix D: Hexagonal geometry with 5 control points, structural score results	85

LIST OF FIGURES

Figure 1. Forced curvature in timber through cambering (Daizen Joinery)	14
Figure 2. “Natural” timber structure, Centre Pompidou Metz (Shigeru Ban Architects).....	14
Figure 3. Diagram representation of oak trees as compass ship timbers (Albion 1926, 3)	15
Figure 4. Cross section of a ship.....	15
Figure 5. Tensile tree fork (left, Fig. 1) vs. Compression tree fork (right, Fig. 2)	16
Figure 6. Arrows show the direction of tree fork trunk fibers (TF), branch fibers (BF), and their intersection at the compaction zone (CZ) (Farrell 7).....	17
Figure 7. Adaptive growth shown in the cross-section of a tree branch.....	18
Figure 8. Plan view of truss with mapped placement of tree forks.....	19
Figure 9. Wood Chip Barn arching truss, completed (Mollica and Self 2016, 140)	19
Figure 10. Connection principle resulting in bifurcating space loops	20
Figure 11. Spatial geometries simulated to align branches with adjacent branch axis with Karamba loadings (Allner and Kroehnert 2018, 4)	20
Figure 12. Standard set of tree fork elements components and assembled (left). Processed and milled tree fork (right). (Von Buelow, Peter, et al. 2018, 2)	20
Figure 13. The basic ParaGen cycle showing the steps used to generate a range of solutions (Von Buelow, Peter, et al. 2018, 5).....	21
Figure 14. Bridge truss system – ground structure (Brütting et al. 2018, 18)	22
Figure 15. Bridge truss – optimization results final topologies (Brütting et al. 2018, 20)	22
Figure 16. Bridge truss – assignment optimization (Brütting et al. 2018, 19).....	23
Figure 17. Iterative form-finding process for inventory constrained design: a) parametrically defined structure with loads and support conditions b) structure elements pre-sorted in descending	

order by length, c) inventory elements pre-sorted in ascending order by length (Bakauskas et al. 2018, 8)	24
Figure 18. Process of acquiring material, digitizing inventory, designing and fabricating (Amtsberg et al.)	27
Figure 19. Tree forks collected and scanned from Somerville site (Amtsberg et al.)	27
Figure 20. Iterative Closest Point (ICP) and Hungarian algorithm matching tree fork material library to given structure (Huang et al.).....	28
Figure 21. Prototype structure (Amtsberg et al.)	28
Figure 22. TreeKeeper database cataloguing all trees in Somerville, MA (“TreeKeeper”).....	29
Figure 23. Visualizations of tree image generation data based on collected branching angles (Aono and Kunii 1984, 15)	30
Figure 24. (Left) Model of tree branching. (Middle) Tree skeleton with equivalent diameters for all branches. (Right) Tree skeleton utilizing Leonardo da Vinci’s rule. (Eloy)	30
Figure 25. Grasshopper sampling methodology visualization.....	31
Figure 26. Line representations of tree forks	32
Figure 27. Brep pipe representations of tree forks.....	32
Figure 28. Oak. 4x7: Hexagonal, 1 Control Curve. 100 samples.	35
Figure 29. Pavilion geometry with 2 control curves.....	36
Figure 30. Potential geometry given x, y, z-coordinate variables for each node.....	37
Figure 31. Hexagonal surface geometry generation process	38
Figure 32. 3 NURBS curves forming hexagonal grid surface	39
Figure 33. Height of lofted curve vs. degree of curvature geometry representation with constant curve angular x-rotation	40

Figure 34. Curve angular x-rotation vs. degree of curvature geometry representation with constant height of lofted curve 40

Figure 35. Original pavilion geometry Matching Score vs. # of Samples..... 42

Figure 36. Matching score vs. Ratio (# of Structural Nodes : # of Samples). Worst performing geometries shown with bold lines: 3x3, 4x3, 5x3, 5x4, 6x3, 6x4, 6x5, 7x3, 7x4, 7x5, 7x6..... 45

Figure 37. Boxed results represent the best matching scores for ash, oak, and fruit (cont.) 47

Figure 38. Example geometries for ash, oak, and fruit species that represent optimal matches (cont.) 48

Figure 39. Hexagonal geometry with 1 control curve, 4x3 & 5x5, homogenous geometries 49

Figure 40. Hexagonal geometry with 1 control curve, 3x7, variant geometries..... 50

Figure 41. Breaking modes: flat-surface (top right), imbedded-branch (top left), and ball-in-socket (bottom) (Farrell 2003, 37) 55

Figure 42. Typical moisture-strength properties of a red spruce (Wilson 1932)..... 56

Figure 43. a) Brep of tree scan, b) plane top/bottom, c) Prototrak top/bottom flat, d) plane 3rd edge, e) Joiner 3rd edge flat..... 57

Figure 44. Fruit tree pre-processed fork 58

Figure 45. Ash tree pre-processed fork..... 58

Figure 46. Fruit tree control cube 59

Figure 47. Ash tree control cube..... 59

Figure 48. Fruit (top) and ash (bottom) tree fork setup – planed top forks sits at the center of the compression 60

Figure 49. Cube setup -- strain gauge attached..... 61

Figure 50. Cracking (top: fruit) and splitting (bottom: ash) in the non-forked branch..... 62

Figure 51. Fruit tree post-testing.....	62
Figure 52. Fruit tree fork testing results: Force vs. Displacement.....	63
Figure 53. Fruit tree cube testing results: Stress vs. Strain.....	63
Figure 54. Ash tree post-testing	64
Figure 55. Ash tree fork testing results: Force vs. Displacement	65
Figure 56. Ash tree cube testing results: Stress vs. Strain	65
Figure 57. Tree fork computational model mesh and point.....	67
Figure 58. Tree fork computational model reactions and principal stresses.....	68
Figure 59. Modeled center corresponding to the natural fibers of the tree fork.....	68
Figure 60. Angle difference between matched node and structural node.....	70
Figure 61. Hankinson equation graphical representation. N/P vs. Angle (“Wood Handbook”) ..	71
Figure 62. Ash. 3x4: Hexagonal, 1 Control Curve. 200 samples.	74
Figure 63. Oak. 4x5: Hexagonal, 1 Control Curve. 50 samples.	74

LIST OF TABLES

Table 1. Tree fork average, minimum, and maximum angles	30
Table 2. Ash, oak, and fruit tree branch angles	36
Table 3. Optimized pavilion geometry sampling matching score results	42
Table 4. Percent difference between structural testing and Wood Handbook of $\sigma_{comp, }$ & E.....	66
Table 5. Ash, oak, and fruit P, Q, σ_V , $ $, and σ bending stress values.....	72

1 Introduction & Literature Review

1.1 Background

While timber structures have seen a resurgence in structural engineering design, the complex structures built tend to disregard the inherent geometric advantages that the wood material contributes. Typically, the organic shapes desired are formed during post-processing of homogenized timber sections through either forced cambering or subtractive fabrication. A wasteful redundancy becomes apparent in which the material is processed several times to achieve characteristics that are present in the original material. Naturally occurring branching tree forks exhibit outstanding strength and material efficiency and are able to sustain a significant amount of structural load as a natural moment connection. The presented project investigates the feasibility of using tree forks as a natural design connection in structural frameworks. This will be conducted through a series of structural capacity testing as well as through sampling of tree fork nodes of various tree species found at a specific site location to form a digital material library.

1.2 Motivation

Utilization of natural grain patterns within trees was readily utilized centuries ago when timber was a more common construction material, specifically Dutch-era shipbuilding practices valued the natural efficiency of complex timber shapes (Albion 1926). However, as design materials shifted to concrete and steel, the perceived abundance and standardization of shapes dissolved the need and practice of harnessing the natural efficiency of timber. The expert skill shipbuilders possessed to select a tree by visually determining the availability of a specific shape needed for the design rather than either inducing a “needle-in-the-haystack” approach for finding a specific

member shape or using an immense amount of labor to form a highly specified member. The practice of utilizing the inherent strength of timber members was not only more labor efficient for shipbuilders, but also created stronger vessels since the wood grain in the pieces used aligned to their desired shape naturally (Gomes, Rosa Varela, et al. 2015). Unfortunately, this workflow has been lost with time, and desirable, “natural,” tree-looking structures are now most commonly produced through forcing curvature or aggressive postprocessing, as seen in Figure 1 and Figure 2. Therefore, one of the goals in this project is to revisit this idea of using the natural grain flow of trees to make a stronger, stiffer structure limiting unnecessary labor costs.



Figure 1. Forced curvature in timber through cambering (Daizen Joinery)



Figure 2. “Natural” timber structure, Centre Pompidou Metz (Shigeru Ban Architects)

This project uses Somerville, Massachusetts as the location of its case studies, due to the availability of extracted trees in the area. The city has been engaging in controlled removals of urban trees as a nature preservation precaution to limit the expansion of an invasive beetle infestation (“Emerald Ash Borer Beetle” 2018) as well as a construction need clear land area for new developments. Instead of processing the trees in a woodchipper for alternate uses, the timber is collected and cut into viable tree fork nodes to be tested and analyzed for this thesis. The goal is to find a methodology to reuse the tree forks and branches in a way that could not only contribute to the community and area that the trees were cut down from but also develop a more general framework to be able to design with existing material systems and geometries. The trees were originally removed with the intention of designing a pavilion using the tree forks of the cut trees, so the target geometries proposed represent this utility. To limit the scope of the design, only the tree forks as connection joints and not the tree branches as beam elements will be considered in the design.

1.3 Literature review

This chapter reviews previous research and usage of natural forms of timber in structural design. The first section discusses previous utilization of natural wood grains as “compass” timbers in shipbuilding, the second section overviews the basic biomechanics of tree joints, the third section reviews several case studies that have utilized repurposed tree forks and branches architecturally, structurally, or computationally, and the fourth section details various instances of designing with existing materials. While there has been previous work regarding highly specific instances of tree fork utilization in structures, there has yet to be a comprehensive methodology of constructing a large material library and understanding of the structural behavior of a tree fork.

1.3.1 Shipbuilding with “compass” timbers

During the fifteenth century, timber was an essential resource for European countries, particularly the Netherlands, providing fuel, transportation, building material, and more. It was in the countries’ strategic interests to take part in forest management and smart use of the limited resource; otherwise, overuse would result in early-stage deforestation, which would be detrimental to the growth of the country. Shipbuilders offered a creative solution by being more mindful of the shape, potential placement, and usage of branches and bifurcations in the ship before cutting a tree down. To find the needed timber pieces, known as compass timbers, with the natural grain, the skilled master carpenter would have to have in his mind a clear view of what shapes were needed within the ship. The compass timbers and their intended placement within a ship are seen in Figure 3 and Figure 4. This approach of utilizing the natural shapes found in trees not only reduced material waste, but also creating the most structurally efficient ship (Albion 1926).

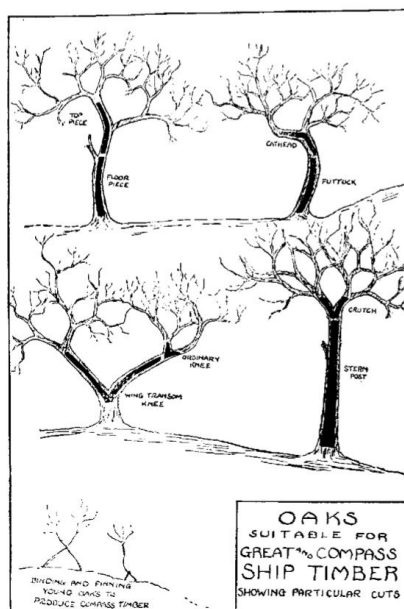


Figure 3. Diagram representation of oak trees as compass ship timbers (Albion 1926, 3)

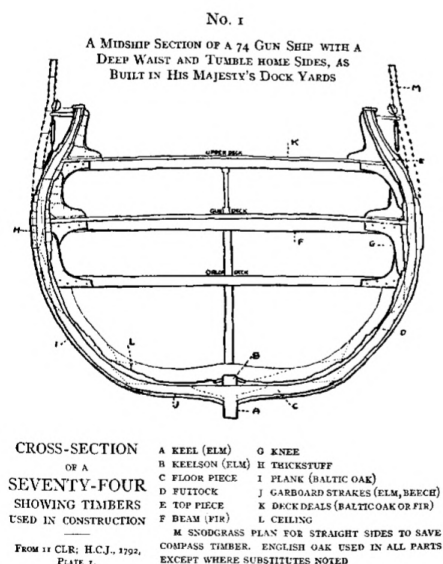


Figure 4. Cross section of a ship (Albion 1926, 4)

Additional factors that contributed to the shipbuilders’ careful tree selection include: age, moisture content, and imperfections (knots). Each of these attributes affects the structural performance of the timber differently, so a thorough understanding of their implications by the shipbuilders was necessary to avoid complications within the built ship. For example, knots represent weak points in the timber structure, because it interrupts the natural grain of the trunk or branch and, with large loads, the timber may generate cracks or even worse, have a sudden failure. However, there is no such things as a perfect tree to convert to perfect timbers. The shipbuilders needed to know how to find the available raw material with an appropriate age, moisture content, and where the knots and cross-grained could be avoided (Gomes, Rosa Verala, et al., 2015). These same natural challenges arise in modern day timber construction and must be accounted for within the design process.

1.3.2 Biomechanics of tree forks

There are two biomechanically different types of tree forks: the tension fork, which consists of two connected stems bent away from each other caused by gravity or wind resulting in tensile stresses in the connective zone, and the compression fork, which consists of two jointed stems pressing against each other (Figure 5). Mattheck and Vorberg (1991) prove the optimized shape of tension tree forks through investigations of their stress distribution. Within their tree samples, it was found that for all tension forks, the inner contour shape remained constant, while the outer contour varied from tree to tree (399). This naturally reoccurring “u-shape” of tension fork demonstrates high levels of efficiency, because it avoids any type of localized stress peaks; the tree automatically wants a fair distribution of loads where no point is exposed to higher stresses than another peak. Ideally, a material library would have mostly tension forks; however, given the external factors that contribute to forming compression forks, it is important to understand their structural implications as well.

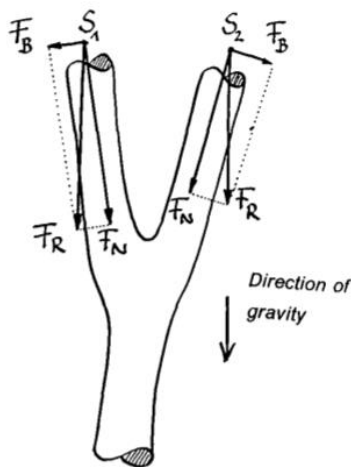


Fig. 1 “Tensile tree fork” characterized by bending the two individual stems of the bifurcation away from each other by gravity leading to tensile stresses in the joint of the two particular stems.

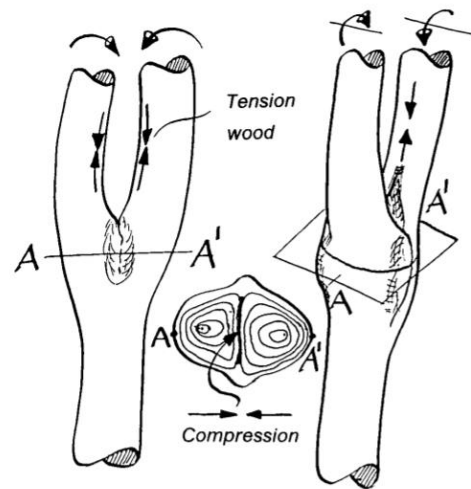


Fig. 2 “Compression tree fork” characterized by bending the two individual stems of the fork towards each other due to reaction wood leading to compressive stresses in the contact zone of the joint.

*Figure 5. Tensile tree fork (left, Fig. 1) vs. Compression tree fork (right, Fig. 2)
(Mattheck and Vorberg 1991)*

The structure of a tension tree fork can be described as the intersection of two expanding cylinders, the branch and the trunk. Shigo (1985) discovered that the trunk is connected to the limb only at the base and sides of the branch attachment, through thousands of tree fork dissections (1392). This means that fibers do not extend from the top of the branch to the trunk above the fork or vice versa, rather the fibers turn to either side and grow around the base of the branch. The zone above the intersection point where branch fibers and trunk fibers turn perpendicular to their respective branches is known as a compaction zone. There is a lack of area for expansion within the compaction zone, so the apex of the tree fork tends to be the weakest point (Farrell 2003, 36). The trunk fibers, branch fibers, and compaction zone can be seen in Figure 6.

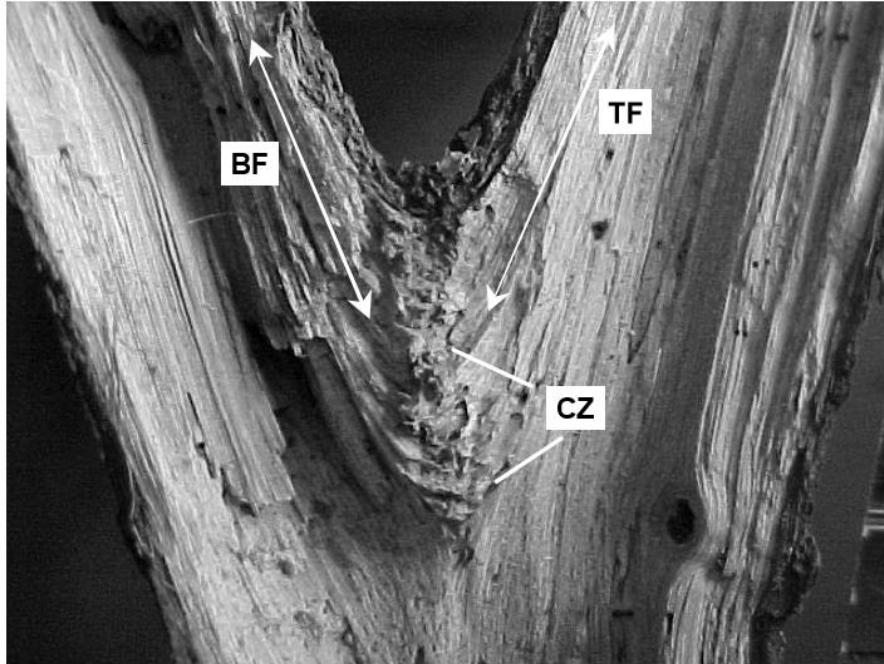


Figure 6. Arrows show the direction of tree fork trunk fibers (TF), branch fibers (BF), and their intersection at the compaction zone (CZ) (Farrell 7)

Trees are highly efficient biomechanical structures whose natural structure is built to resist gravity and wind loads. Tree forks, specifically, act as natural moment connections between the trunk and horizontal branches. These natural structures react to changes within their environment as well as changing gravity and lateral loading conditions, such as snow, wind, etc. by displaying adaptive growth. One result from this response is that the cross-section of a branch changes as it becomes more horizontal and is subject to more bending loads caused by self-weight rather than wind loads. Trees respond to these newfound compressive stresses by growing more cells in that area, and since the maximum compressive stresses due to self-weight occur on the underside of horizontal branches, the result is that the horizontal branches grow downwards and becomes more oval-shaped, shown in Figure 7. The tree fork vector shifts from the centroid of the circular branch to the center of branch rings that have shifted upwards. Adaptive growth in tree fork branches can affect the structural behavior of the fork by changing the modeled vector from what can be assumed to several degrees of center (Burgess and Pasini, 2004 186). Adaptive growth will not be considered during this thesis when simulating tree forks, however, it is important to understand the variation that may occur when using natural materials such as repurposed timber.



*Figure 7. Adaptive growth shown in the cross-section of a tree branch
(Burgess and Pasini 2004, 186)*

1.3.3 Tree fork geometry case study precedents

Previous work regarding utilizing tree fork branches as components in structural frameworks have focused on either singular case studies or broad investigations of polygonal forms that fit the general “Y” fork shape.

1.3.3.1 Hooke Park

The Design & Make School of Architecture in the United Kingdom, executed a singular case study to understand the geometric strategies for exploiting the tree fork inherent form through non-standard technologies. A photographic 2D survey was first conducted of 204 trees to approximate two-dimensional fork representations, and then, after analysis, 25 trees were cut down and a 3D-scan of each branch was conducted to build a database of available tree geometries. For this project, a Vierendeel-style arching truss configuration was designed. Rhino and Grasshopper were used to organize and dynamically place each of the 3D-scanned branch elements along the truss’ target curves and each truss element was placed through three main transformations: 1) moving to another point 2) rotating 3-dimensionally and 3) a second rotation to define the axis. This placing logic was repeated for every component in each iteration of the optimization to minimize the tensile forces; the optimization goal was to minimize the total deviation of the tree forks from the target curves given the constraint of the 20 discrete forks, and the final structure decided upon can be seen in Figure 8. Lastly, in the connection definition and fabrication phase, the strategy was to maximize use of compression transfer through timber-to-timber bearing and to use steel connections for tension and shear limitations. A six-axis robot was used to mill the elements. Mortise and tenon connections were used to connect branch elements to top chords. The structure was assembled successfully, as seen in Figure 9. Future work suggested documenting a larger library of tree components and an analysis of considerations of wood’s grain patterns (Mollica and Self 2016).

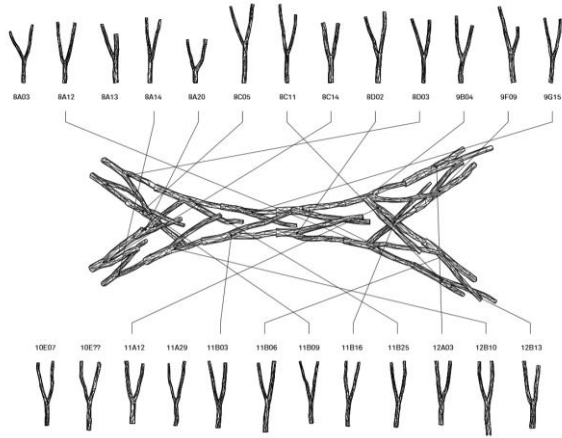


Figure 8. Plan view of truss with mapped placement of tree forks (Mollica and Self 2016, 146)



Figure 9. Wood Chip Barn arching truss, completed (Mollica and Self 2016, 140)

1.3.3.2 IASS 2018

Allner and Kroehnert (2018) presented their research at the IASS 2018 conference regarding forked branches as a new, natural construction material (1). They specifically explored the heterogeneous material properties and grown form of forked branches as optimized structural nodes. They began developing a set of design rules and to use these irregular parts of trees in structural and architectural designs. Each piece was 3D-scanned to simplify the tree fork's complexity into a basic typological principle axis model; then, that information was translated into an axis model, which serves as the reference geometry when designing and configuring. The y-branch nodes were joined to form closed cells to provide general structural integrity and bracing (Figure 10), which when configured together, assembles into bifurcating space loops (Figure 11). Using Rhino, Grasshopper, Wasp, and Kangaroo, spatial frameworks were formed by duplicating and aggregating forks. Basic structural analysis was conducted using Karamba3D on the spatial frameworks (Figure 11), but no work was conducted on the structural capacity of the forks themselves. Further works suggests investigating the structural performance of tree forks, which will be carried out in the current project (Allner and Kroehnert 2018, 4).

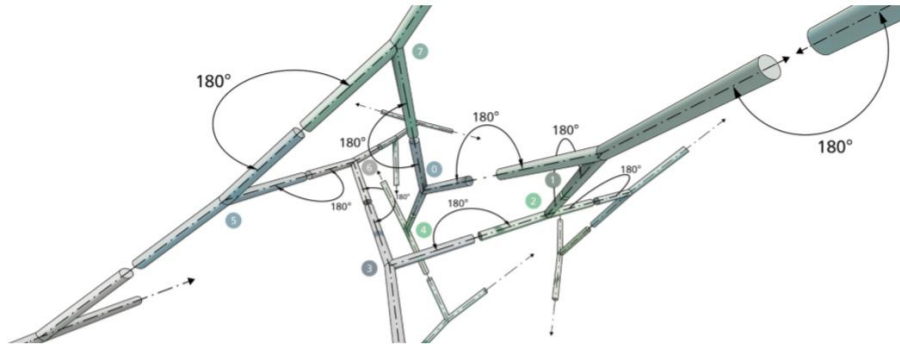


Figure 10. Connection principle resulting in bifurcating space loops (Allner and Kroehnert 2018, 3)

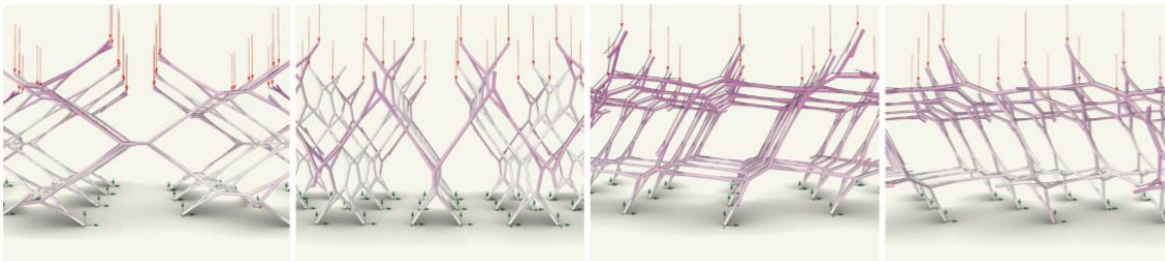


Figure 11. Spatial geometries simulated to align branches with adjacent branch axis with Karamba loadings (Allner and Kroehnert 2018, 4)

Von Buelow et al. (2018) presented work aligned with the goals of this thesis that explore the use of natural timber elements as design connections in timber construction at the IASS 2018 conference. The group developed a methodology that combines parametric form generation and design exploration to produce wooden reticulated shells using natural tree crotches. Their intent was to simplify the complicated design process associated with natural tree forks by developing a standard set of parts that could be organized and produced in various ways for different circumstances as seen in Figure 12.



Figure 12. Standard set of tree fork elements components and assembled (left). Processed and milled tree fork (right). (Von Buelow, Peter, et al. 2018, 2)

Their methodology executed in Rhino/Grasshopper consisted of 4 steps: 1) selecting a base topology grid (target structure), 2) executing a dynamic relaxation of the grid using the plugin Kangaroo to find a compression shell, 3) apply gravity loads using the Karamba plugin and analyze the structural implications, and 4) export the final images using the Ladybug plugin. A solutions space to find and display the best structures for the tree fork library was constructed through Paragen, a design aid developed by the University of Michigan. This system combines parametric form generation through Kangaroo and an analysis tool (Karamba); a non-destructive dynamic population genetic algorithm is applied to search for solutions that fit the applied criteria and the results are saved to a Structured Query Language (SQL) database. The process is designed to be cyclical and interactive such that clients can instantaneous react to the designs created through the solution exploration (Von Buelow, Peter, et al. 2018). The basic design process is shown in Figure 13.

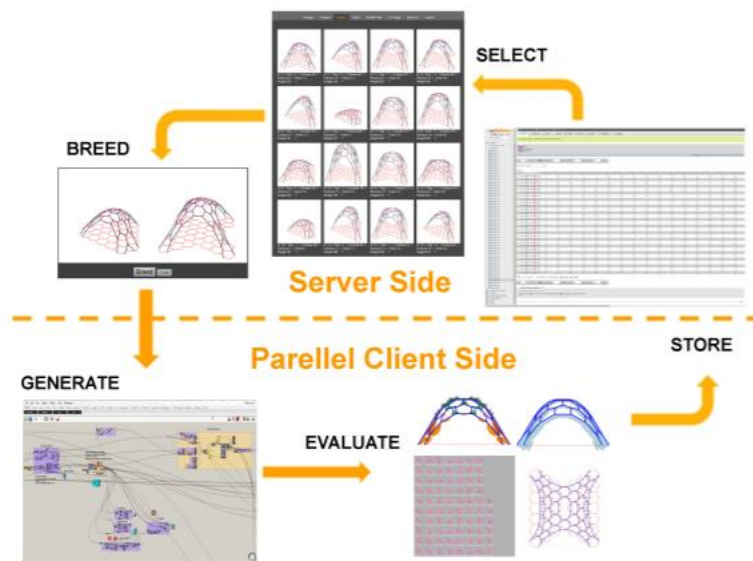


Figure 13. The basic ParaGen cycle showing the steps used to generate a range of solutions (Von Buelow, Peter, et al. 2018, 5)

1.3.4 Designing with existing materials

The contemporary mindset for structural engineering is a design of abundance and standardization; there is an assumption that there are infinite supplies of reoccurring elements. This approach does not work for instances where structural materials are available in finite quantities or not available at all, and design mentality must change to use resources more mindfully. Additionally, environmentally and economically there is an interest to design with less embodied carbon or amount of material through structural optimization, usage of local materials, or utilization of new technologies. There have been some custom enterprises utilizing found tree forms, such as specializing in ad hoc railings made from branches, but these ventures tend to have an artisan component that is difficult to implement at a larger scale. Conventional approaches for finding solutions with finite quantities of material, methods to reuse existing material, or designs based on an available material library are slow or ineffective, requiring time-consuming trial and error to

develop viable designs, or not findings solutions at all. New computational strategies are key to tackling this problem and developing methodologies of using existing materials in design.

Brütting et al. (2018) researches the reuse of structural components in design to reduce the environmental impact of building structures. Their work utilizes structural optimization formulations to design truss systems from reusable steel elements; weight minimization and embodied energy serve as objective functions subject to ultimate and serviceability constraints. The methodology utilized in their research is a two-step method in which the original structure undergoes a topology optimization followed by a geometry optimization. Specific case studies were conducted on: 1) simple roof truss systems with predefined geometry and topology and 2) geometry optimization to better match the optimal topology found for trusses in the form of a simple cantilever, a bridge (Figure 14), and a complex roof with available stock length elements. In each of these case studies, Brütting et al. (2018) compares the structural shape, size of the members, mass, embodied energy, displacement, and element capacity utilization between the structure made from reused elements versus new material. The result of the optimized shape for the bridge truss is shown in Figure 15 and the compared values are in Figure 16. This research concludes that even though structures made from reused elements have a higher mass and lower element capacity utilization, they embody significantly less energy and carbon with respect to structures made of new elements (Brütting et al. 2018, 19). The two-step methodology is sufficient to locate local optima, but a more efficient solution explored in the present tree fork optimization would simultaneously optimize element assignment, topology, and geometry.

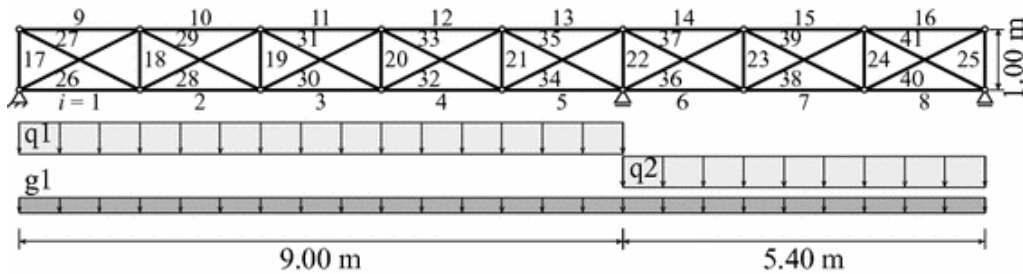


Figure 14. Bridge truss system – ground structure (Brütting et al. 2018, 18)

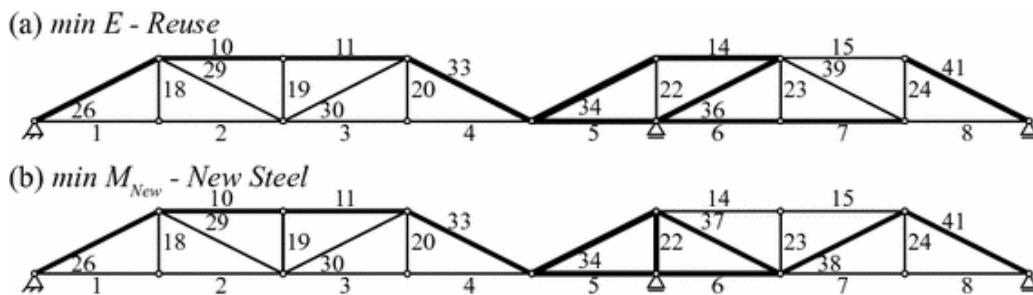


Figure 15. Bridge truss – optimization results final topologies (Brütting et al. 2018, 20)

System C	Reuse - Objective			New steel
	$\min M$	$\min \Delta M$	$\min E$	$\min M_{new}$
M_{tot} [kg]	219.4	216.0	210.6	–
m [kg]	189.1	195.9	189.9	179.8
ΔM [kg]	30.3	20.1	20.7	–
E [MJ]	711.6	700.6	683.2	2378.6
u [mm]	18.3	17.1	17.8	19.0
util. [%]	64.4	56.7	59.0	64.9

Figure 16. Bridge truss – assignment optimization (Brütting et al. 2018, 19)

Bukauskas et al. (2018) explores naturally-occurring small-diameter round timbers as a viable existing structural material to be utilized with minimal processing. The group has developed an approach that makes it easier for engineers and architects to design using these low embodied-energy, inventory-constrained materials. Bakauskas et al. has proposed the concept of an “assignment” of inventory elements to structural elements, which is a set of instructions necessary to assemble a structure from the given set of inventory elements. Additionally, rather than minimizing the structural problem for mass or structural stiffness, an offcut-ratio, the ratio of offcut waste mass to the mass of inventory material consumed, is applied. The off-cut ratio better for this instance, because it is a helpful benchmarking tool when comparing the relative performance of assignments for different designs. An example of this methodology can be seen in Figure 17 of how a designer can use this approach to parametrically design a roof truck with a constrained inventory (Bakauskas et al. 2018, 8).

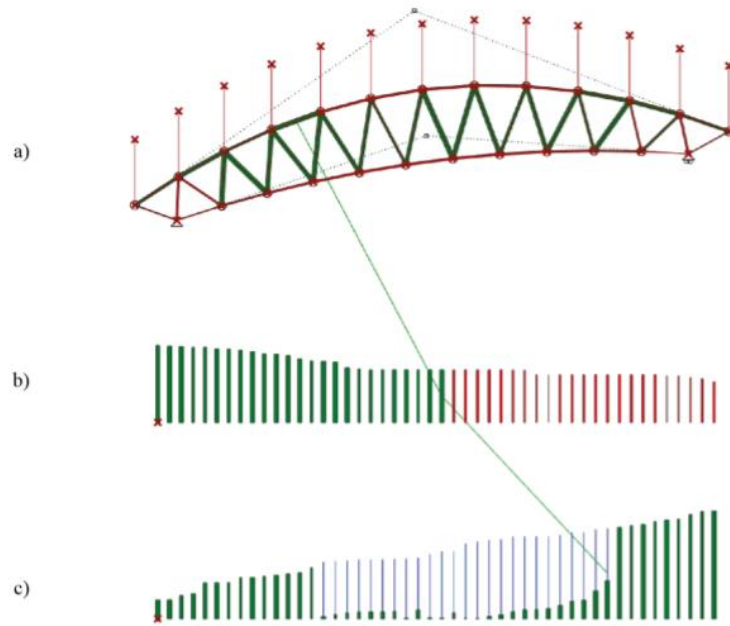


Figure 17. Iterative form-finding process for inventory constrained design: a) parametrically defined structure with loads and support conditions b) structure elements pre-sorted in descending order by length, c) inventory elements pre-sorted in ascending order by length (Bakauskas et al. 2018, 8)

Previous work regarding using existing materials has focused on finding specialized solutions for truss structures reusing steel elements as well as developing a specific metric for usage of small-diameter round timbers. The research presented in this thesis aims to understand tree forks as an existing material and develop a comprehensive scoring metric for matching and performance of proposed structural designs. With continued research in this field, modern technology, when applied, will make designing with available materials more accessible and available reality for the future.

1.4 Research objective

This project will focus on two goals: 1) exploring the extent and limitations of the material library on the structural design by conducting a thorough sampling of tree fork nodes of various tree species found at the site location, and 2) creating a model that allows the user to understand the relationship between varying the geometry, the number of tree forks in the material library, the structural percentage match of the tree fork vector angles to the nodes and the percent allowable variation in the geometry of the original structure. The above plans will be carried out through physical structural tests as well as software analysis through Grasshopper in Rhino. The research question posed for the matching-based design method and structural performance of tree nodes are listed.

Matching-based design method:

- 1) How many samples are necessary to get the “best match” for a desired structure? Is there a point where the matching score exhibits diminishing returns as number of samples in the material library increases?
- 2) How do various tree species perform on different target geometries?
- 3) What is the relationship between tree species, number of samples, and target geometry?
- 4) What is the ratio of tree nodes available to inventory size needed that results in a good match?

Structural performance of tree branch nodes:

- 1) What kind of reaction (e.g. splitting, crushing, cracks, etc.) occurs during a moment test of a tree fork branch?
- 2) Is there an angular cutoff in which there is a significant decrease in performance of tree forks?
- 3) Which tree species provides the best structural score? Which tree species is recommended for use in structural design?

2 Matching-based design methods and results

2.1 Conceptual overview of design process

2.1.1 Previous work

Previous work has been conducted by Caitlin Mueller, Felix Amtsberg, Kevin Moreno Gata, and Yijiang Huang in designing an algorithm to fit natural tree fork connections into a pre-described structure. Their research goal was to quantify the mismatch between a three-valence node on a design geometry and a tree fork and to create a computational algorithm to find the optimal matching that minimizes the overall “mismatch error” calculated. A material library was collected and analyzed, a computational algorithm was developed, the available tree forks were matched to a design, robotic fabrication was utilized to cut the joints to shape, and a prototype of the design was constructed (Figure 18).

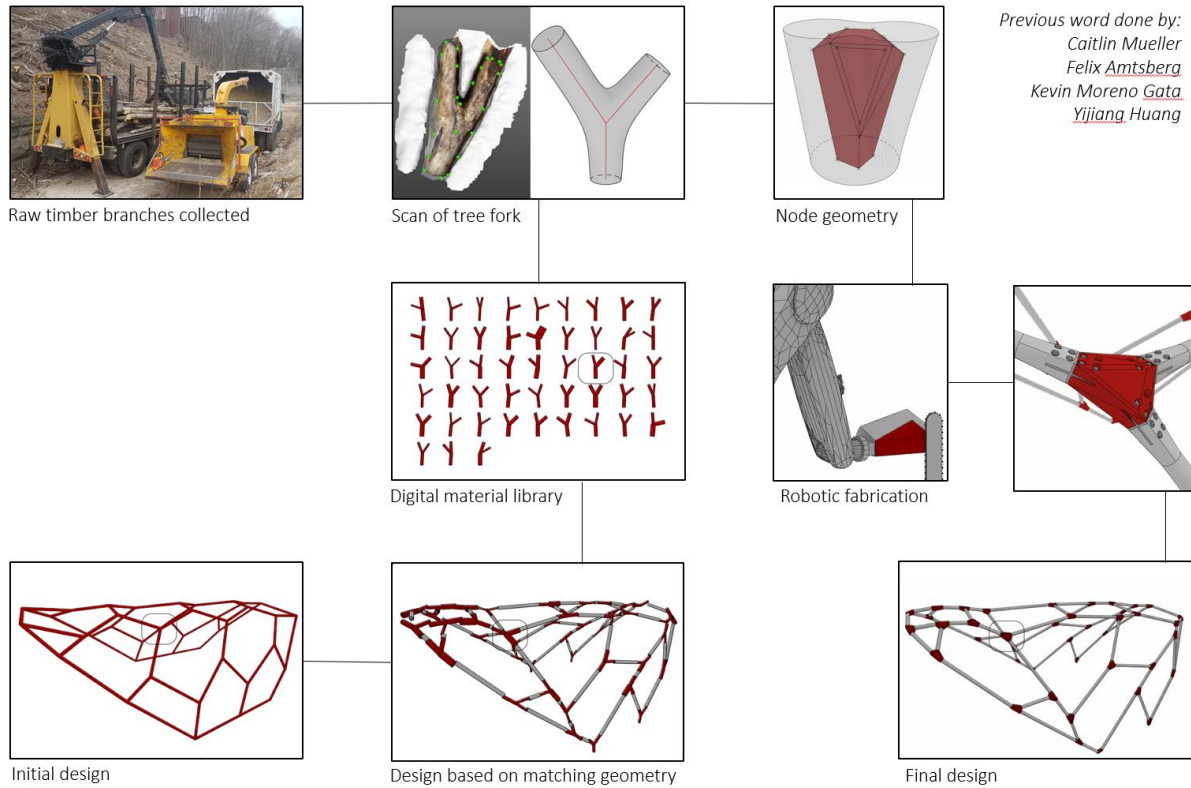


Figure 18. Process of acquiring material, digitizing inventory, designing and fabricating (Amtsberg et al.)

A library of 46 tree forks of various species were collected from Somerville, Massachusetts and catalogued for use in this project. A few examples of the tree forks obtained to be analyzed are shown in Figure 19. Low-cost 3D-scanners were used to generate a rudimentary material library from which a mesh was uploaded in Rhino to be cleaned and simplified. The Rhino model contained branch diameter and angle information to be referenced later in a computational algorithm.



Figure 19. Tree forks collected and scanned from Somerville site (Amtsberg et al.)

An algorithm was constructed through the combination of the Hungarian algorithm and Iterative Closest Point algorithm that takes the nodal center points of the tree forks in the library and matches them to the nodal points of the pre-described structure at the best vector angle fit, which will be detailed in section 2.1.2.6 Matching score (Figure 20).

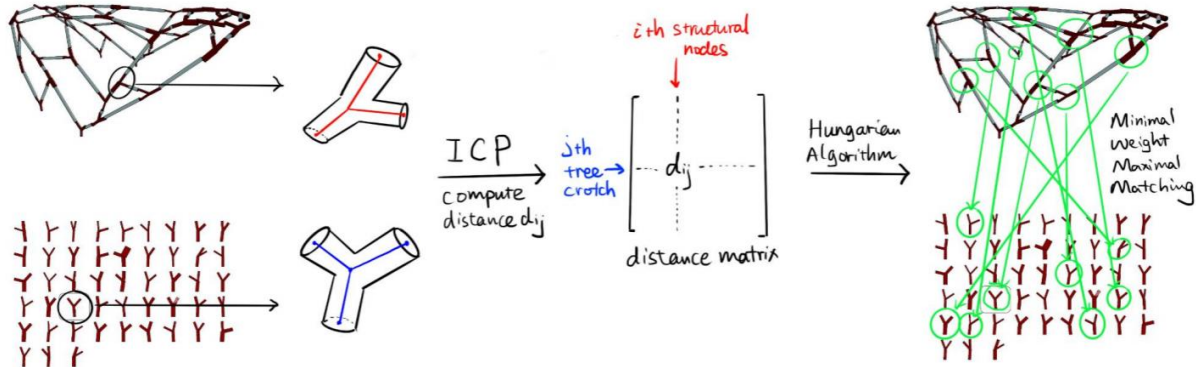


Figure 20. Iterative Closest Point (ICP) and Hungarian algorithm matching tree fork material library to given structure (Huang et al.)

The matching algorithm was used to design a small, specialized prototype that could test the design-to-fabrication process. The fabrication sequence of the matched tree forks to a proposed structure are shown in Figure 21.



Figure 21. Prototype structure (Amtsberg et al.)

This previous work provided a starting point for this research project by generating a methodology that gives a quantitative value that represents the quality of match between available tree forks in a material library to a target design. Since the matching score improves as the fit of the tree fork vectors to the structure has less variance, this thesis explores various methods that change the target structure to best match the available tree forks.

2.1.2 General methodology

In order to generate a new, simulated material library of 50, 100, 200, 250, 350, 500, 750, and/or 1000 samples, basic tree morphology data is necessary: the tree species present at the site, the branch angle range for different species, the branch diameter ratio between the main branch and the two branching out forks. With the necessary data, a new material library can be randomly generated for a project. For the purposes of this thesis, material libraries consisting of branches of the same species will be analyzed for matching ability to a prescribed structure.

2.1.2.1 Tree species

The original study conducted by Caitlin Mueller, Felix Amtsberg, Kevin Moreno Gata, and Yijiang Huang was based on existing trees cut down from a high school in Somerville, Massachusetts, so for consistency, a sampling was conducted based on the trees found at that location. This data was found in the Somerville TreeKeeper database, a software website used to track the economic and ecological benefits of each tree in the city, and is shown in Figure 22 (“TreeKeeper”). Navigating through the online database, on the side panel there is an option to build a report based on site; selecting the Somerville High School option gives the number of trees of each species in that location. The main tree species at the site are: maple, crabapple, ash, dogwood, oak, and various fruit trees.

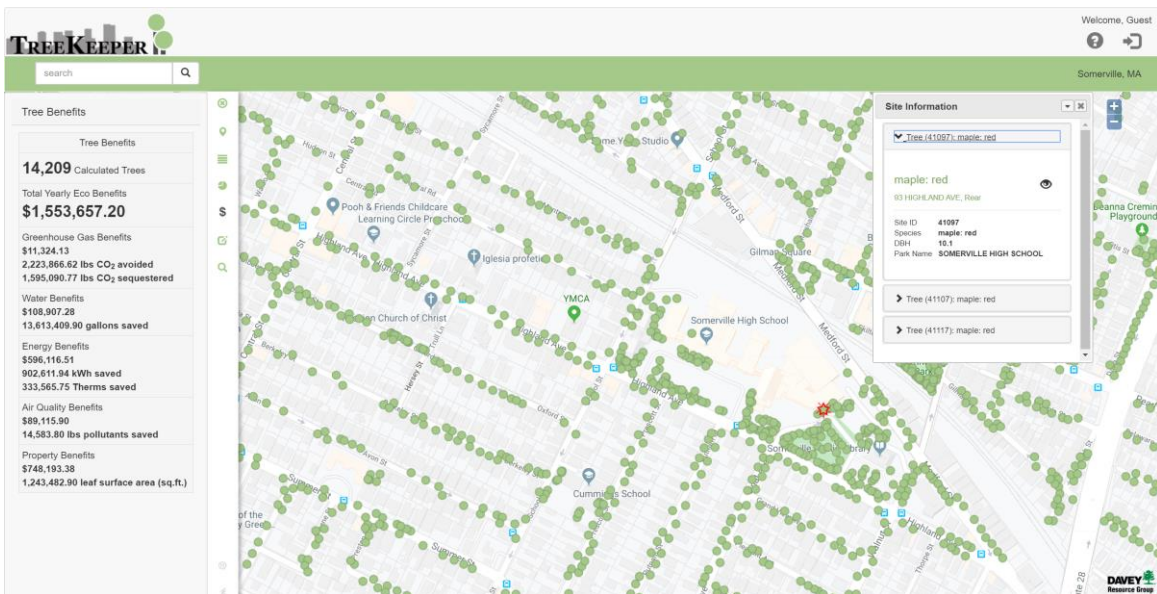


Figure 22. TreeKeeper database cataloging all trees in Somerville, MA (“TreeKeeper”)

2.1.2.2 Branch angles

The necessary tree branch angles are found through botanical tree image generation data, which provides a maximum, minimum and average branching angle. This data was collected by Masaki Aono and Toshiyasu L. Kunii from the University of Tokyo to model botanical trees through geometric modeling in a computer graphics system. Visualizations of the trees generated are shown in Figure 23. Since the trees sampled are in Japan, a common genus (i.e. birch or ash or maple) and similar characteristics of the trees were cross-referenced between the data collected by Aono and Kunii (1984) and the Somerville High School tree species (19). This information is shown in Table 1; the tree name is from the paper followed by the common name/characteristics, its match to the Somerville High School tree, the total number of that species in Somerville, and the average/maximum/minimum angle data. In Grasshopper, the branching angle variable range is set between the minimum angle divided by 2 to the maximum angle divided by 2 for the right and left branch angle. A third z-angle variable is set for the right and left forks at a range of zero to 30 degrees as evidenced from literature and the original data library (Pradal et al 2008).⁹

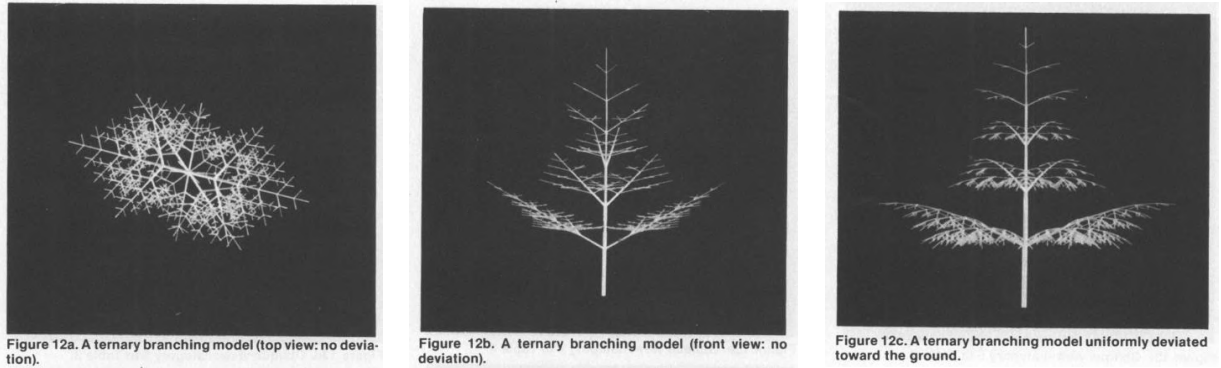


Figure 23. Visualizations of tree image generation data based on collected branching angles (Aono and Kunii 1984, 15)

Table 1. Tree fork average, minimum, and maximum angles

Tree Name	Common Name/Characteristics	Match to location tree type	# of species at location (Total = 14k)	Aver. Angle	Max. Angle	Min. Angle
Betula platyphylla	Birch	Birch	173	60	86	35
Cornus controversa	Dogwood, med-size, deciduous	Dogwood	71	60	88	40
Liquidambar formosana	Sweet gum, deciduous	Ash	1052	64	99	25
Lithocarpus edulis	Stone-oak	Oak	730	54	86	32
Myrica rubra	small-med-size, fruit tree	Crabapple	208	60	85	30
Liriodendron tulipifera	Poplar, large, deciduous	Maple	7	56	83	25

2.1.2.3 Tree branch diameters

Tree branch diameters were obtained through utilization of Leonardo da Vinci’s rule, which states that the sum of the cross-sectional area of all tree branches above a branching point at any height is equal to the cross-sectional area of the trunk or branch immediately below the branching point (Minamino and Tateno 2014). This rule is visually displayed in a computer-simulated tree example in Figure 24.

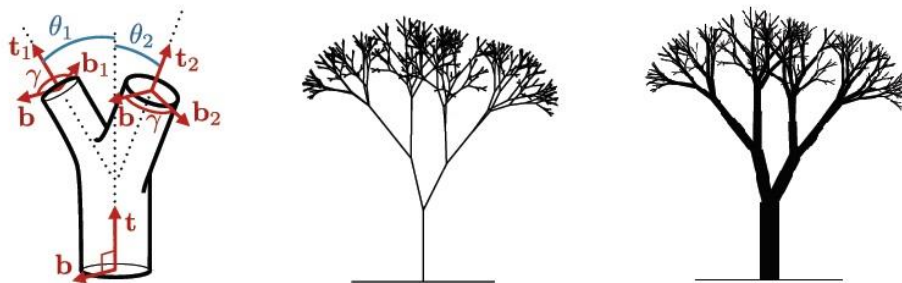


Figure 24. (Left) Model of tree branching. (Middle) Tree skeleton with equivalent diameters for all branches. (Right) Tree skeleton utilizing Leonardo da Vinci’s rule. (Eloy)

Mathematically, this means that if a tree fork with a trunk branch diameter (D) splits into an arbitrary number (n) of secondary branches of diameters (d_1, d_2, \dots), the sum of the secondary diameters squared equals the square of the original branch's diameter.

$$D^2 = \sum_i d_i^2 \quad (1)$$

The Grasshopper model sampling aims to reproduce tree forks similar in size to those previously scanned and recorded within the material library with reasonable variability. The trunk branch diameter varies between 6 and 10 inches, and one of the forking branches varies between 3 and 5 inches. The random sampling selects a value within these ranges and subsequently calculates the last forking branch diameter according to Leonardo da Vinci's rule.

2.1.2.4 Methodology for simulating random tree fork library

Since there is a generous amount of variability even within each tree species depending on various environmental and location specific factors, a random sampling of the tree image data provides a satisfactory database for the simulated tree forks. A random uniform sampling is completed in Grasshopper for Rhino through the Sampling component found in the Design Space Exploration plugin. The five variables inputted into the Sampler are: 1) the right branch angle, 2) the left branch angle, 3) z-axis rotation angle, 4) diameter of the trunk branch, and 5) diameter of one of the forks. A sampling is conducted for the three most common species in the Somerville High School location: ash, oak, and crabapple for 50, 100, 200, 250, 350, 500, 750, and/or 1000 samples. This information is then inputted into the Grasshopper code that takes the values and creates tree fork representations that can be inputted into the matching algorithm. This process is shown in Figure 25. The "Rotation of Branch Angles" and "Line Branch Visualization" section takes the angle values and creates line representations (Figure 26), and the "Diameters" and "Line to Brep" sections create pipe representations to be displayed in the Rhino model (Figure 27).

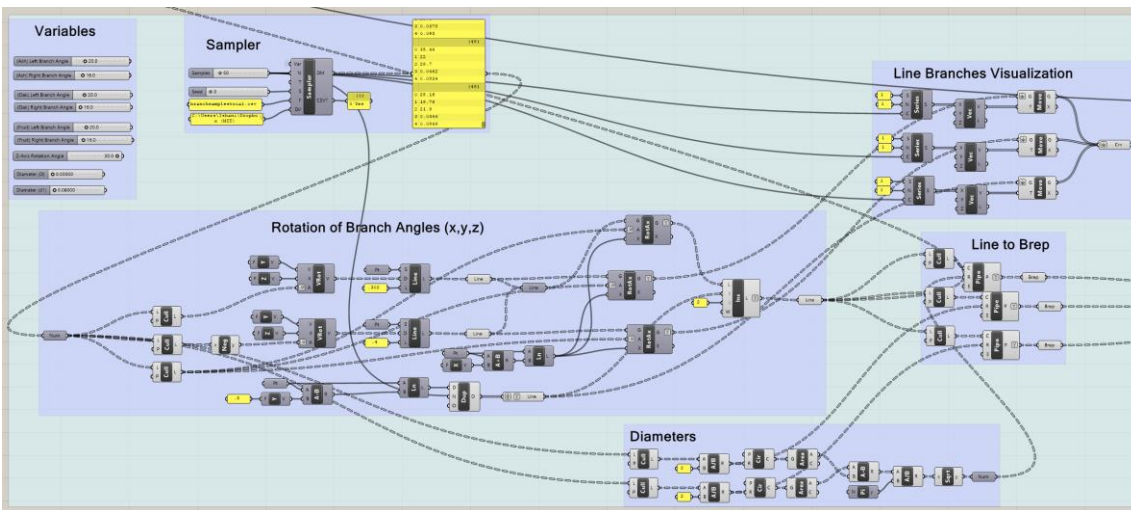


Figure 25. Grasshopper sampling methodology visualization



Figure 26. Line representations of tree forks



Figure 27. Brep pipe representations of tree forks

The newly generated samples are then input into the Grasshopper code that vectorizes and matches the nodes to the structure.

2.1.2.5 Target structures

The prototype structures are designed within Grasshopper to allow for geometric variation through either control curves or points, changing the variables that manipulate these components alters the geometry of the structure. The computational matching algorithm automatically updates the tree forks matched to each node for the best fit as the geometry changes, which allows for an optimization algorithm to use the control curves or points as variables and the matching score as a minimization objective. This geometric variation aims to answer the research question of whether or not there is a best fit structure that fits the tree forks available in a material library.

The structures simulated in Grasshopper within this thesis aim to limit the number of variables used to manipulate the geometry of the structure while maintaining a generous control space for the structure to shape to multiple forms. An unsuccessful iteration that designated each x, y, and z-value of each node a variable resulted in erratic geometries and nonconvergence when optimized.

Additionally, when designing potential structures as options for utilizing the tree forks simulated in the sampling and subjected to the computational matching algorithm as structural nodes, it is important to ensure that the prototype structure's nodes have three beam elements meeting at each singular joint. Any nodal configurations with more or less than three vectors meeting at joint causes an error within the computational algorithm resulting in no matching.

2.1.2.6 Matching score

A computational model was constructed through the combination of the Hungarian algorithm and Iterative Closest Point algorithm to develop 1) a metric calculating the mismatch between the tree fork vectors to matched nodal vectors, known as the matching score and 2) a method of matching the tree forks in the available material library to the nodal points of a proposed structure that minimizes the overall mismatch score. The mismatch metric is defined based on the Iterative Closest Point (ICP) method and the Hungarian algorithm is used to find the minimal distance matching. As mentioned in 2.1.1 Previous work, this computational algorithm was implemented in Grasshopper by Yijiang Huang.

The matching problem formulation is fundamentally a map that uses the notion of distance to measure the gap between the vectors of the structural nodes to the vectors in the tree forks, and it can be formulated as:

$$\min_{c \in \text{Perm}(\{m\})} \sum_{i=1}^n d(N_i, M_{c(i)}) \quad (2)$$

where d is the mismatch metric needed to be designed, N_i represents the n three-valance structural target nodes where $i \in \{1, \dots, n\}$, and $M_{c(i)}$ represents the n three-valance tree fork nodes where $i \in \{1, \dots, n\}$ and $c(i)$ is the integer index of the point in M that corresponds most closely with the i -th point in N .

The ICP is implemented first and computes the mismatch metric, d , between a design node N and tree fork M by finding the optimal rotation, translation, and distance to vectors of the structure's node and then computing the sum of squared matched end point distances. Three vectors generate a central line skeleton that represents each target structure node and each tree fork in the material library. The set of three vectors use the four end points of the skeleton line segments: $N_i = \{u_0^{N_i}, u_1^{N_i}, u_2^{N_i}, u_3^{N_i}\}$ and $M_i = \{v_0^{M_i}, v_1^{M_i}, v_2^{M_i}, v_3^{M_i}\}$, where $u_0^{N_i}$ and $v_0^{M_i}$ are the central points that have a valence of three. A joint optimization of rotation, translation, and skeleton line correspondence produces a distance, so the mismatch measure problem can be formulated as matching the two vectors sets:

$$d(N, M) := \min_{R, t, c} \sum_{i=0}^3 \|R \cdot u_i^{N_i} + t - v_{c(i)}^{M_i}\|_2^2 \quad (3)$$

$$\text{s. t. } R^t = R^{-1}, R \in \mathbf{R}^3$$

$$t \in \mathbf{R}^3$$

The Iterative Closest Point algorithm alternates between solving for Rotation, R , translation, t , and the correspondence, c , separately and then finds the closest rotated and translated tree fork.

Theorem: Let $X' = \{x_i - \mu_x | i \in [n]\} = \{x'_i\}$ and $P' = \{p_i - \mu_p | i \in [n]\} = \{p'_i\}$ where $\mu_x = \frac{1}{n} \sum_{i=1}^n x_i$ and $\mu_p = \frac{1}{n} \sum_{i=1}^n p_i$ denotes the center of masses. Let $W = \sum_{i=1}^n p'_i \cdot x'_i{}^T$, and its

Singular Value Decomposition, SVD, is $W = U \begin{bmatrix} \sigma_1 & 0 & 0 \\ 0 & \sigma_2 & 0 \\ 0 & 0 & \sigma_3 \end{bmatrix} V^T$, where $U, V \in \mathbb{R}^{3 \times 3}$ are

unitary and $\sigma_1 \geq \sigma_2 \geq \sigma_3$ are the singular values of W . Then, if the $\text{rank}(W) = 3$, the optimal solution of $E(R, t) = \frac{1}{n} \sum_{i=1}^n \|R \cdot x_i + t - p_i\|^2$ is unique and given by:

$$R^* = U \cdot V^T \quad (4)$$

$$t^* = \mu_p - R^* \cdot \mu_x \quad (5)$$

The minimal value of the error function, known as the matching score, is $E(R^*, t^*) = \sum_{i=1}^n (\|x'_i\|^2 + \|p'_i\|^2) - 2(\sigma_1 - \sigma_2 - \sigma_3)$. (Rusinkiewicz and Levoy 2001).

The Hungarian algorithm, a combinatorial optimization algorithm, is processed on each of the node vector matches to minimize the distance difference between the tree fork vector and the structural node vectors and gives a matching score value. It takes the distance d , which measures the mismatch, a mismatch distance matrix $D \in \mathbb{R} n \times m$ can be constructed by having $D_{ij} = d(N_i, M_j)$. Then, the Hungarian algorithm takes this distance matrix D as an input and outputs the optimal match, c (“The Hungarian Algorithm”). An open source C# implementation of the Hungarian algorithm is used in the Rhino/Grasshopper environment.

The mismatch metric generated in Equation (3) can be solved through the following steps:

1. Given an initial R and t , the correspondence, c , is calculated by calculating the Euclidean distance through the Hungarian Algorithm.
2. Use c to solve R^* and t^* using Equations (4) and (5)
3. If the new mean error, matching score, $\frac{1}{4} \sum_{i=0}^3 \|R \cdot u_i^{N_i} + t - v_{c(i)}^M\|^2$ does not exhibit any change within a specified tolerance since the last iteration, then go to step 1 and repeat, otherwise exit.

The matching score is tabulated as the mean error for the whole structure of all the matched tree forks to the target structure nodes; the Hungarian algorithm calculates the Euclidean distances between the tree forks and target nodes resulting in the R , t , and c values and the iterative closest point theorem outputs the mean error, matching score, described above as $E(R^*, t^*) = \sum_{i=1}^n (\|x'_i\|^2 + \|p'_i\|^2) - 2(\sigma_1 - \sigma_2 - \sigma_3)$ tabulated from inputting Equations (4) and (5) into Equation (3).

The larger the matching score value, the worse the matching result, so a minimal matching score is desired for a “good” matching structure.

2.1.2.7 Optimization

In this research thesis, structural optimization formulations are utilized to design target structures from available tree forks in a material library. Minimization of the matching score is the objective function subject to target structure geometry design variables.

The optimization is conducted in a built-in component in Grasshopper, Galapagos. This optimizer tool is able to optimize a shape so that it best achieves a user defined goal. For the Galapagos component to work, it needs a series of variables or “genes” to sample, and a defined objective or “fitness value.” In the geometries tested in the following case studies, the variables adjusting the 2 control curves, 5 control points, and 1 control curve are the input “genes,” and for all the cases, the matching score is the “fitness value.” Galapagos does not try every single possible combination of the options to find an optimum solution; instead, it aims to “learn” from each successive round of experiments or “generations” to progressively get to the best answer.

Within Galapagos, the Simulated Annealing solver was utilized to minimize the matching score (the lower the score, the better the match). Simulated annealing is a heuristic optimization method, which uses random numbers and statistical methods to improve a design until a satisfactory result is reached. This method, though effective for optimizations in a large sample space, may still

provide a local minimum depending on the starting point of the problem. For consistency in the sampling results, the target structure geometry was reset to the original structure before a new optimization was conducted.

The colors of the tree branches matched to the target structure qualitatively and relatively demonstrate the better and worse matches for the tree fork to structural node. Colors range from green to yellow to orange to pink representing best to worse matches; an example of the color matching is seen in Figure 28 for a 4x7 hexagonal grid target structure with oak tree forks matched. It would be optimal to have a matching score equal to zero and all representative tree forks to be colored green.

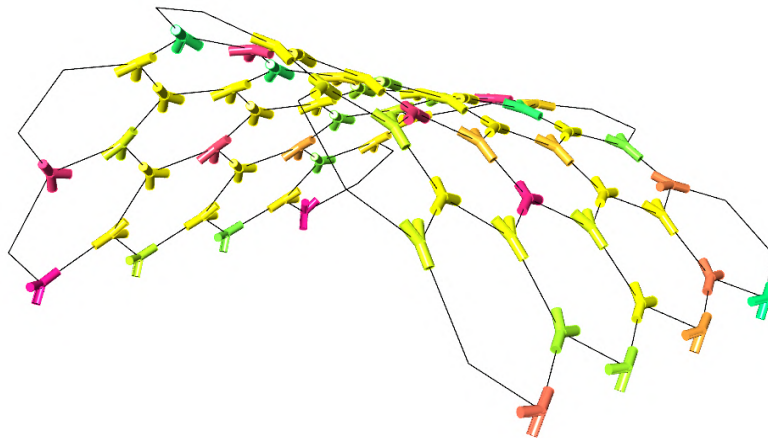


Figure 28. Oak. 4x7: Hexagonal, 1 Control Curve. 100 samples.

2.2 Simulated inventories and case studies

There are 46 samples in the original digital material library; the new sampling method coded within Grasshopper generates any number of tree forks for the computational matching algorithm to correspond to the nodes to any designed template structure. This research comprises of iterated samplings of the material library on three distinct prototype structures to investigate three questions: 1) how many samples are necessary to get the “best match” for a desired structure, at what point are there diminishing returns? 2) are some geometries better target structures than others? 3) what tree species have the best fit for the structures tested?

The geometries are matched with three commonly found tree species found from the original material library location in Somerville, Massachusetts: ash, oak, and a wide-ranging fruit species. These tree species were correlated to trees sampled in Japan through a common genus that has the same characteristics to obtain the angular tree morphology data collected in the study done by Aono and Kunii explained in section 2.1.2.2 Branch angles. The angles for the ash, oak, and fruit tree are shown in Table 2.

Table 2. Ash, oak, and fruit tree branch angles

Ash		Oak		Fruit	
Angles:	Average: 64	Angles:	Average: 54	Angles:	Average: 60
	Maximum: 99		Maximum: 86		Maximum: 85
	Minimum: 25		Minimum: 32		Minimum: 30

2.2.1 Pavilion geometry with 2 control curves (4 variables)

The initial structure used for the sampling analysis is the original pavilion from previous work designed for a high school in Somerville, Massachusetts where the tree forks were collected. The original structure was modeled by Mueller, Amtsberg, and Gata in Rhino (Figure 29a), and its shape can be manipulated with two control curves generated in the Grasshopper environment (Figure 29b). The two lines of curvature have four variables that control the strength and amount of curvature the structure follows (Figure 29c).

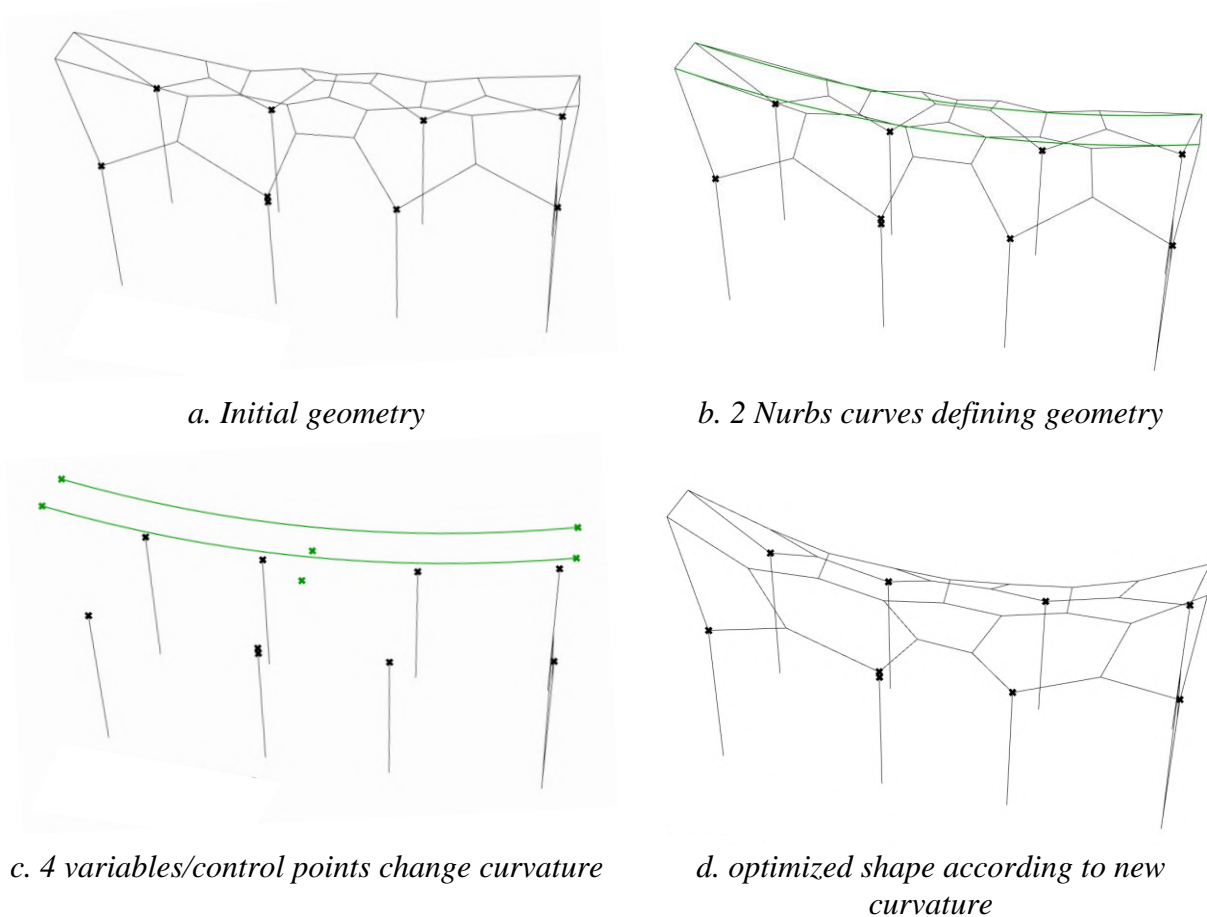


Figure 29. Pavilion geometry with 2 control curves

The geometry of the target structure changes based on the two control curves such that the nodes on the structure shift according to the curvature changes (Figure 29d). The Galapagos optimizer plugin is utilized to vary the four variables controlling the curvature shape of the structure to

minimize the matching score by automatically placing the best fit tree forks from the generated material library onto the target structure.

An iteration of the original pavilion geometry was tested by changing the variables from the broad control curves to the x , y , and z -coordinates of each node of the target structure. The reasoning for this approach speculated that if the x , y , and z coordinates of the target structure are able to be shifted within a range, then there will be a structure that has a matching score equal to zero where every tree fork is a theoretical perfect fit to the target structure. This trial was unsuccessful for two reasons: 1) the optimization failed to converge on a single solution because there were too many variables, and 2) if a solution was found, it was incongruous and therefore, unlikely to be a viable architectural shape. A potential geometry using this control point system is shown in Figure 30.

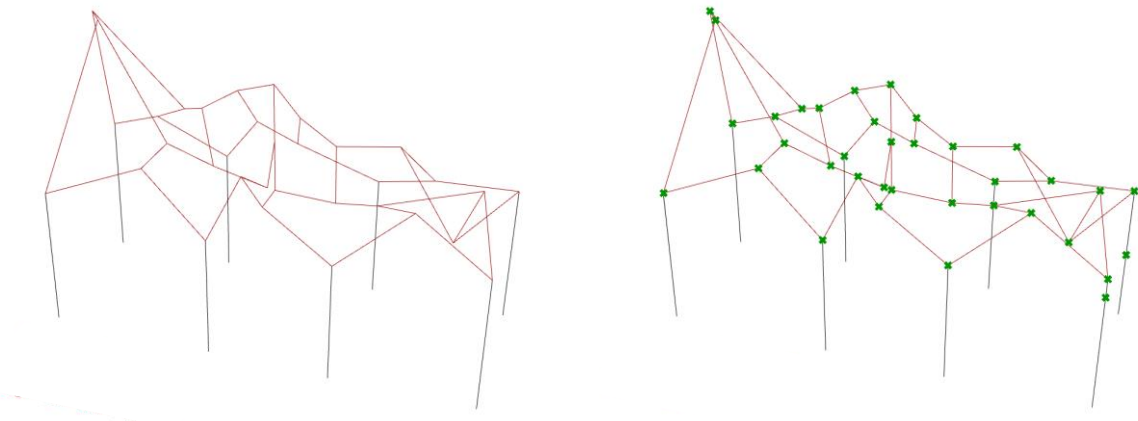


Figure 30. Potential geometry given x , y , z -coordinate variables for each node

2.2.2 Hexagonal geometry with 5 Control Points (5 variables)

To understand the sampling effects of the tree fork matching on a more conventional geometry, a hexagonal grid of varying x -direction and y -direction densities was generated and projected on a surface with 5, z -direction control points. Hexagonal grids are distinctive in that every node has three beam elements meeting a singular connection point, so a hexagonal surface is a model target geometry for tree fork matching. The process of generating the hexagonal grid and projecting it on a square surface constructed from 9 points is shown in Figure 31.

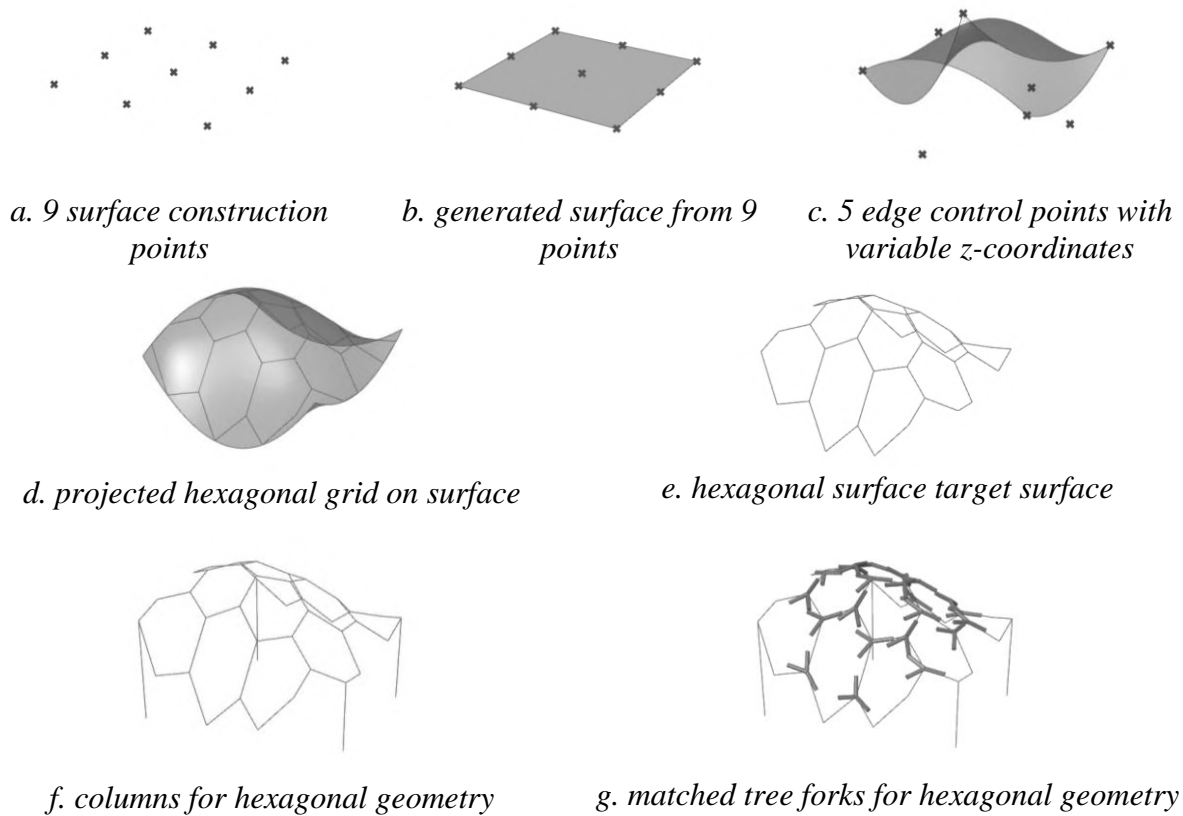


Figure 31. Hexagonal surface geometry generation process

The results of the sampling experiments are discussed in section 2.3.2 Hexagonal geometry with 5 control points (5 variables) results.

2.2.3 Hexagonal geometry with 1 Control Curve (3 variables)

The hexagonal initial geometry was iterated to create a more rigid geometry with fewer variables to create more consistent final geometries. The hexagonal grid now has fixed connections along the edge points in the x-direction, and the curvature of the structure is manipulated with 3 variables composing one control curve. The base surface the hexagonal grid is projected on is 20'x20' square. The x-direction hexagonal grid density controls the number of support points fixed to the ground, and the y-direction hexagonal grid density represents the number of hexagons across the target structure. The number of hexagons in the x and y-direction are varied to observe if varying the initial grid structure while all other variables remain constant would produce varying matching score results answering the question, are some geometries better target structures than others?

The geometry controlling the curvature of the structure is a non-uniform rational b-spline, NURBS, curve, which is a mathematical formulation that has a high level of flexibility and precision restrained by a set of control points. The singular NURBS curve controlling the hexagonal geometry has three variables: 1) the height of the lofted curve, 2) the degree of curvature, and 3) an angular x-rotation of the curve. This NURBS curve dictates the final surface through three

additional NURBS curves formed from the endpoints and midpoints of the NURBS curve and the two x-direction edges fixed at the ground (Figure 32). An assortment of the geometric variations resulting from altering the variables that control the NURBS curve are shown in Figure 33 and Figure 34.

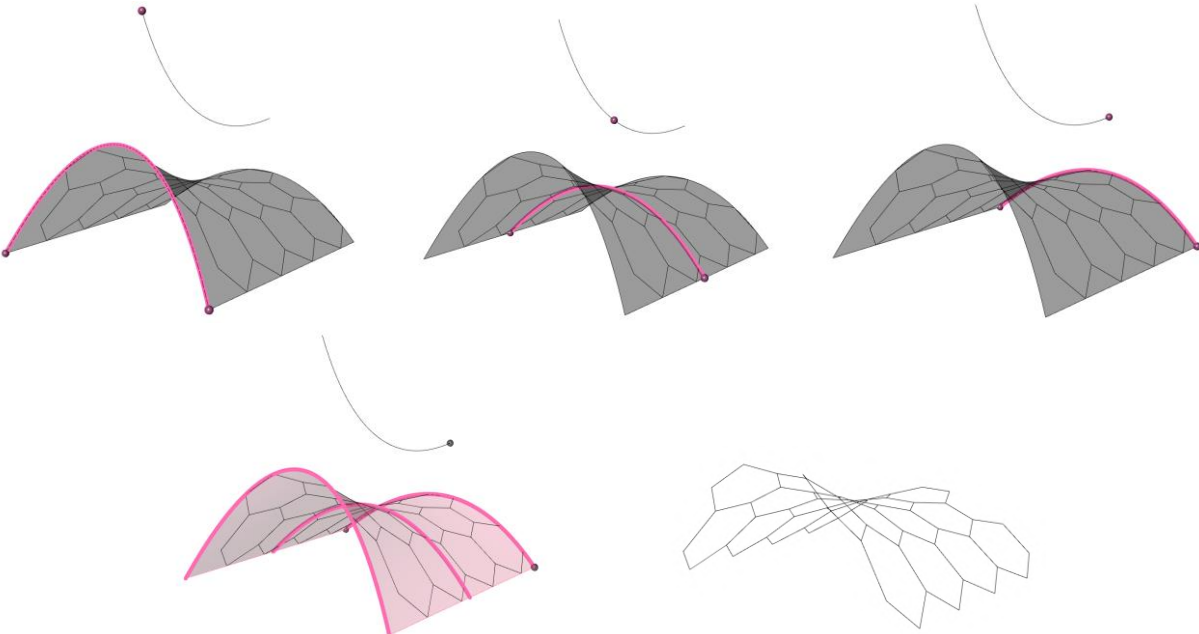


Figure 32. 3 NURBS curves forming hexagonal grid surface

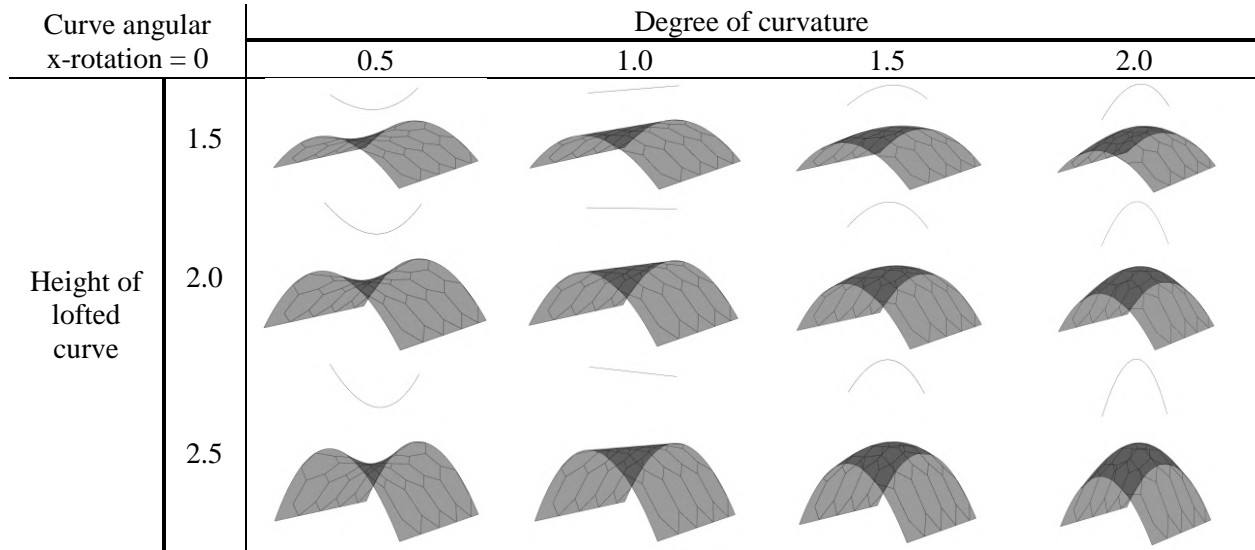


Figure 33. Height of lofted curve vs. degree of curvature geometry representation with constant curve angular x-rotation

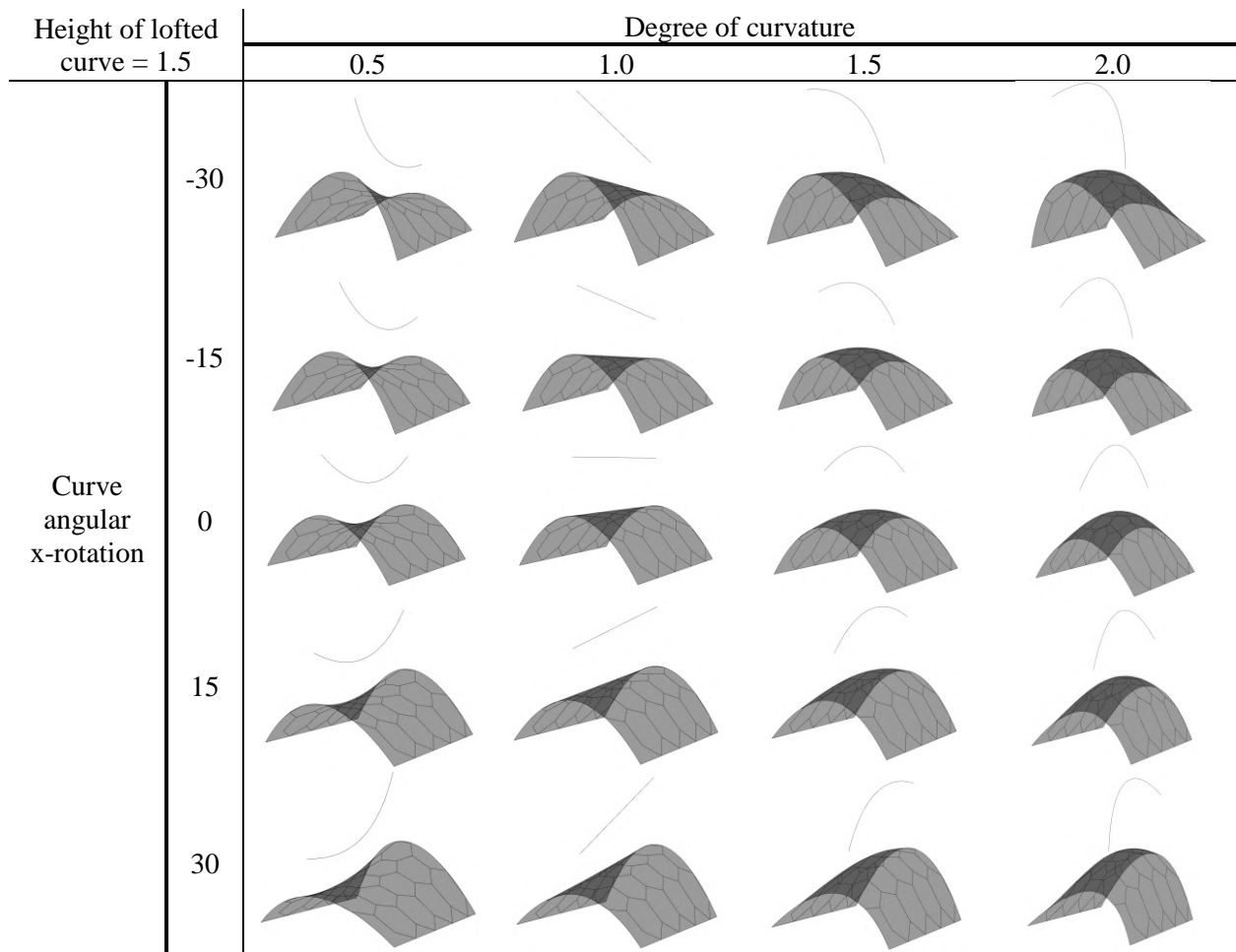


Figure 34. Curve angular x-rotation vs. degree of curvature geometry representation with constant height of lofted curve

The hexagonal geometry with one control curve is optimum for a scenario in which a particular final geometry configuration is desired; there is ample geometric variation with the variable constraints which allows for analogous final geometries. Extensive sampling tests were conducted for material library sizes of 50, 100, 200, 350, and 500 tree forks and for all combinations of varying the number of hexagons in the x and y-direction ranging from 3 to 7, inclusive. This resulted in a total of 15 experiments per geometry, 5 per species for each of the material library sizes, and 25 individual geometries to test. The results of these experiments are discussed in section 2.3.3 Hexagonal geometry with 1 control curve (3 variables) results and the data is in collated Appendix B.

2.3 Results

2.3.1 Pavilion geometry with 2 control curves (4 variables) results

The matching score results for the sampling of the original pavilion geometry for 50, 100, 250, 500, 750, and 1000 samples are shown in Table 3 and graphed in Figure 35. The data shows that the ash species has a significantly better matching score for each number of samples. This can be attributed to the wider maximum angle of ash; oak and fruit have no variation in their maximum angle value and slight variation in their minimum angle value resulting in expected overlapping results. The wider angle in ash producing better matching scores may also be specific to this original pavilion structure provided. A different original structure with narrower angles may result in a different outcome, which suggests results can be highly dependent on the starting structure; further testing is suggested to validate this claim.

The point of diminishing returns at which increasing the number of samples does not improve the matching score occurs at 500 samples, which is about ten times the number of nodes on the structure. Geometries generated with greater than 100 samples are considered good matches, since the most significant improvement in matching score (15-26% decrease) occurs between 50 and 100 samples. Matching score improvements between 100-250 samples and 250-500 samples are significant with an 8-18% and 12-18% decrease, respectfully, so if the number of tree forks are available for these material library sizes, it would be preferred in a design scenario. Additionally, there is an exponential time tradeoff as the number of samples is increased; the more samples, the more time required to conduct the sampling and matching: 50, 100, and 250 samples take a couple minutes, 500 samples take about 10 minutes, 750 samples take about 20 minutes, and 1000 samples take about 30 minutes.

Table 3. Optimized pavilion geometry sampling matching score results

# of samples	Ash	Oak	Fruit
	Angles: Aver: 64 Max: 99 Min: 25	Angles: Aver: 54 Max: 86 Min: 32	Angles: Aver: 60 Max: 85 Min: 30
	Matching Score		
50	25,331	47,251	44,405
100	18,646	35,312	37,993
250	17,105	31,834	31,338
500	13,943	27,228	27,559
750	13,347	28,341	26,735
1000	13,320	26,519	26,245

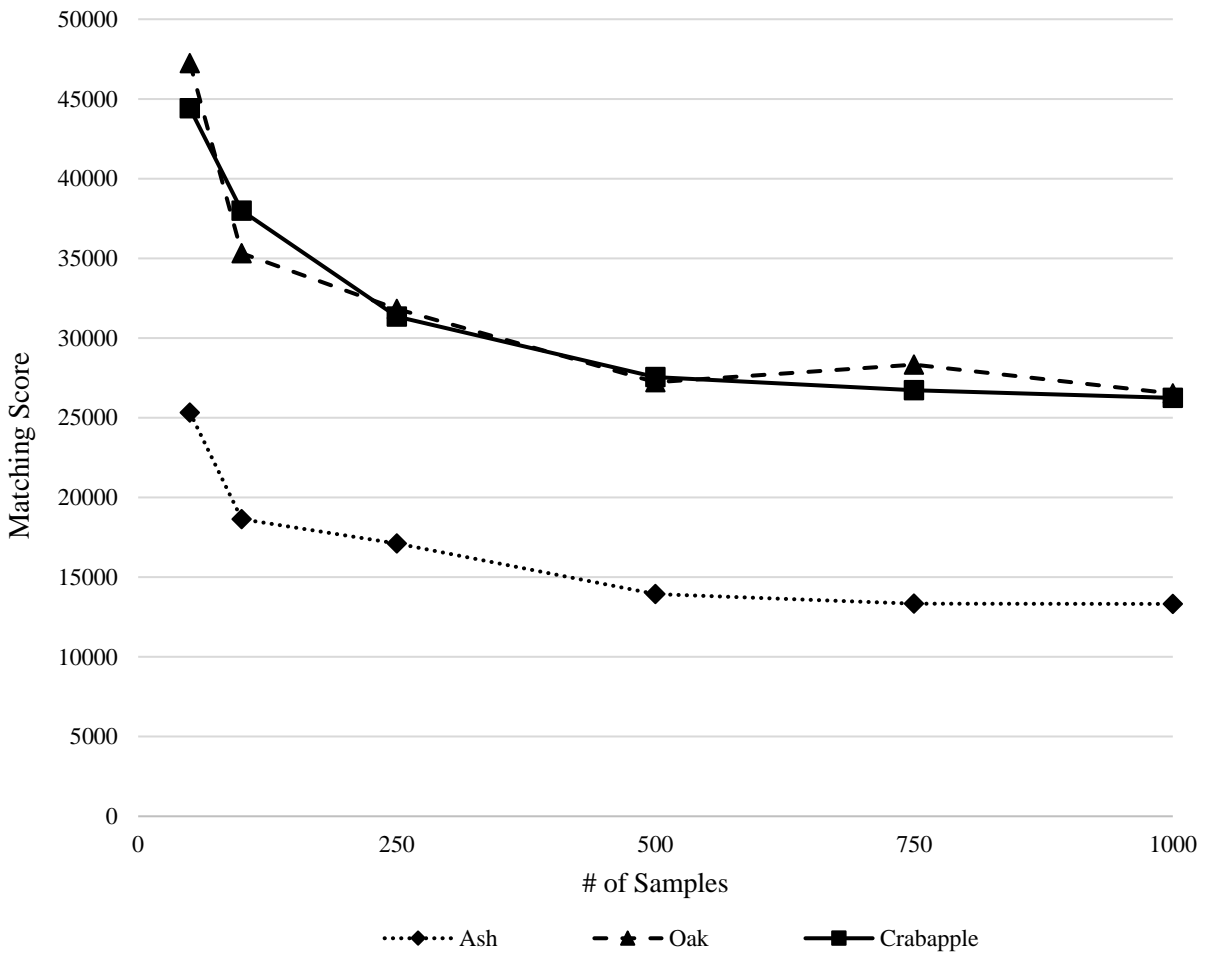


Figure 35. Original pavilion geometry Matching Score vs. # of Samples

2.3.2 Hexagonal geometry with 5 control points (5 variables) results

This hexagonal geometry was examined briefly in conjunction with the sampled tree fork libraries, but due to the structural implications of the design further testing was ceased. The pinned columns at the corner points of the surface would experience a sizeable horizontal thrust force that would be difficult to resolve with a matched tree fork member. A more comprehensive structural solution would be necessary to address this design challenge.

The advantage of this hexagonal geometry with 5 control points is that for each sampling scenario varying the number of samples and the number of hexagons in the x and y-direction, there was a considerable amount of geometric variation. This geometry manipulation with a moderate number of variables is a useful option for brainstorming potential final geometries and scenarios where no specific configuration is desired for the structure.

The conducted sampling results are collated in Appendix A for a 9'x21' surface with a projected hexagonal grid with a fixed x-direction hexagonal density of one and a varying y-direction hexagonal density ranging from two to nine. For each of the hexagonal grid geometries, material library sizes of 50, 100, 250, 350, 500, and 750 tree forks were generated and matched to the target geometry to be optimized for matching score performance. Only the ash tree species was implemented in this brief case study.

The matching score incurred an exponential decrease when the number of samples increased, as expected. An acceptable matching score was available at just 50 samples in the material library justified by the low ratio of number of structural nodes to number of tree forks as well as the high degree of variation in the geometry promoting more accurate fits to the available tree forks. Each successive iteration of the hexagonal geometry with increased samples resulted in a wide range of geometries as seen in Figure 37 obtainable due to the appreciable z-direction range of the 5 control points.

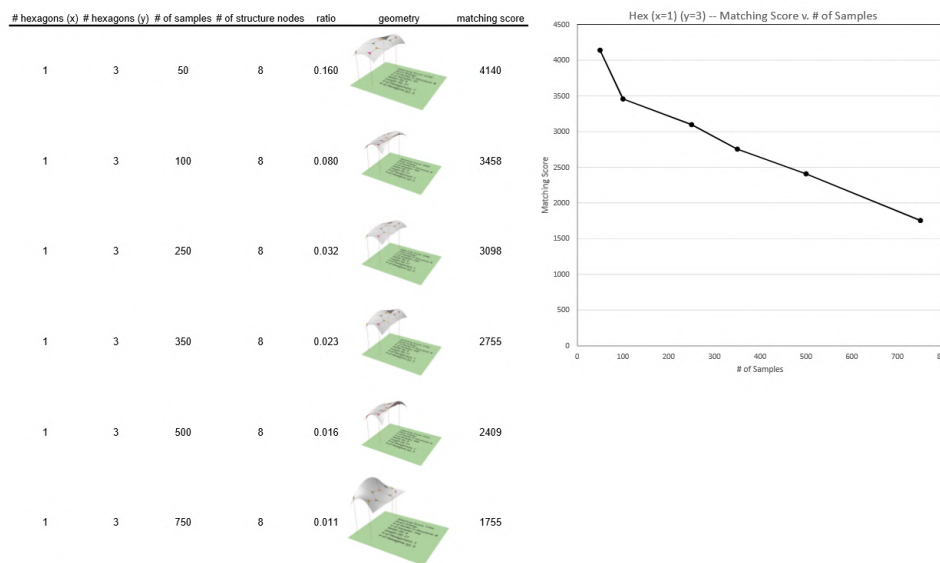


Figure 32. Hexagonal geometry with 5 control points ($x=1$) ($y=3$)

2.3.3 Hexagonal geometry with 1 control curve (3 variables) results

The results for the hexagonal geometry with 1 control curve are compiled in Appendix B for a generated sampling of 50, 100, 200, 350, and 500 samples for the ash, oak, and fruit tree species. The data collected validated the pavilion geometry results with similar results. The ash tree species performed the best for every tested geometry, and the oak and fruit trees performed nearly the same as each other. These performance results are most attributed to the range of angles available for each of the tree fork species with the ash tree species expressing the widest range and the oak and fruit tree species having nearly identical angle values. The maximum angle of the tree species and the total range are the most significant values that determine the matching quality of the tree species to the target structure.

The hexagonal geometry with 1 control curve sampling not only validated the pavilion geometry results with similar findings but allowed for increased understanding of the effects expanded upon multiple geometries for each of the three species tested. For all the geometries tested, the matching score exponentially decreased as the number of samples available in the material library increased. The point of diminishing returns for all geometries, regardless of the number of nodes in the target structure, occurred with 350 generated tree fork samples. Significant decreases in matching scores were also observed between 50 to 100 and 100 to 200 samples, which make these material library sizes of 100 or 200 tree forks viable options depending on the availability of material for the target structure project.

To compare the performances of each of the geometries tested for each tree species matched, the ratio of the number of structural nodes to the number tree fork samples was calculated and graphed with the corresponding matching scores as seen in Appendix C and Figure 36. The ratio of structural nodes to the number of available samples are displayed on a logarithmic scale to more clearly view the diminishing returns of the matching score as the ratio decreases. An optimal tree fork matching geometry would have a high ratio of structural nodes to available tree forks and a low matching score. The higher the ratio, the less need to have a disproportionate material library for the target structure proposed, and the lower the matching score, the better the tree forks match to the structural nodes. For the ash, oak, and fruit tree species, the worst performing geometries tended to be those that had a higher x-direction than y-direction hexagonal grid density: 3x3, 4x3, 5x3, 5x4, 6x3, 6x4, 6x5, 7x3, 7x4, 7x5, 7x6 (Figure 36). These geometries tend to have a) narrower hexagonal shapes and b) less flexibility with the control curve, that results in the higher matching score.

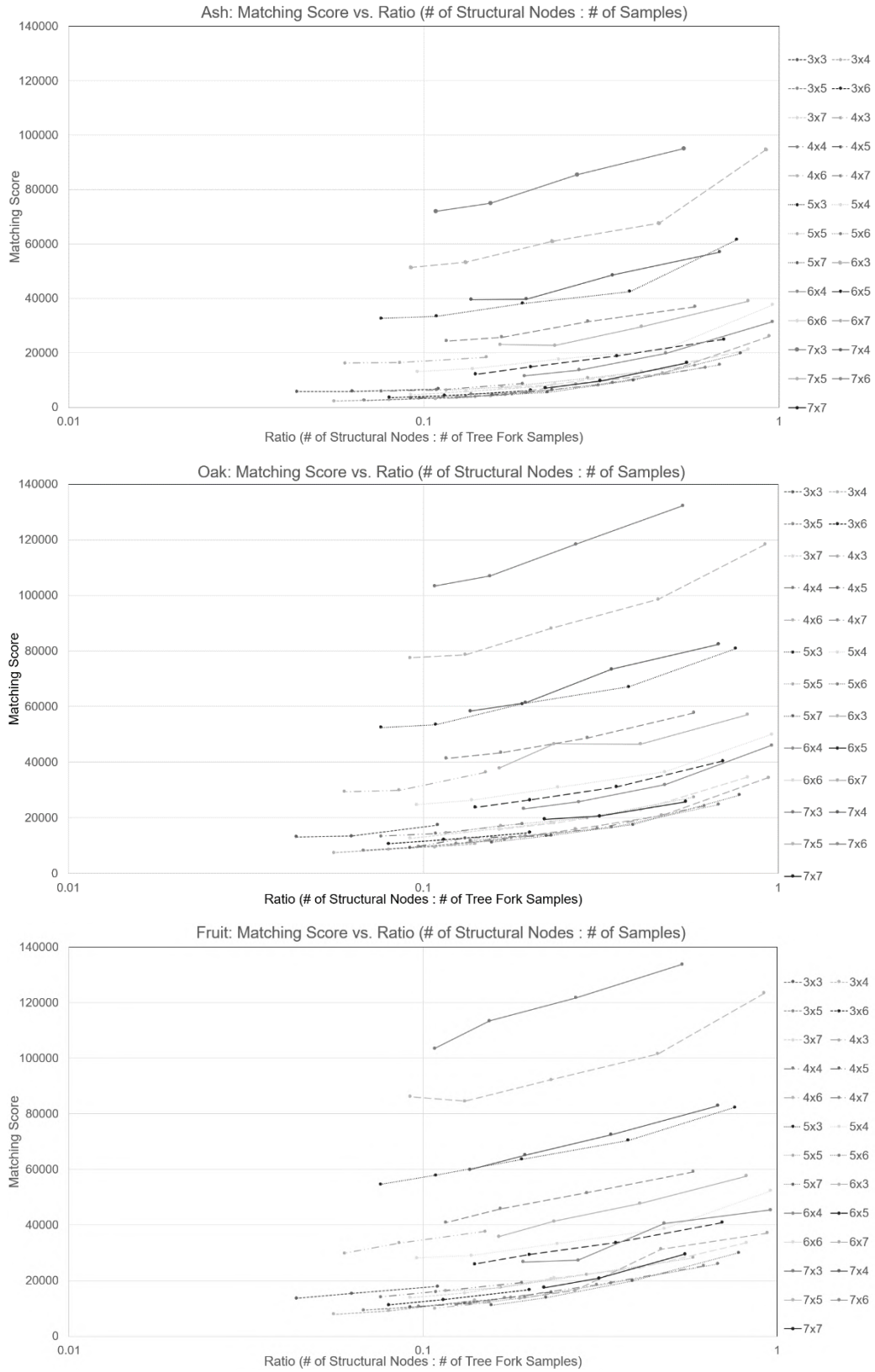


Figure 36. Matching score vs. Ratio (# of Structural Nodes : # of Samples). Worst performing geometries shown with bold lines: 3x3, 4x3, 5x3, 5x4, 6x3, 6x4, 6x5, 7x3, 7x4, 7x5, 7x6

The majority of the other structures tend to perform moderately similar to one another and are clustered in the bottom right corner. The best matches occur when the ratio of structural nodes to number of available tree fork samples is high and the matching score is low. Figure 37 highlights the area on the graph that have the most practical designs in which the target structure has a reasonably low matching score and material library. The lower the matching score, the better the match to the target structure. Figure 38 displays a few example geometries that are considered to be optimal matches with minimal matching scores. The geometries displayed in Figure 38 are more commonly optimized with a concave up curve (ash: 4x5, 7x7, 4x7, 5x6; oak: 4x6, 3x4, 5x6, 5x7; fruit: 4x6, 3x4, 5x6, 5x7) than a concave down curve (ash: 5x7; oak: 4x7; fruit: 4x7). This distribution of geometry results is representative of all the geometries tested; the majority of optimized structures manipulate the control curve into a concave up shape.

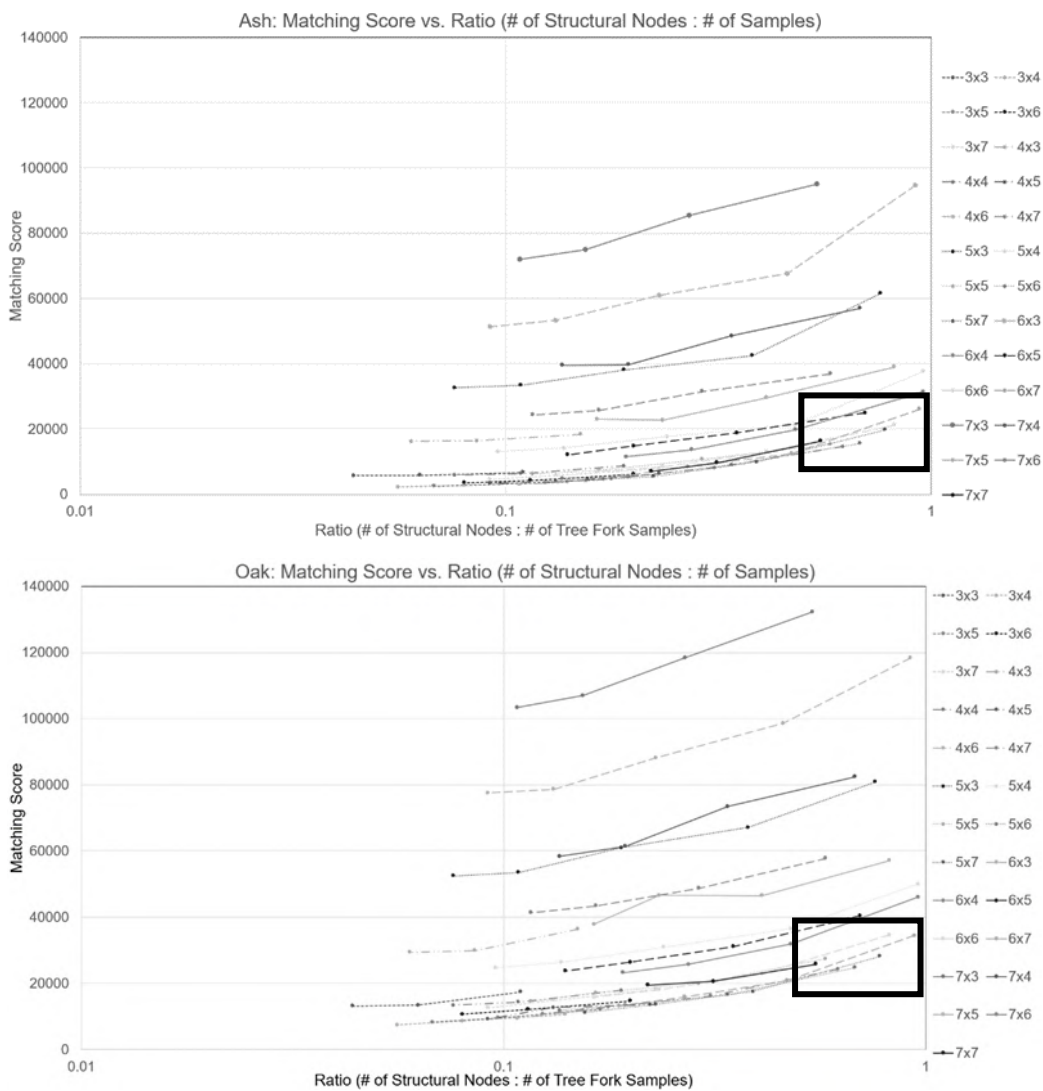


Figure 37 Boxed results represent the best matching scores for ash, oak, and fruit

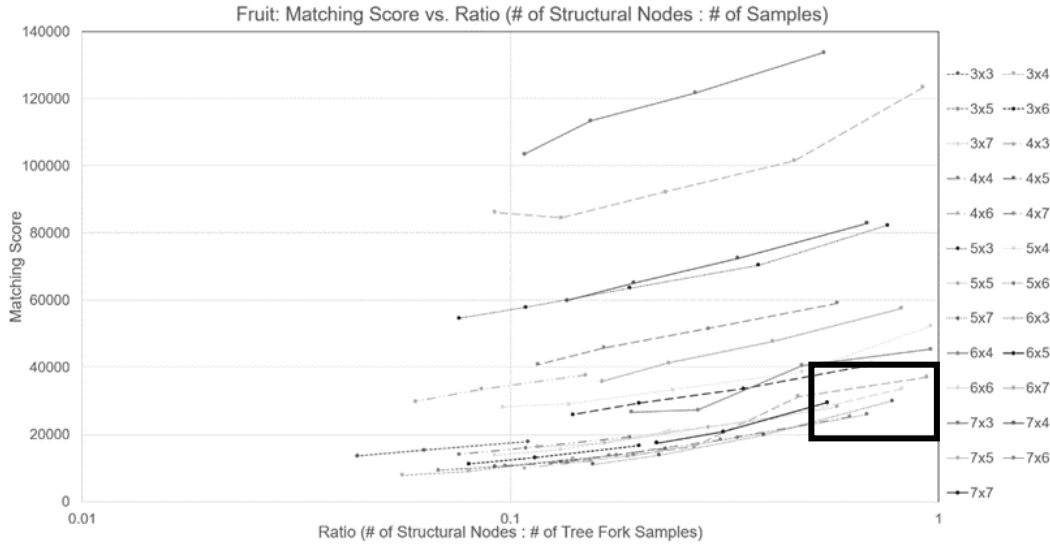


Figure 37. Boxed results represent the best matching scores for ash, oak, and fruit (cont.)

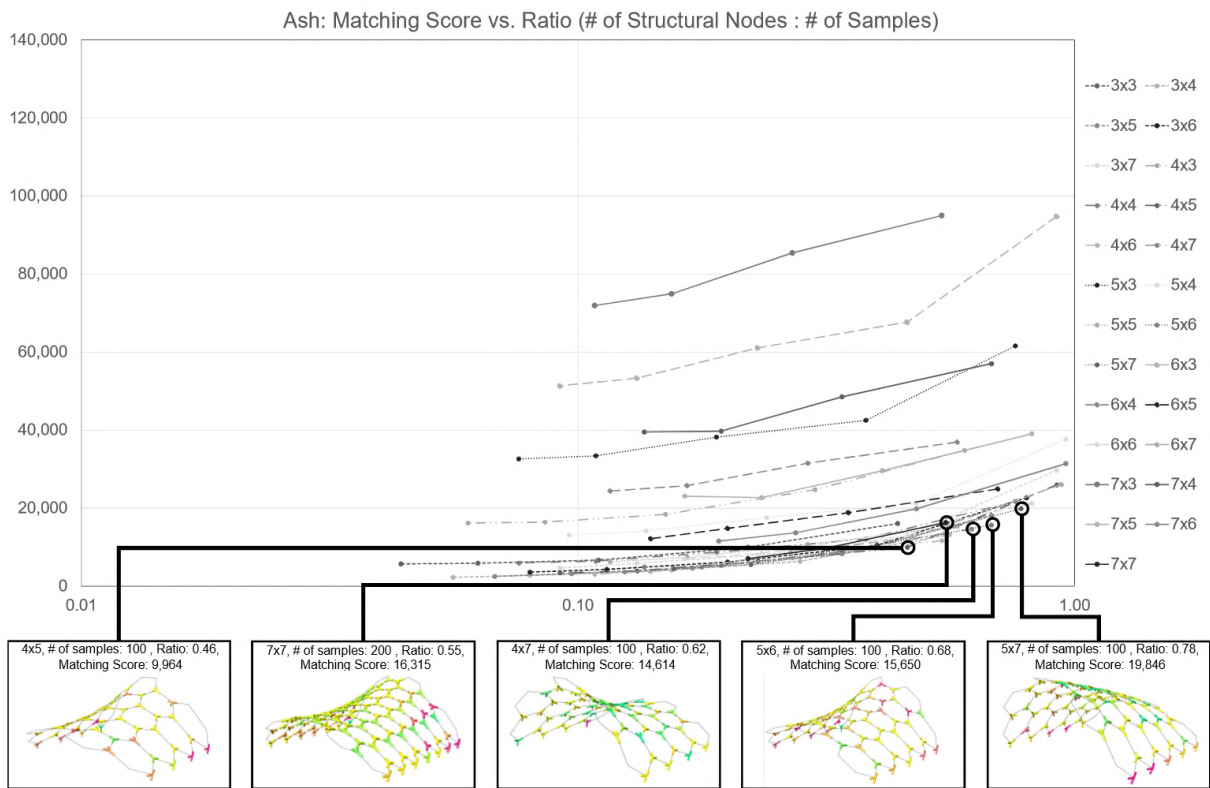


Figure 38. Example geometries for ash, oak, and fruit species that represent optimal matches

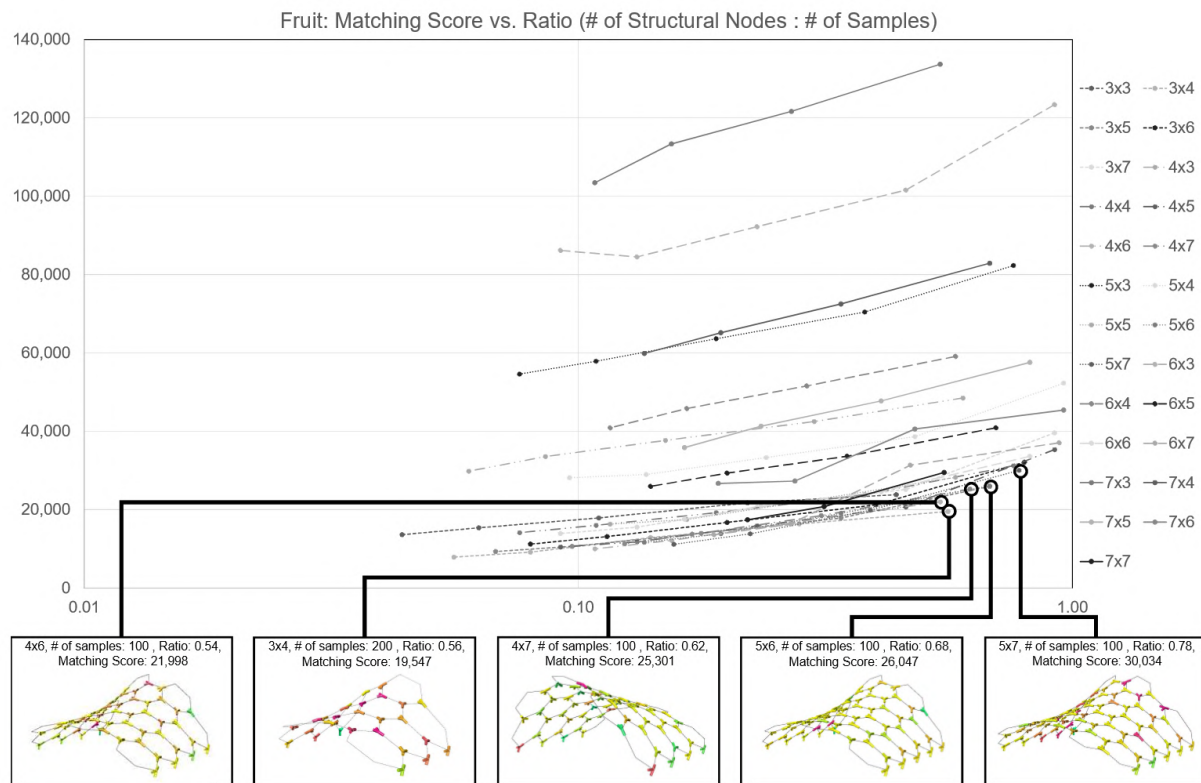
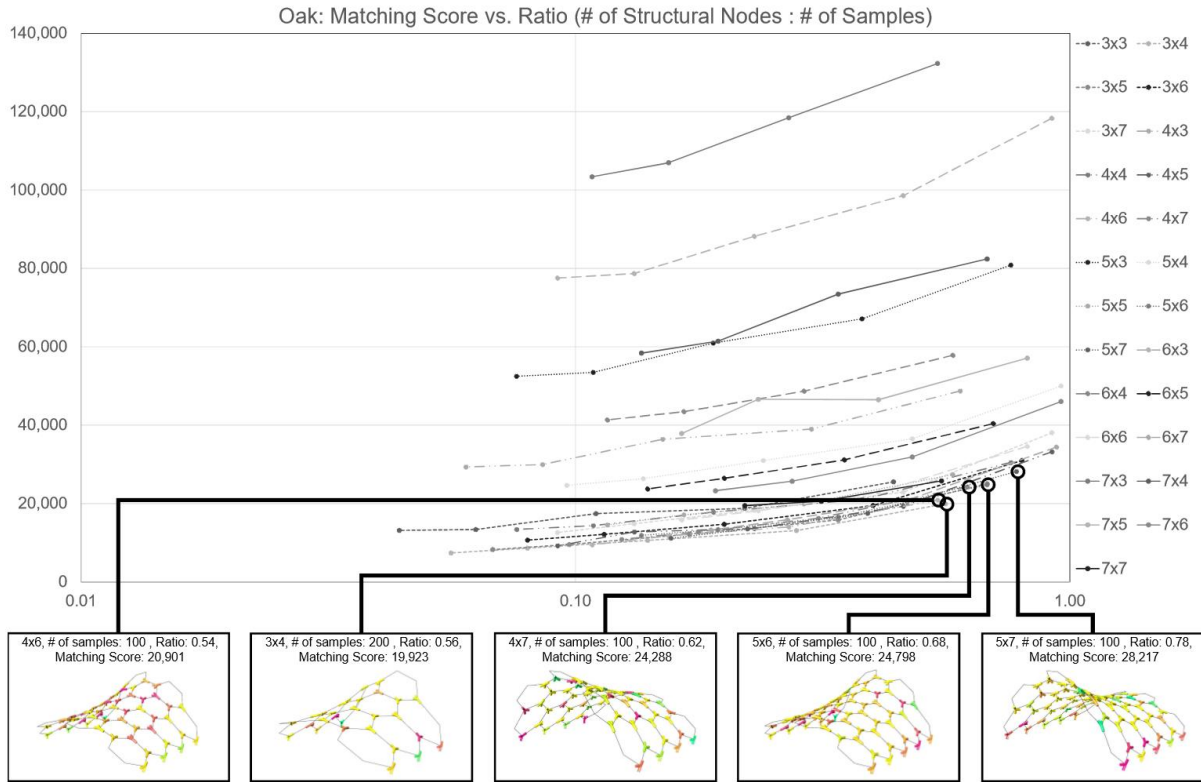


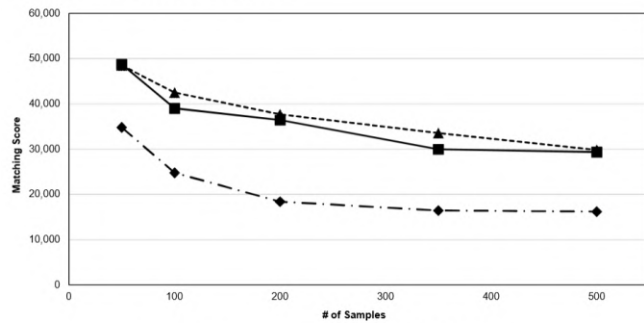
Figure 38. Example geometries for ash, oak, and fruit species that represent optimal matches (cont.)

The results for each hexagonal grid setup tend to produce mainly homogenous geometries regardless of the number of samples available in the material library or the tree species.

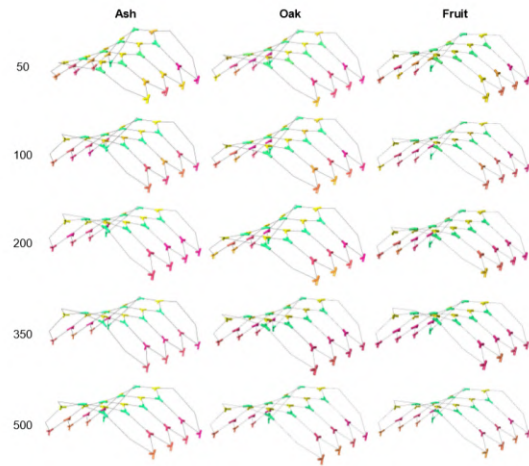
Figure 39 shows hexagonal grid densities 4x3 and 5x5 that display the consistent geometry.

Figure 40 displays an example of hexagonal grid variation 3x7 that presents more variation, but even in this case, the resulting geometries have a degree of similarity unlike the results of the hexagonal geometry with 5 control points.

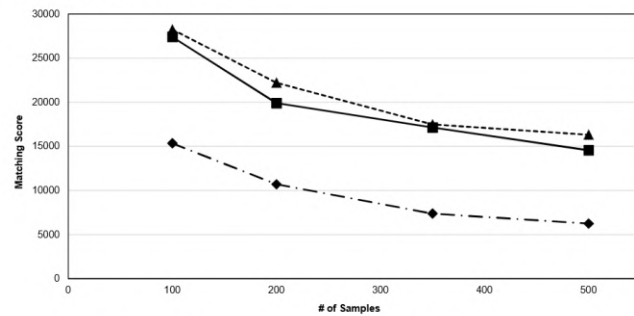
4x3: Hexagonal, 1 Control Curve



# of samples	Ratio (# structural nodes: # of samples)	Matching Score		
		Ash	Oak	Fruit
50	0.60	34,816	48,745	48,502
100	0.30	24,758	39,006	42,500
200	0.15	18,401	36,426	37,676
350	0.09	16,429	29,966	33,546
500	0.06	16,198	29,358	29,822



5x5: Hexagonal, 1 Control Curve



# of samples	Ratio (# structural nodes: # of samples)	Matching Score		
		Ash	Oak	Fruit
50	0.58	15,345	27,409	28,253
100	0.29	10,702	19,911	22,212
200	0.17	7,369	17,140	17,488
350	0.12	6,249	14,555	16,316

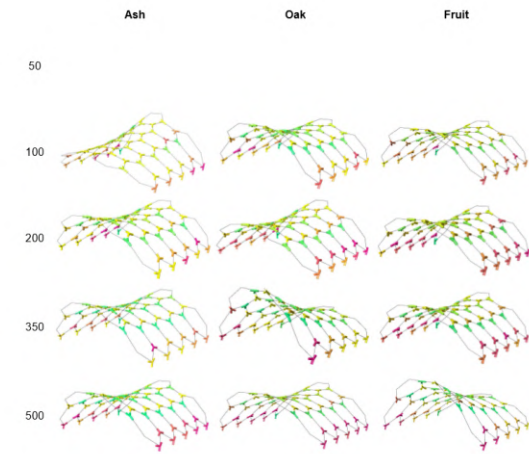


Figure 39. Hexagonal geometry with 1 control curve, 4x3 & 5x5, homogenous geometries

3x7: Hexagonal, 1 Control Curve

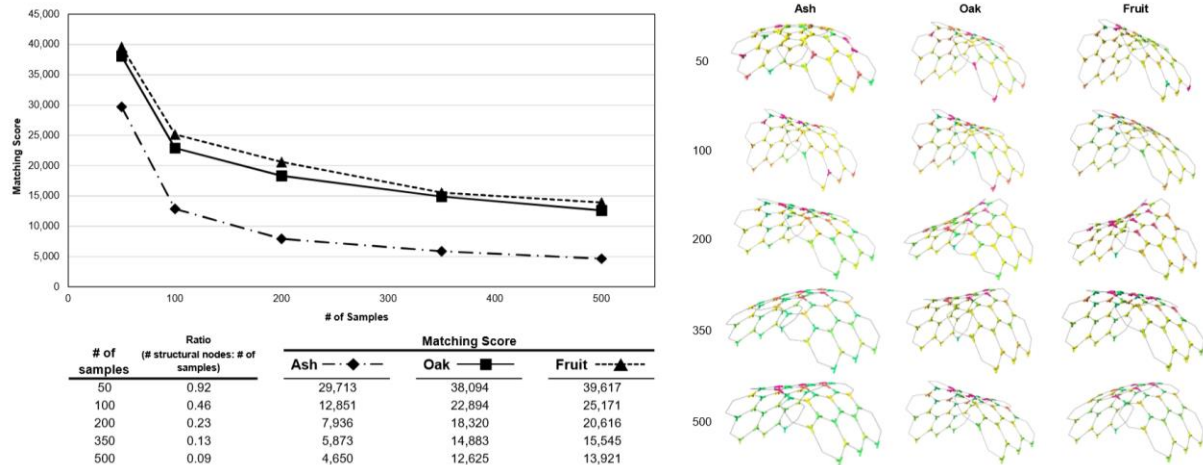


Figure 40. Hexagonal geometry with 1 control curve, 3x7, variant geometries

2.4 Discussion and conclusion

The matching-based sampling for each of the geometry case studies showed an exponential decrease in matching score as the number of tree forks in the material library increased. This proves that there is a point of diminishing returns at which the matching score does not perform better regardless of increase in available material library. An advantageous target structure would have a high ratio of available tree forks in the material library to number of nodes on the matching geometry. Based on the extensive testing conducted on the hexagonal geometry with 1 control curve by varying the densities of the x and y-direction hexagonal grid, there are certain structures that are a much better fit with lower matching scores than others. Sampling conducted for each of the three target geometries demonstrated that the ash tree species produced significantly lower matching scores than the oak or fruit tree species. This variance can be attributed to the wider branch angle between the two forking branches from the trunk. This allows for better matches between the tree forks and the three vectored nodes of a target structure. Further work for this research project includes continuing to test various geometry configurations to understand the relationship between the target structure, tree species, and matching scores.

A material library size that is twice the size of the number of nodes on the target structure is recommended for use in design. It is a realistic and feasible to assume in a design scenario that twice as many tree forks will be available to utilize in a project. Minimal material excess is projected compared to using material libraries five or ten times the number of nodes of the target structure. Twice as many nodes also provides leeway for fabrication errors, imperfections in the natural wood grain of the catalogued forks, or design modifications.

There is potential for improvement within the matching-based algorithm to address the specialized nodes of the target structure – the edge nodes along the hexagonal grid geometries that have two rather than three vectors entering a single node. This thesis omitted these nodes within the matching algorithm and sampling analyses; however, a method in which a modified two-vectored tree fork can match to these nodes is recommended to be developed in continued work.

Integrating structural capacity testing of tree forks with the matching-based algorithm would be a beneficial next step to understanding the angle of tolerance allowable between the beam element and the node vector to maintain sufficient structural capacity of the tree fork node. This recommendation is explored further in section 3.3 Structural performance computational model.

3 Structural performance of tree branch nodes

3.1 Background on tree mechanics and previous testing

3.1.1 Tree fork structural mechanics

Trees forks are highly efficient biomechanical structures of a tree; their structure allows them to continually resist gravity and wind loads as the tree matures. Their inherent structural efficiency is sought to be utilized by engineers, particularly in this thesis, through reutilization of found tree forks in a structural design.

To understand the basic reactions that occur in a naturally occurring tree fork, it is helpful to compare the structural features found in trees to those used in engineering. Tree branches can most simply be represented as a fixed-end cantilever and tree forks act as a natural moment connection resisting the bending stresses from the branch (Burgess and Pasini). Tree fork breaking strength can be calculated as being equal to the maximum bending stress measured in the branch section proximal to the fork at the moment of failure. The section modulus of a circular section with diameter d , is given by:

$$S = \frac{\pi d^3}{32} \quad (6)$$

The section modulus can be used to characterize the bending resistance of a cross section in a single value, and it can be substituted into a flexure formula to calculate the maximum bending stress in a cross section:

$$\sigma = \frac{M}{S} \quad (7)$$

The section modulus in turn can be substituted into the maximum bending stress equation to calculate the breaking strength for the tree forks:

$$\sigma = \frac{32M}{\pi d^3} \quad (8)$$

Computational models to calculate stresses along theoretical tree branches, particularly for tapered cantilever beams orientated horizontally or at an angle, have been developed by Shahbazi et al. (2015); however, these models only considered stress due to the weight of the branch with no external loads being applied at any angle to the grain or any moment capacity calculations.

3.1.2 Previous work

Several researchers have also previously tried to determine relationships to why and how tree forks fail with both conclusive and conflicting results. Branch angle and branch-trunk diameter ratio have been investigated as the main predictors for the strength of the tree forks. Buckley et al. (2015) concludes that the strength of tree bifurcations varied with their angle of inclination, while Kane et al. found no relationship between the attachment angle and strength. The relationship between branch-trunk diameter ratios and strength have been studied by Farrell (2003), Kane et al (2008), and Buckley et al. (2015), concluding that larger forces were required to pull apart narrow branches attached to a thicker trunk, forks that have relatively similar diameter for each branch were the weakest, and branches with larger diameters had lower breaking stresses.

Physical testing has been carried out by Özden, et al. (2017) on hazel trees and Farrell on maple, oak, and pear trees to understand the potential failure mechanisms and quantify the stress at failure of the tree forks. One area in particular that presents a weak point is the apex of bifurcation between the branch and main trunk. Thus, it can be inferred that these bifurcation points when exposed to large stresses can result in splitting and failure.

3.1.3 Breaking modes and characteristics

There are three main breaking modes for failures observed in tree forks: flat surface, imbedded branch, and ball-in-socket. Each of these failure modes demonstrate the significant impact the grain pattern of a tree fork has on the behavior of tree forks. Understanding the characteristics of each tree species and the tree forks in the material library is essential to utilization in structural design. Flat surface failures occur when the tree fork breaks parallel to the trunk grain and the trunk splits roughly in half, imbedded-branch failures are similar to flat-surface but rather than splitting down the middle, the trunk branch broke out leaving a groove in the trunk, and the ball-in-socket failure is highly correlated to the branch location and occurs when slowly pulled apart (Figure 41). Farrell (2003) discovered that the breaking mode observed is highly correlated to diameter ratio calculated by dividing the branch diameter of the smaller stem by the trunk diameter of the larger stem; ball-in-socket failures are most common for ratios between 0.2-0.67, imbedded

branch failures tend to occur for diameter ratios between 0.67-0.89, and flat-surface failures happen for diameter ratios between 0.8-1.0 (49).

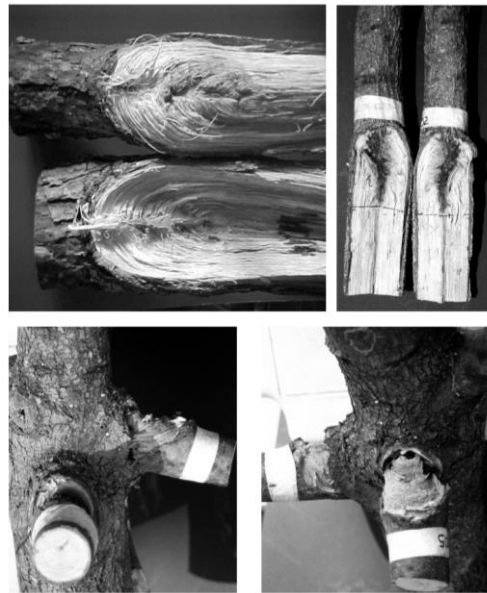


Figure 41. Breaking modes: flat-surface (top right), imbedded-branch (top left), and ball-in-socket (bottom) (Farrell 2003, 37)

To use the tree forks as a natural connection in structural engineering, it is essential to understand their behavior under various loading conditions and characterize the mechanical properties. In previous work, structural testing studies have worked to characterize the failure breaking modes (Farrell 2003), effect of branching angles on strength (Matteck and Kubler 1997), or bending strength based on tensile tests (Özden et al. 2017). There is a gap in knowledge for understanding how tree forks behave when loaded at various angles not strictly parallel or perpendicular to the grain; a distinctive bending moment and shear reaction is expected and desired to be characterized. The physical testing conducted in this thesis aims to increase the understanding of the failure mechanisms of natural tree forks as well as quantify their structural performance for use in design.

The moisture content also has substantial effects on the failure characteristics as well as the stiffness and strength of tree fork specimens. Performance differences between wet (green) and dry (12% moisture content) tree forks are attributed to their changed molecular composition. Within wet timber, the molecular cells are filled with water, which dramatically softens the cell walls and promotes hydrogen bonds between cellulose and water rather than cellulose and cellulose. The cellulose-water hydrogen bonds soften the internal microfibrils making it easier to stretch the wood fibers as well as decrease the stiffness of the wood. This relationship is shown in Figure 42.

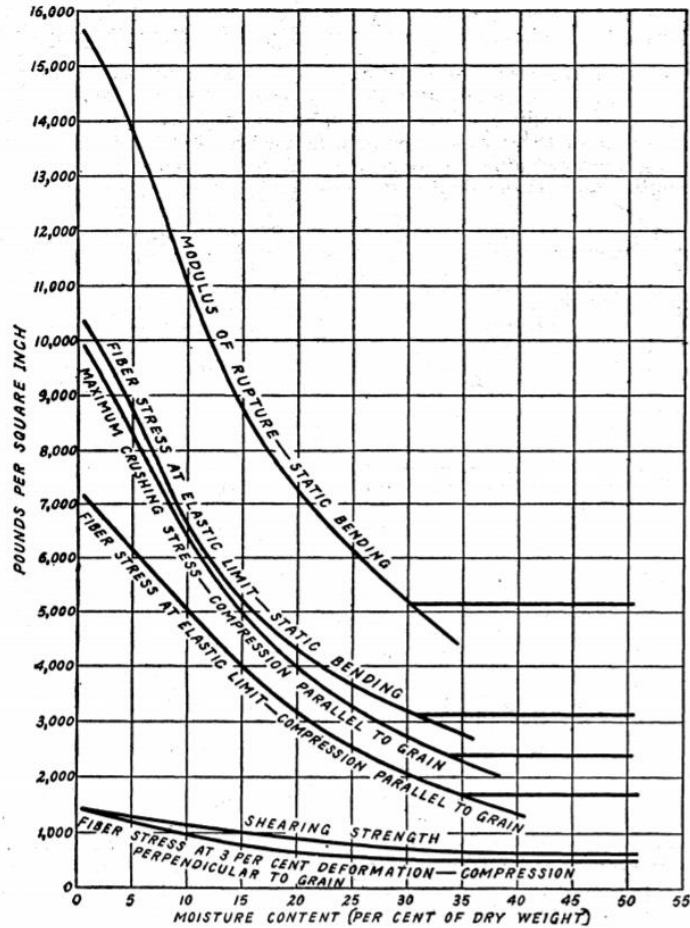


Figure 42. Typical moisture-strength properties of a red spruce (Wilson 1932)

3.2 Physical load tests

Physical load testing was conducted on tree fork specimens to understand and characterize the load capacity, force flow, and fracture properties that occur in these natural joints that are available material library.

3.2.1 Pre-processing of tree forks

Since natural tree bifurcations grow naturally based on environmental conditions, each fork has an inimitable three-dimensionality. Considerations must be taken for a) the tree branch vectors not contained on center xy-plane, b) the curvature of the main trunk that must sit flat on the testing table, and c) the loading surface on the branch that the machine will come in contact with that must be parallel to the testing table. These requirements necessitated pre-processing of the tree fork specimens in order to safely test them on a standard load compression machine in the Pierce laboratory. The fabrication process, and the resulting tree fork joint, can be seen in Figure 43. a) Brep of tree scan, b) plane top/bottom, c) Prototrak top/bottom flat, d) plane 3rd edge, e) Joiner 3rd edge flat (Figure 43).

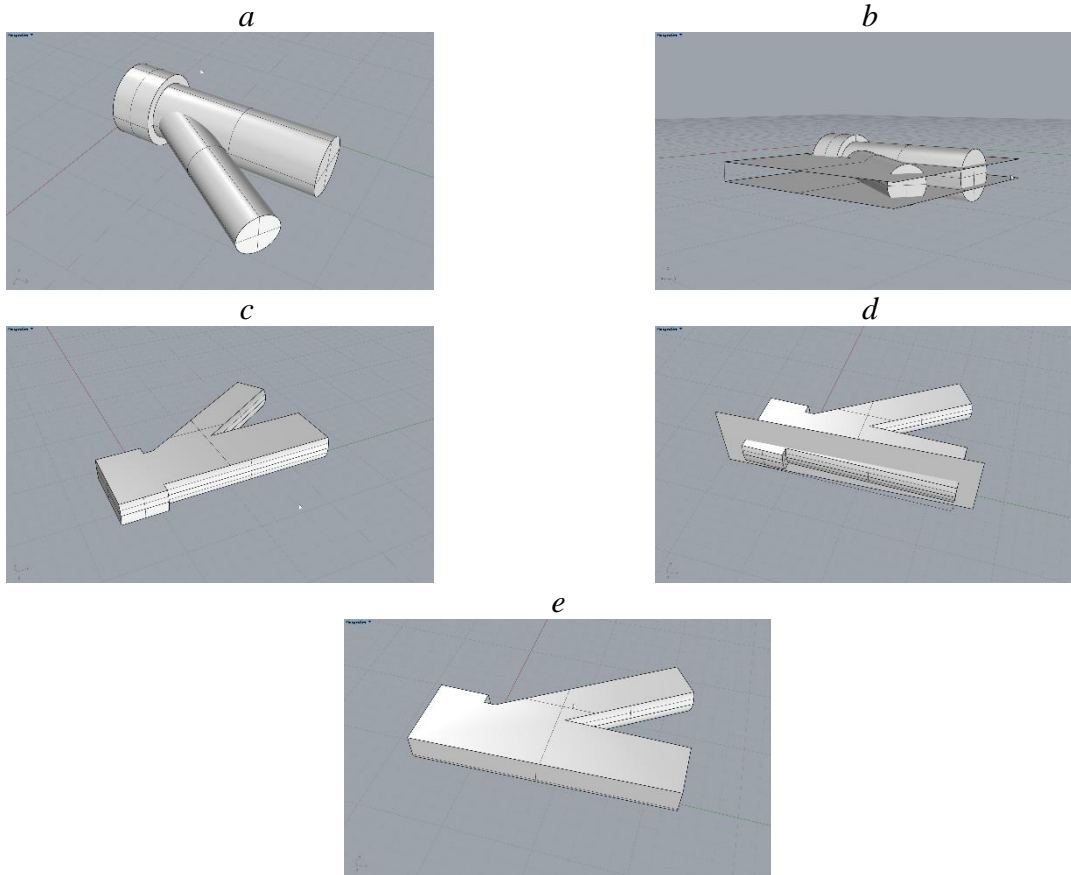


Figure 43. a) Brep of tree scan, b) plane top/bottom, c) Prototrak top/bottom flat, d) plane 3rd edge, e) Joiner 3rd edge flat

The first step was to assess the tree fork and understand the potential cuts and machines necessary to plane the fork; this was required each time due to the high variability in every tree fork. Figures 5b and 5c demonstrate how a Prototrak machine was used to flatten the top and bottom of the tree fork to a consistent xy-plane. Figure 5d and 5e show how a Joiner machine was used to flatten the trunk branch to allow for it to sit sturdily on the flat testing bed. Figure 5f demonstrates how a bandsaw was used to create a surface parallel to the surface in 5e. The processed tree forks are shown in Figure 44 and Figure 45.



Figure 44. Fruit tree pre-processed fork

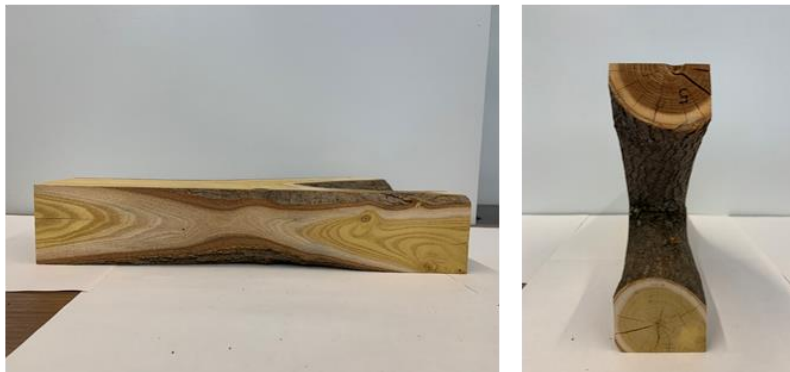


Figure 45. Ash tree pre-processed fork

Additionally a control test specimen in the shape of a 2” from the tree branch was milled into a 2” cube to be tested alongside the fork to gather general properties of the wood as seen in Figure 46 and Figure 47.



Figure 46. Fruit tree control cube



Figure 47. Ash tree control cube

It is important to also note the moisture content of the wood before testing, since specimens with a higher moisture content are more flexible, while less drier specimens are more brittle. The fruit tree was taken from open-air, outdoor conditions and tested with days and had a 100% moisture content (green), and the ash tree was taken from a specimen air-drying indoors for about a year with a moisture content of 15% (analyzed as 12% as seen in the Wood Handbook).

The fruit tree will be evaluated as a cherry tree, because it qualitatively has the most similar bark and grain features and is the most similar to a commonly found crabapple tree from the original site.

3.2.2 Testing

All load testing was executed in the Pierce laboratory at the Massachusetts Institute of Technology under the direction of Stephen Rudolph. A 60,000 lb INSTRON hydraulic compression machine was used to apply a point load to the angled branch to incite a moment reaction in the center of the tree fork node as seen in Figure 48. Load continued to be applied until there was a failure in the tree fork or the load reached a plateau.

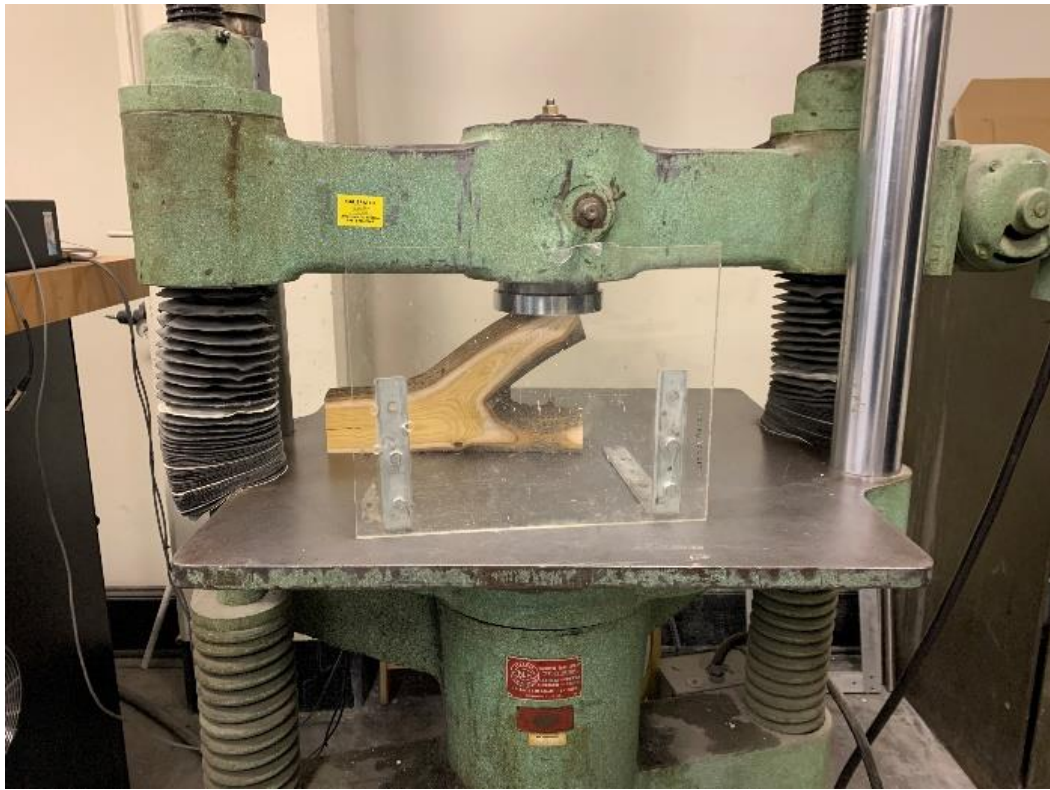


Figure 48. Fruit (top) and ash (bottom) tree fork setup – planed top forks sits at the center of the compression

The control cubes with a strain attached were tested on the 60,000 lb INSTRON hydraulic compression machine as well (Figure 49). These cubes were tested to determine the compression parallel to the grain, $\sigma_{\text{comp},\parallel}$, and the modulus of elasticity, E , of the wood.



Figure 49. Cube setup -- strain gauge attached

3.2.3 Results

The results of these experiments were initially unexpected, but with further structural analysis, the tree fork failure demonstrated a predictable behavior. In both specimens tested, a tensile failure at the back trunk-branch (non-forked member) was observed.

The fruit tree demonstrated more flexible bending in the branch and node resulting in a more gradual failure as seen in Figure 50, Figure 52, and Figure 53. Sounds of cracking were heard before any visual signs of splitting were seen on the branch, which insinuates the members within the branch were breaking from inside out. The force at failure of the fruit tree fork was 10,170 lb. This maximum force occurred when the angled branch compressed onto the bottom branch on the table as seen in Figure 12. Continued loading after this point resulted in minimal displacement as seen in the graph below due to the load being applied perpendicular to the grain of two stacked branches. The control cube when tested for stress of compression parallel to the grain, $\sigma_{\text{comp},\parallel} = 3030 \text{ lb/in}^2$ and the modulus of elasticity, $E = 7.27 \times 10^5 \text{ psi}$. When compared to values in the Wood Handbook, the compression parallel to the grain, $\sigma_{\text{comp},\parallel} = 3540 \text{ lb/in}^2$ and the modulus of elasticity, $E = 1.31 \times 10^6$.



Figure 50. Cracking (top: fruit) and splitting (bottom: ash) in the non-forked branch



Figure 51. Fruit tree post-testing

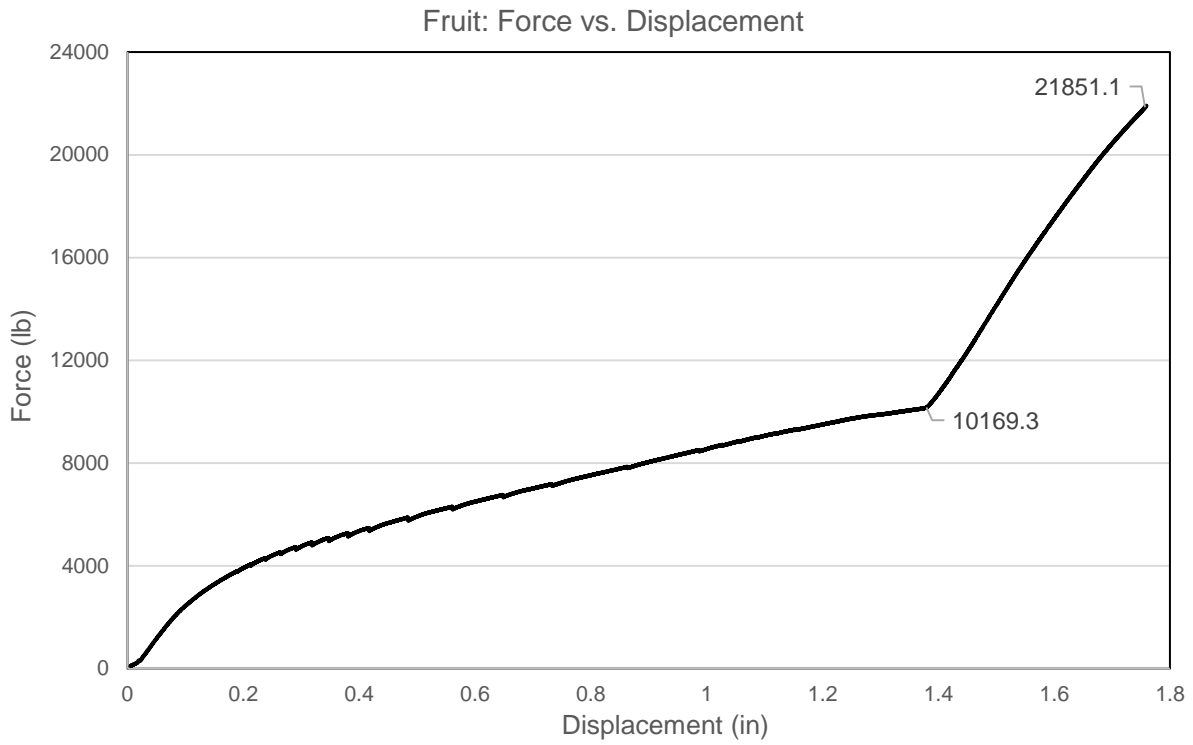


Figure 52. Fruit tree fork testing results: Force vs. Displacement

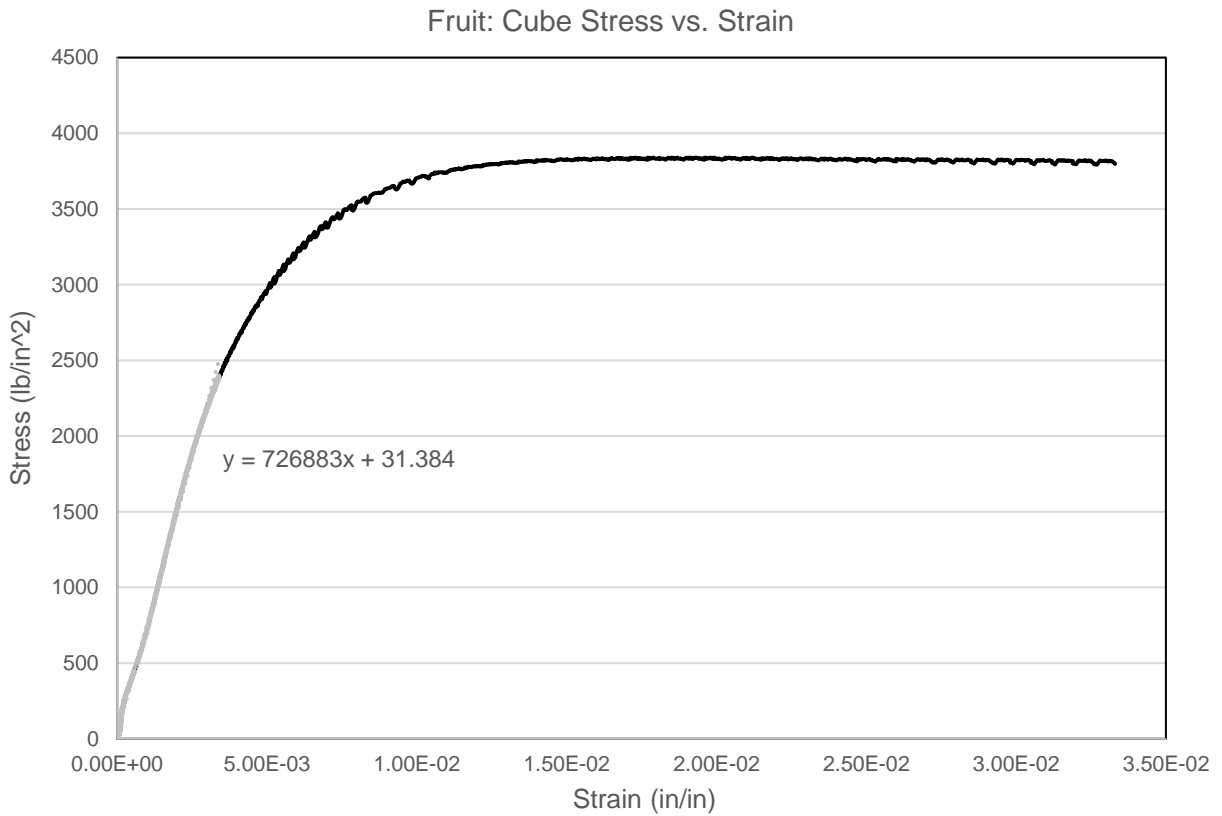


Figure 53. Fruit tree cube testing results: Stress vs. Strain

Post-testing, the fruit tree fork displayed some inelastic bending resulting in a deformed fork. There was a large amount of compression at the apex of the bifurcation as seen by the crushing of the bark on the outside. It was also shown that the plane milled that the force was applied on top of should be a smaller surface area if possible, because it would allow the branch to exhibit more bending action in the node rather than a compression perpendicular to the grain.

The ash tree fork had a more sudden failure; the non-forking member split open quickly after the first crack as seen in Figure 54, Figure 55, and Figure 56. The maximum force at failure occurred at 9,100 pounds of force. The control cube when tested for stress of compression parallel to the grain, $\sigma_{\text{comp},\parallel} = 6480 \text{ lb/in}^2$ and the modulus of elasticity, $E = 8.75 \times 10^6 \text{ psi}$. When compared to values in the Wood Handbook, the compression parallel to the grain, $\sigma_{\text{comp},\parallel} = 7080 \text{ lb/in}^2$ and the modulus of elasticity, $E = 1.66 \times 10^6$.



Figure 54. Ash tree post-testing

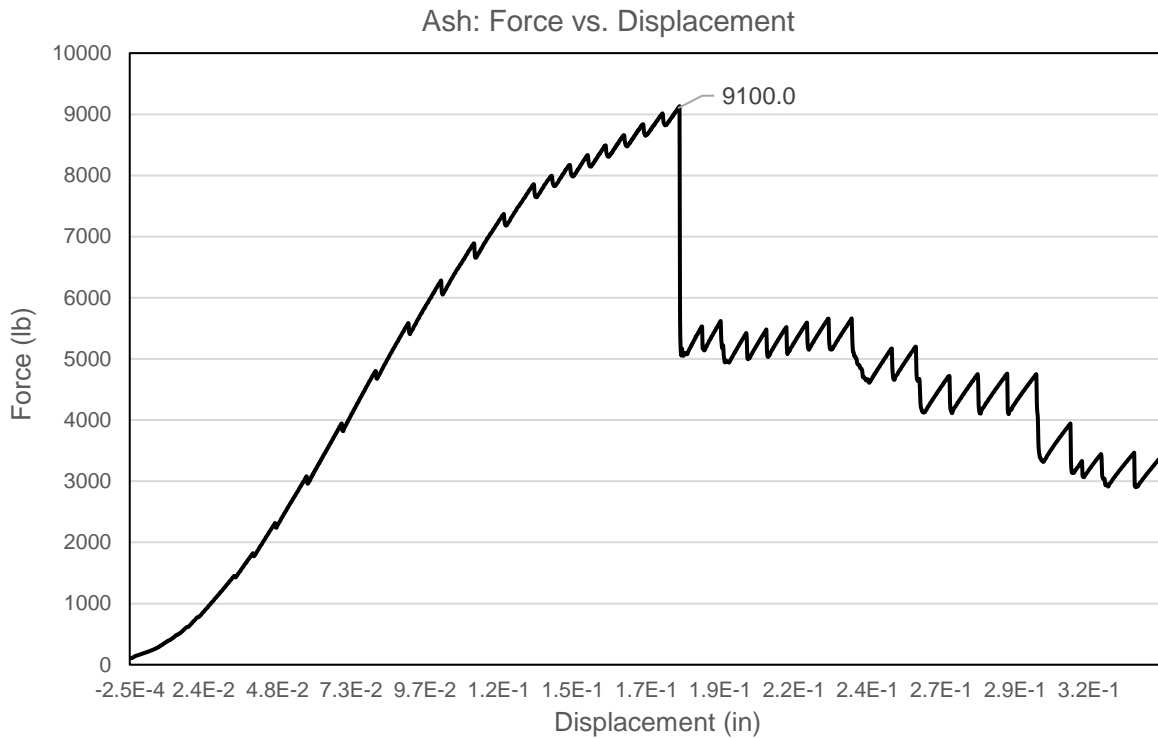


Figure 55. Ash tree fork testing results: Force vs. Displacement

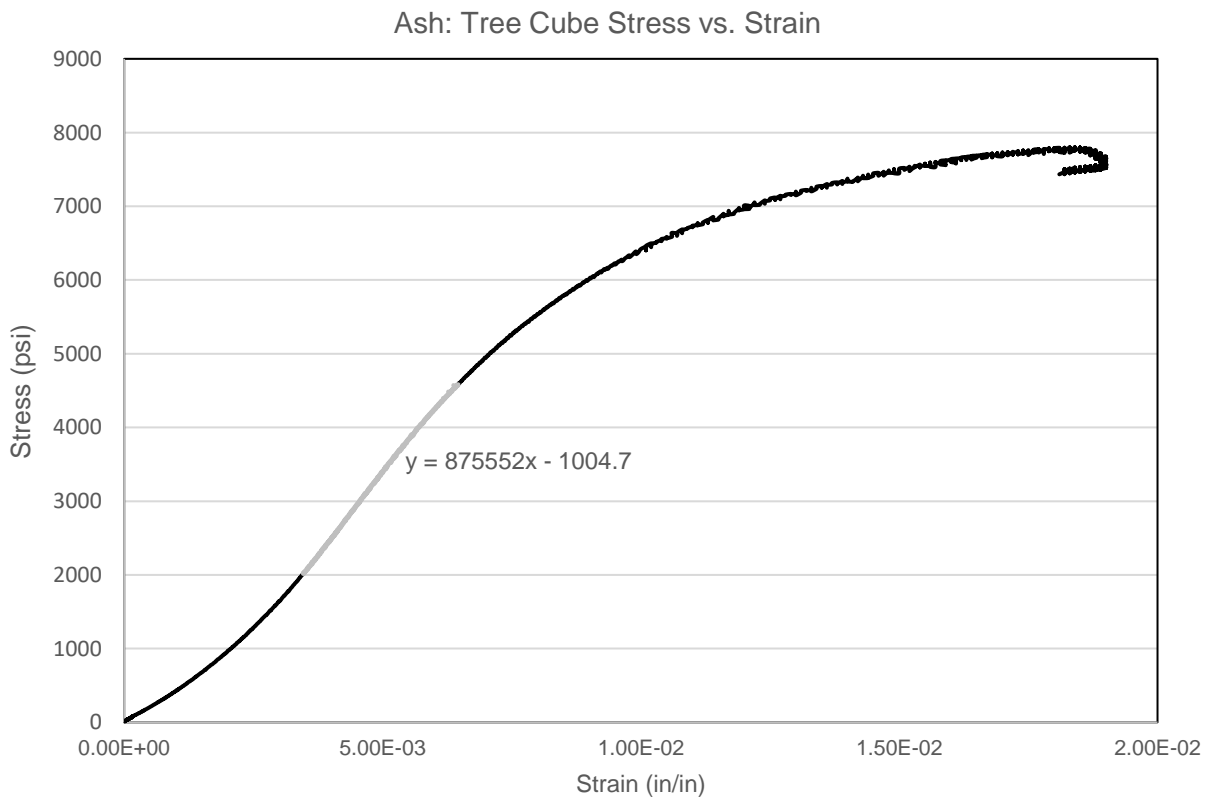


Figure 56. Ash tree cube testing results: Stress vs. Strain

The testing of the ash tree resulted in a complete splitting of the fork into two pieces. The failure behavior resembles an imbedded branch failure; the tree fork split off center from the middle and left a groove in trunk with fibers from the trunk still intact (Figure 54). The more dramatic failure can be attributed to the moisture content of the branch compared to that of the fruit tree; the ash tree had a moisture content of 12%, while the fruit tree was green and had a moisture content of 100%. The higher the moisture content, the more flexible the timber element (Figure 42); the lower the moisture content, the more brittle the failure.

A comparison between the tested and theoretical values of the compression parallel to the grain, $\sigma_{comp,||}$, and modulus of elasticity, E , results of the fruit and ash tree are shown in Table 4. The Wood Handbook is a comprehensive resource that presents properties of wood and summarizes wood as an engineering material; the strength property values given represent average values taken from extensive sampling and testing of each tree species category. The compression parallel to the grain and modulus of elasticity are found in Table 5-3b. within the Wood Handbook. The actual and theoretical compression parallel to the grain of both the fruit and ash tree species are statistically similar within 15% of each other. This substantiates the usage of the compression parallel to the grain values found in the Wood Handbook for structural calculations. Further testing is recommended with the available material library to validate this conclusion, but appreciable merit is assumed so the computational analysis conducted in section 3.3 Structural performance computational model, uses the values from the Wood Handbook. The considerable percent difference between the actual and theoretical modulus of elasticities for both the fruit and ash tree species can be attributed to a structural testing fault with pre-processing the 2” cube. The machines utilized for milling the cube, though accurate, were not as precise as necessary for the strain gauge control test. The cube’s top side and bottom side proved not to be exactly parallel to one another causing unbalanced loading on the surface, which resulted in lower than expected modulus of elasticity values. Future specimens should be ensured to be perfectly parallel before testing.

Table 4. Percent difference between structural testing and Wood Handbook of $\sigma_{comp,||}$ & E

	$\sigma_{comp, }$, actual	$\sigma_{comp, }$, theoretical	% difference	E , actual	E , theoretical	% difference
Fruit	3030 lb/in ²	3540 lb/in ²	15.5%	7.27 x 10 ⁵ psi	1.31 x 10 ⁶ psi	57.2%
Ash	6480 lb/in ²	7080 lb/in ²	8.8%	8.75 x 10 ⁵ psi	1.66 x 10 ⁶ psi	61.9%

Both of the tree forks tested experienced a tensile failure at the main trunk branch rather than moment induced failure at the compaction zone. This failure mechanism should be expected in hindsight due to the loading conditions and constraints applied to the tree fork during testing. The compression force applied to the top surface of the angled branch experiences an opposite, parallel reaction force directly underneath on the testing table surface. This force couple not only acts as a stabilizing agent to keep the tree fork steady on the testing apparatus, but also generates forces within the main trunk branch of the tree fork. For this thesis, the main trunk was not restrained, since it was postured the moment capacity of the structural joint. Therefore, the compressive force on the angled branch induced a tensile, uplift force in the back half, main trunk portion of the tree fork resulting in splitting.

3.2.4 Computational model of behavior

A computational prototype of the tree fork was modeled in Rhino and Grasshopper to visually demonstrate the tensile failure behavior observed during the structural capacity testing and the consequential splitting. Theoretical reasoning explained in section 3.2.3 Results of the tree fork testing model postulates the observed tree fork behavior during testing.

Within Rhino, an elevation view of the tree fork was input as a reference for the geometry inputs of the Grasshopper model. The perimeter of the tree fork was outlined to generate closed surface area to be meshed as a timber material, the top edge line was divided into points to apply negative vertical forces, and the bottom edge was divided into points to represent supports along the testing apparatus table. The mesh was implemented in Karamba through the *Mesh Breps* and *Mesh to Shell* elements with the perimeter outline, top edge line, and bottom edge line as inputs; images of the generated mesh and the points of the mesh are shown in Figure 57. During assembly, the modelled shell was given the isotropic material properties of wood.

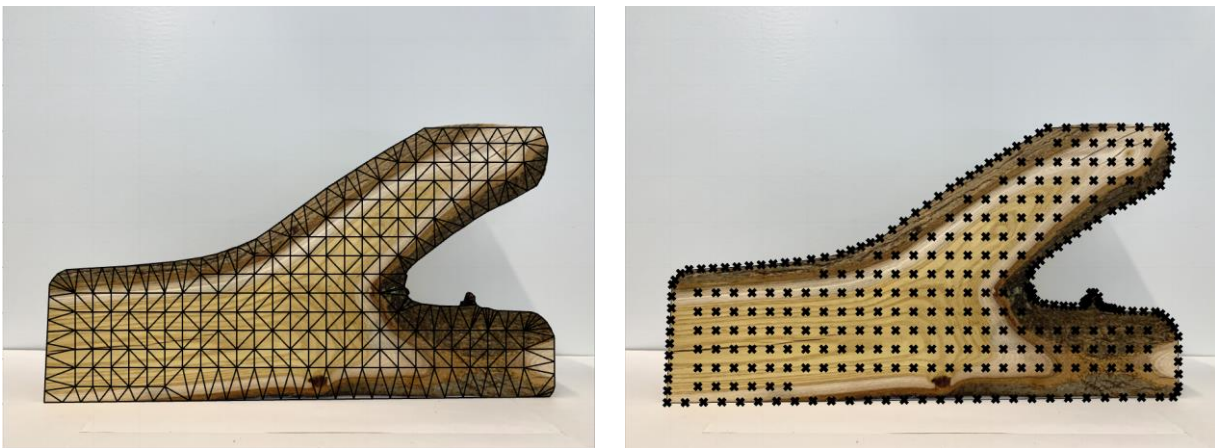


Figure 57. Tree fork computational model mesh and point

The supports along the bottom edge of the tree fork are all pinned supports except for the support at the very left edge which is a fixed support; this configuration is meant to replicate the behavior as if there were a constraint restricting the main trunk branch. The top edge points were assigned 1-kip negative vertical loads. The shell, material, supports, and loads are input to the *Assemble* element to generate the computational model. The *ModelView* and *ShellView* elements in Karamba visually display the resulting behavior based on the inputs of the assembly.

The *ModelView* reactions and the *ShellView* principal stresses displayed in Figure 58 characterize the behavior of the tree fork and prove the parallels between the computational model and the structural tested tree fork. The reaction forces are opposite and largest at the points along the bottom edge that are parallel to the applied compressive forces. The inferred resulting tensile uplift forces are displayed along the bottom edge points of the main trunk branch. The principal stresses of the computational model follow the observed behavior of the tested tree fork: the largest principle stresses occurred at the compaction zone which is the weakest point of the tree fork, and the principal stresses generated a circular pattern at what would be the naturally occurring center where the natural tree fork fibers meet (Figure 59).

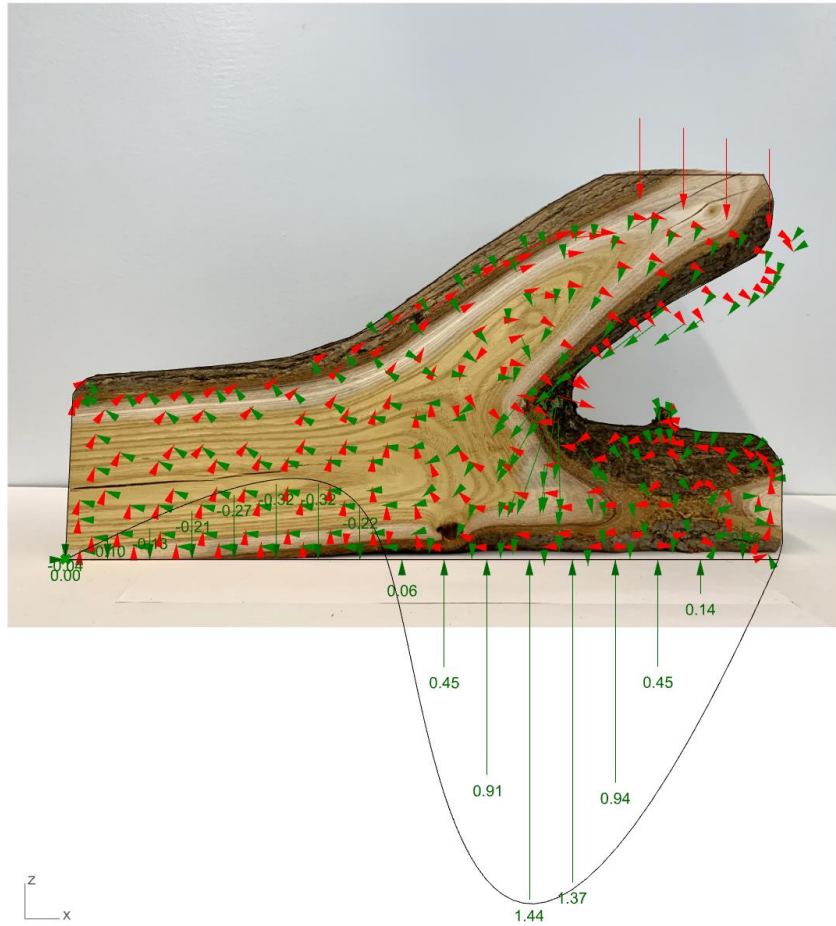


Figure 58. Tree fork computational model reactions and principal stresses

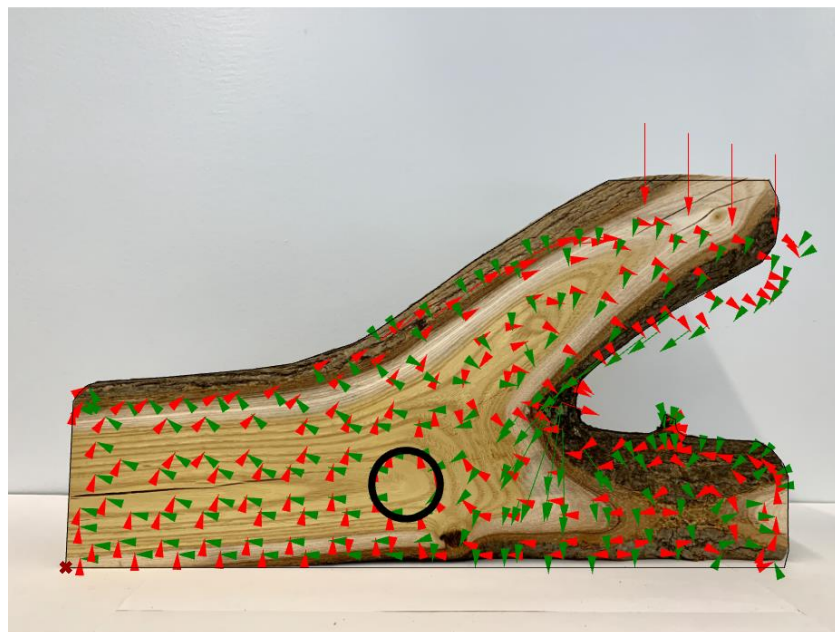


Figure 59. Modeled center corresponding to the natural fibers of the tree fork

3.3 Structural performance computational model

A method to integrate structural capacity testing of tree forks with a matching-based algorithm is explored within this thesis to a) understand the effects of different tree species on structural performance, and b) compare the resulting geometries obtained from a structural score versus matching score optimization problem. The structural score developed accounts for the angle of tolerance allowable between the beam element and the node vector to maintain sufficient structural capacity of the tree fork node and compares the strength values of the target structure nodes with those of the matched tree fork. The matching-based algorithm, Hankinson's equation, and a strength equation are utilized to develop the structural score described in 3.3.1 Design framework.

3.3.1 Design framework

The formulation of the structural score is based on the shear and moment stress to strength ratios of the target structure design values to the capacity of the matched tree forks. The shear and moment stress to strength ratios are squared and combined to quantify the capacity of the tree forks in the material library to resist the force reactions expected at the nodes of the target structure. The utility equation is inspired by a modification of the Mohr's circle equations as a method of combining stresses to quantify the distribution of shear and moment capacity within the tree fork. A conservative metric was utilized due to the high variability of the tree forks due to the idiosyncratic natural grain patterns of each fork as well as the simplification of the utility equation developed. The strength equation is shown in Equation (9).

$$Utility = \left(\frac{V_u}{V_n}\right)^2 + \left(\frac{M_u}{M_n}\right)^2 < 1 \quad (9)$$

$$V_u = \sqrt{V_y^2 + V_z^2} \quad (10)$$

$$M_u = \sqrt{M_y^2 + M_z^2} \quad (11)$$

$$V_n = Area \times \frac{N}{P} \times \sigma_{V,\parallel} \quad (12)$$

$$M_n = S \times \frac{N}{P} \times \sigma_{bending} \quad (13)$$

Where:

V_u = ultimate shear, target structure

V_n = nominal shear, tree fork

V_y = y-direction shear, in-plane

V_z = z-direction shear, out-of-plane

M_u = ultimate moment, target structure

M_n = nominal moment, tree fork

M_y = y-direction moment, in-plane

M_z = z-direction moment, out-of-plane

N = strength at angle, θ , from fiber direction

P = strength parallel to the grain

$\sigma_{V,\parallel}$ = shear stress parallel to the grain
 S = section modulus (Equation (6))
 $\sigma_{bending}$ = bending stress

The ultimate shear and moment of the structural nodes are determined for each of the three branch vectors entering a singular node through a Karamba analysis conducted on the target structure explained in section 3.3.2 Structural analysis setup. The resultant beam forces are coordinated to each target beam vector which is then matched to the material library tree fork branch. The square root of the squared values of the shear and moment in the y and z-direction (in-plane and out-of-plane) are calculated to determine the ultimate shear and moment (Equation (10) and Equation (11).

The nominal shear and moment of the material library tree forks is determined by combining basic structural mechanics equations and the Hankinson's equation in order to account for the angle tolerance between the beam element and the node vector (Equation (12) and Equation (13)). The ideal matched tree fork would have a perfectly parallel force flow between the incoming beam to the tree fork branch vector; however, as seen from the previous matching-based design case studies, the majority of tree forks when matched results in some degree of angle difference from the expected versus matched fork Figure 60.

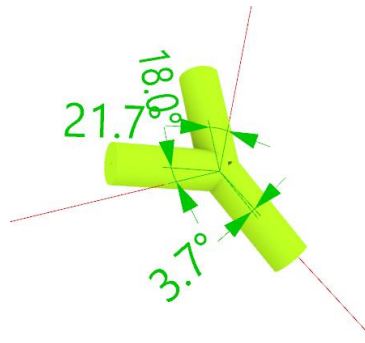


Figure 60. Angle difference between matched node and structural node

The Hankinson's equation was originally developed to quantify a strength metric to be used in situations where the direction of important stresses does not coincide with fiber orientation of the natural axes of fiber orientation in the wood. The Hankinson formula, Equation (14), approximates the strength properties at an angle, θ , from the fiber direction to obtain a proportioned strength, N , accordingly.

$$N = \frac{PQ}{P \sin^n \theta + Q \cos^n \theta} \quad (14)$$

Where:

- N = strength at angle Θ from fiber direction
- P = strength parallel to the grain
- Q = strength perpendicular to the grain
- n = empirically determined constant, 2
- θ = angle from fiber direction

The empirical constant, n , is obtained from literature and for tensile, compression, and bending strength, the value equals two. The Grasshopper model provided the angles between the intended fiber direction and that provided by the matched tree fork, and the strengths parallel and perpendicular to the grain of each species were referenced from the Wood Handbook mechanical properties tables. The N/P ratio utilized in Equations (12 and (13. represents the fraction of the property, shear or moment in this instance, that is viable given the variable angle to fiber direction; Figure 61 visually represents the relationship between the fraction N/P value and angle to fiber direction. An angle mismatch of up to 20 degrees maintains a significant amount of strength. No angle cutoff is administered in this problem formulation, but this constraint can be considered in a future iteration.

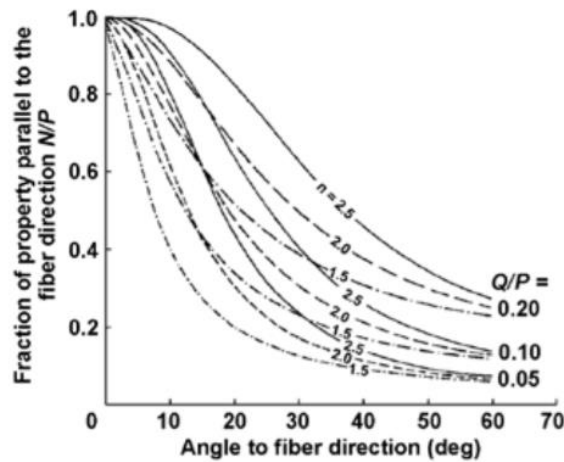


Figure 5-4. Effect of grain angle on mechanical property of clear wood according to Hankinson-type formula. Q/P is ratio of mechanical property across the grain (Q) to that parallel to the grain (P); n is an empirically determined constant.

Figure 61. Hankinson equation graphical representation. N/P vs. Angle (“Wood Handbook”)

The N/P ratio is input in the utility equation by appropriately proportioning the available strength of the tree fork’s vectored branches given the angle of difference between the fork and adjoining fiber direction. The strength reduction is calculated by multiplying the N/P fraction by the available shear, $V = Area \times \sigma$, and moment, $M = S \times \sigma$, resulting in Equations (12 and (13.

The utility equation formulated postulates that if the combined squared shear and moment ratios equals less than one, the tree fork has the available capacity to resist the expected shear and moment and is considered to be a satisfactory match. If the utility equation is greater than or equal to one, then a penalty score is added. The tree fork structural score is calculated as follows:

$$\begin{aligned}
& \text{Structural score} = 0 \\
& \text{For each connection, } i \\
& \quad \text{If } \text{Utility}(i) < 1 \\
& \quad \quad \text{Penalty} = 0 \\
& \quad \text{else} \\
& \quad \quad \text{Penalty} = \text{Utility}(i)^2 \\
& \text{Structural score} = \text{Structural score} + \text{Penalty} \\
& \text{end}
\end{aligned} \tag{15}$$

The utility equation is calculated for each of the matched tree forks; if the score is greater than one, it is cubed and cumulatively summed to generate the structural score. An optimum structural score has a value of zero where all the matched tree forks are structurally sound for the target structure's node.

Table 5. Ash, oak, and fruit P , Q , $\sigma_{V,\parallel}$, and σ_{bending} stress values

	Ash	Oak	Fruit
P	7.08 kip/in ²	3.44 kip/in ²	3.54 kip/in ²
Q	1.31 kip/in ²	0.61 kip/in ²	0.36 kip/in ²
$\sigma_{V,\parallel}$	1.26 kip/in ²	1.21 kip/in ²	1.13 kip/in ²
σ_{bending}	1.50 kip/in ²	1.50 kip/in ²	1.50 kip/in ²

The color distribution for the structural score testing was modified to represent each branching vector's angle differences between the matched tree fork vector target node vector. An angle difference of 0°-10° is green, 10°-20° is yellow, and greater than 20° is red.

3.3.2 Structural analysis setup

The hexagonal geometry with 1 control curve described in section 2.2.3 was utilized again for the optimization of the structural score experiments. The 25 hexagonal grid structures were constructed identically on the 20'x20' surface and subject to the same NURBS curve variable constraints (Figure 32, Figure 33, and Figure 34). The sampling was conducted for generated material libraries of 50, 100, and 200 samples to simulate practical obtainable material libraries for structures of the provided size and number of target nodes.

The structural analysis of the structure was executed with Karamba, a plugin within Grasshopper/Rhino. The line elements of the structure were transformed into beam elements with the *LineToBeam* component, the points along the x-axis were defined as fixed supports with the *Supp* element, and the material of structure was selected to represent wood mechanical properties through *MatSelect*. A three times amplified gravity load was applied to more clearly see the effects and behavior of the structure. Future iterations of the structural testing should apply various case

study lateral and gravity loadings to understand these effects in practical design applications. The *LineToBeam*, *Supp*, and *MatSelect*, components were inputted into the *Assemble*, *Analyze*, *ModelView*, and *BeamView* Karamba components to analyze and visually display the computed reactions, displacements, and stresses of the structure.

The individual beam forces, in-plane and out-of-plane shear and moment, were extracted through the *B-Forces* component to input into Equations (10 and (11). The *B-Forces* component provides the shear and moment values according to the beam element organization instead of the reaction correlated to the associated tree fork branch vector attached to the beam needed. A simple python algorithm was implemented by Yijiang Huang to match the beam endpoint indices and correlated shear and moment values to the corresponding matched tree fork branch.

The Karamba analysis updates instantaneously as the target structure shape is modified, so the input values in the utility metric to calculate the structural score provides real-time interaction and results.

3.3.3 Results

The results for the structural score computational experiments are compiled in Appendix D for a generated sampling of 50, 100, 200 samples for the ash, oak, and fruit tree species on the hexagonal geometry with 1 control curve. For every grid density, the ash and oak trees species proved to provide a structurally viable structure; the structural score minimized to a value of zero meaning that each tree fork resisted the applied shear and moment forces of the target structure. The fruit tree results from the optimization evidenced that this species should not be used for structural design construction; the majority of geometries tested resulted in structural scores greater than 1, which means that there were tree forks that did not adequately resolve the structural design conditions. The reason for the poor performance of the fruit tree forks can be attributed to the lower compression parallel to the grain, compression perpendicular to the grain, and shear parallel to the grain compared to those of the ash and oak tree species.

For each of the oak and ash tree species, as the number of samples increased, the matching score decreased linearly, which is expected with a larger material library with a wider-range of tree forks available. The new matching scores correlated with the structural score optimization are significantly larger than the original matching scores from the optimization of the matching score. This percent difference is irrelevant when considering the structural performance of a structure; however, the lesser the new matchings score, the less angle variation between the vectors inherently resulting in a more efficient structure. The ash tree sampling of 200 tree forks performed the best for each geometry under this metric with the lowest matching score and a structural score equal to zero.

The best performing result for the ash tree species was for the 3x4 hexagonal grid with 200 samples shown in *Figure 62*; this experiment resulted in a structural score equal to 0 and a matching score of 4,559. The structural performance of this geometry is sufficient, and the new matching score is comparable to the previously generated optimized matching score.

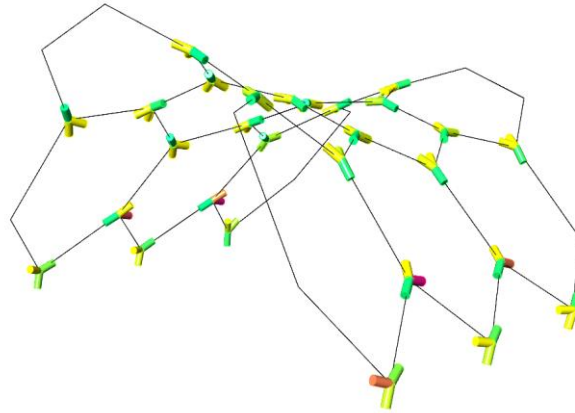


Figure 62. Ash. 3x4: Hexagonal, 1 Control Curve. 200 samples.

The best performing result for the oak tree species was for the 4x5 hexagonal grid for 50 samples shown in *Figure 63*. This structure had a structural score of 0 and a matching score of 6,328. This geometry was one of the few experiments that the structural score optimization resulted in a new matching score that was much lesser than the original matching score equal to 33,222.

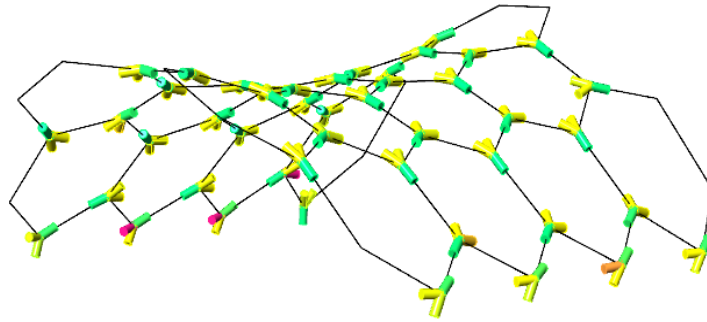


Figure 63. Oak. 4x5: Hexagonal, 1 Control Curve. 50 samples.

The structural score model developed outputs a local minimum for the possible feasible solutions that may be present from an initial target geometry. The optimizer only provided the first local minimum solution geometry found even though other potential solutions were located; a future iteration of this problem is recommended to develop a design framework that records all solutions that are a “good” structural fit.

3.4 Discussion and conclusion

For the structural testing, the pre-processing of the tree forks went through iterations as testing continued. It was determined that creating flat surfaces in the xy-plane (as seen on the ash species pre-processing) may be unnecessary for testing depending on the angle of difference between the center points of the two branches on top of each other. Small angle differences in the z-direction between the top branch with load being applied on top of and the bottom branch resting atop the testing table would be insignificant as the force applied on the angled branch would be resolved at a point parallel to the point of application on the bottom branch (as seen in the fruit tree fork), but

a large angle difference could create a torsional reaction when tested that could be dangerous or result in inconclusive results.

Both of the tree species tested displayed a tensile failure resulting in cracking and splitting in the main branch of the trunk. This behavior was expected and proved with a theoretical computational model outline in section 3.2.4 Computational model of behavior. The ash tree displayed more dramatic failure versus the more gradual failure of the fruit tree. This behavior can be attributed to the moisture content differences between the two specimens; the ash tree was dry resulting in brittle behavior, while the fruit tree was green and had flexible properties. To prevent the tension splitting in a practical design scenario, it is recommended to attach a collar to the perimeter of the branch to provide resistance. Further testing to characterize the behavior of a constrained tree fork with a collar is recommended to understand other failure mechanisms and observe if cracking still occurs internally in the tree branch.

The compression parallel to the grain stress results of the ash and fruit trees tested were significantly similar to those found in the Wood Handbook as seen in Table 4. The modulus of elasticity values displayed more variability from the values in literature due to errors in pre-processing the control cubes. Future iterations, are recommended to ensure that the plane that the compression force is being applied upon be perfectly parallel. Unfortunately, due to time limitations within the laboratory, only two specimens were able to be tested. Further testing of the tree forks are recommended to validate the results of the structural capacity testing and correlate the tested values with those found in the Wood Handbook.

The structural score developed provides a conservative metric of the behavior of the tree fork nodes matched to a target structure. Squaring the shear and moment ratios of the stress to strength in Equation (9) provides a load factor for the metric. During testing, it became apparent that multiple target geometries could be potential matches for a given material library, but the optimizer only displayed the first found local minimum geometry. Future work is recommended to develop a tool that finds multiple local minimum and displays their target geometries. This would be a beneficial tool for structural engineers during the concept design phase to visually compare and contrast the various feasible geometries that would all be structurally sound options given an available material library.

4 Conclusion

The matching-based algorithm, structural capacity testing, and structural score development presented here are important steps in making structural design with existing, found materials, such as tree forks, a feasible option in the conceptual design process. The expandable and iterative format of the sampling methodologies resulting in the matching and structural scores generate quantitative definitions to interpret the interaction behavior between available tree forks in a material library and the nodes of a target structure.

4.1 Summary of contributions

The three contributions presented and demonstrated through case studies are a matching-based design algorithm, structural capacity testing, and a structural performance computational model. Previous instances of reutilizing tree elements in a structural design, such as the Wood Chip Barn in Hooke Park, have been implemented, but these projects were architecturally-driven and hard to replicate at scale due to the highly specified design strategy. This thesis develops a workflow that uses any available or generated material library to compute a metric describing the quality of matching for any input target geometry. The relationship between tree species, target geometry, and number of samples in the material library was determined, and a point of diminishing returns, independent of the number of nodes in the target structure, was identified at which the matching score plateaued. A material library that is twice the size as the number of target nodes is sufficient to generate “good” matches with minimal material waste.

Structural testing of tree bifurcations in previous work has correlated relationships between tree morphology and failure mechanisms and quantified conventional timber mechanical properties,

while this thesis used structural testing to experimentally characterize and quantify the failure when tree forks are loaded in compression at an angle to the fiber direction. Tensile splitting failure was displayed, and a computational model was developed to demonstrate the theory of the reaction forces of this behavior.

A structural performance computational model was developed to assign a score metric that quantifies the performance of presented structures; this real-time model allows a designer to understand the feasibility of a design given an available material library within a few minutes. This instantaneous feedback with a combinational matching and structural scoring algorithm is a novel workflow. Within the structural score testing, it was found that the fruit tree species performed the worst and is not recommended for use in structural design, while the ash tree forks proved to be an excellent option as a construction material.

4.2 Potential impact

The development of a real-time matching and scoring metric model makes designing with available existing materials a more feasible option. A streamlined conceptual design process makes the mindful design mentality demonstrated by the Dutch shipbuilders more obtainable for the fast-paced reality within design firms. This thesis promotes utilization of the now, readily available computational tools to develop a widespread methodology to design according to an existing material library. There are economic and environmental benefits for reusing structural materials or utilizing found material in design; new material costs and designs of material abundance can be avoided. Current design mindset assumes an infinite supply of resources, but this approach is environmentally taxing and unsustainable long-term, so a mindset shift to more conscious design is necessary to utilize available resources more mindfully and efficiently. The computational tools developed in this thesis provide a framework for more conscious design.

4.3 Future work

It is intended that the computational models and tools developed will continue to evolve to incorporate more features, increase speed and efficiency, and become more comprehensive. Within the matching-based computational model, the current problem formulation only allows for three-branched tree forks to be matched to three-vectored target nodes; developing an algorithm to match three-branched tree forks to two-vectored target nodes will create a more and accurate matching capability and scoring system. Additional geometry case studies with various target geometries would continue to enhance understanding of the relationship between tree species, target geometry, and number of samples. Geometry recommendations include hexagonal grids with assorted hexagon sizes rather than uniform grids utilized in this work and combination hexagonal and pentagonal grids.

Continued structural testing of the available tree forks in the catalogued material library is recommended to characterize the capacity of the tree fork joints and validate the stress values correlated used to those available in the Wood Handbook. Additional case studies within the structural score optimization framework will increase understanding of the structural score implications, what constitutes better target geometries for structural performance, and confirms the poor performance of the fruit tree species.

4.4 Concluding remarks

The framework developed in this research has the potential to help designers develop real-time, interactive optimized structures given an available material library. Current design processes for more specialized projects with limited material libraries are slow or ineffective, requiring time-consuming trial and error. With the algorithms developed in this thesis, computational models for projects utilizing existing or limited material libraries and constraints can be more easily implemented in practice. The availability of these tools will create a more comprehensive concept design development and understanding of the basic structural behavior resulting in more consciously designed structures.

5 References

- Albion, Robert Greenhalgh. *Forests and Sea Power*. Harvard University Press, 1926.
- Allner, Lukas, and Daniela Kroehnert. “Conceptual Joining: Branch Formations.” *Proceedings of the IASS Symposium 2018*, pp. 1–4.
- Aono, Masaki, and Toshiyasu L. Kunii. “Botanical Tree Image Generation.” *IEEE Computer Graphics and Applications*, vol. 4, no. 5, 1984, pp. 10–34.,
doi:10.1109/mcg.1984.276141.
- Brütting, Jan, et al. “Design of Truss Structures Through Reuse.” *Structures*, vol. 18, 2019, pp. 128–137., doi:10.1016/j.istruc.2018.11.006.
- Brütting, Jan, et al. “Optimization Formulations for the Design of Low Embodied Energy Structures Made from Reused Elements.” *Advanced Computing Strategies for Engineering Lecture Notes in Computer Science*, May 2018, pp. 139–163.,
doi:10.1007/978-3-319-91635-4_8.
- Buckley, Gareth, et al. “Angle of Inclination Affects the Morphology and Strength of Bifurcations in Hazel (*Corylus Avellana*L.).” *Arboricultural Journal*, vol. 37, no. 2, Mar. 2015, pp. 99–112., doi:10.1080/03071375.2015.1064265.
- Bukauskas, Aurimas, et al. “Form-Fitting Strategies for Diversity-Tolerant Design.” *Proceedings of the IASS Symposium 2018*, pp. 1–8.
- Burgess, S. C., and D. Pasini. “Analysis of the Structural Efficiency of Trees.” *Journal of Engineering Design*, vol. 15, no. 2, 2004, pp. 177–193.,
doi:10.1080/09544820410001658517.
- Daizen Joinery. “Curve bending before fabricate into truss.” Daizen Joinery, Daizen Joinery Ltd., 2020, daizen.com.

- Eloy, Christophe. Leonardo da Vinci's rule example: computer-simulated tree. *American Physical Society*.
- “Emerald Ash Borer Beetle Detected in Somerville.” *Emerald Ash Borer Beetle Detected in Somerville / City of Somerville*, 22 Aug. 2018, www.somervillema.gov/news/emerald-ash-borer-beetle-detected-somerville.
- Farrell, Robert William. 2003, pp. iii-57.
- Gomes, Rosa Varela, et al. *The Management of Iberian Forest Resources in the Early Modern Shipbuilding: History and Archaeology*. Instituto De Arqueologia e Paleociências, 2015.
- “The Hungarian Algorithm.” *Steps of the Hungarian Algorithm - HungarianAlgorithm.com*, www.hungarianalgorithm.com/hungarianalgorithm.php.
- Kane, Brian, et al. “Failure Mode and Prediction of the Strength of Branch Attachments.” *Arboriculture & Urban Forestry*, vol. 34, no. 5, 2008, pp. 308–316.
- Mattheck, C., and U. Vorberg. “The Biomechanics of Tree Fork Design.” *Botanica Acta*, vol. 104, no. 5, 1991, pp. 399–404., doi:10.1111/j.1438-8677.1991.tb00248.x.
- Mattheck, Claus, and Hans Kubler. “The Mechanical Self-Optimization of Trees — Five Theorems.” *Wood - The Internal Optimization of Trees Springer Series in Wood Science*, 1997, pp. 21–21., doi:10.1007/978-3-642-61219-0_3.
- Minamino, Ryoko, and Masaki Tateno. “Tree Branching: Leonardo Da Vincis Rule versus Biomechanical Models.” *PLoS ONE*, vol. 9, no. 4, Aug. 2014, doi:10.1371/journal.pone.0093535.
- Mollica, Zachary, and Martin Self. “Tree Fork Truss, Geometric Strategies for Exploiting Inherent Material Form.” *Advances in Architectural Geometry*, 2016, pp. 138–153.

- Özden, Seray, et al. “Fracture Properties of Green Wood Formed within the Forks of Hazel (Corylus Avellana L.)” *Trees*, vol. 31, no. 3, Mar. 2017, pp. 903–917.,
doi:10.1007/s00468-016-1516-0.
- Pradal, C., et al. “PlantGL: A Python-Based Geometric Library for 3D Plant Modelling at Different Scales.” *Graphical Models*, vol. 71, no. 1, 2009, pp. 1–21.,
doi:10.1016/j.gmod.2008.10.001.
- Rusinkiewicz, S., and M. Levoy. “Efficient Variants of the ICP Algorithm.” *Proceedings Third International Conference on 3-D Digital Imaging and Modeling*, May 2001,
doi:10.1109/im.2001.924423.
- Shahbazi, Zahra, et al. “Mechanical Stress Analysis of Tree Branches.” *American Journal of Mechanical Engineering*, vol. 3, no. 2, 2015, pp. 32–40., doi:10.12691/ajme-3-2-1.
- Shigeru Ban Architects. *Stronger Than Steel: Shigeru Ban’s Glulam Revolution*, Architizer,
<https://architizer.com/blog/inspiration/collections/shigeru-ban-glulam>.
- Shigo, A.L. 1985. How tree branches are attached to trunks. *Canadian Journal of Botany*.
63:1391-1401.
- “TreeKeeper 8 System for City of Somerville, MA.” *TreeKeeper 8 System for City of Somerville, MA*, somervillema.treekeepersoftware.com/.
- Von Buelow, Peter, et al. “Combining Parametric Form Generation and Design Exploration to Produce a Wooden Reticulated Shell Using Natural Tree Crotches.” *Proceedings of the IASS Symposium 2018*, pp. 1–8.
- Wilson, Thomas Randall Carson. *Strength-Moisture Relations for Wood*. 1932.
- Wood Handbook: Wood as an Engineering Material*. Forest Products Society, 2011.

Zyga, Lisa. "Leonardo Da Vinci's Tree Rule May Be Explained by Wind." *Phys.org*, Phys.org, 4 Jan. 2012, phys.org/news/2012-01-leonardo-da-vinci-tree.html.

6 Appendix

The Appendix contains the complete testing results and analyzed data for the executed sampling for both the matching and structural score frameworks. The order and contents of each appendix are as follows:

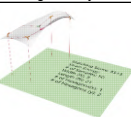
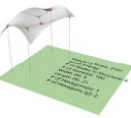
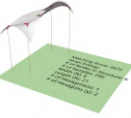
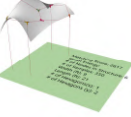


Appendix A: Hexagonal geometry with 5 control points, matching score results

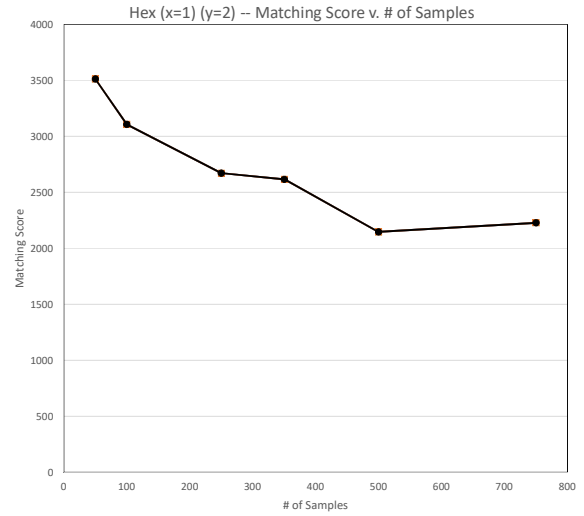
Appendix B: Hexagonal geometry with 1 control curve, matching score results







Appendix C: Hexagonal geometry with 1 control curve, matching score vs. ratio graphs

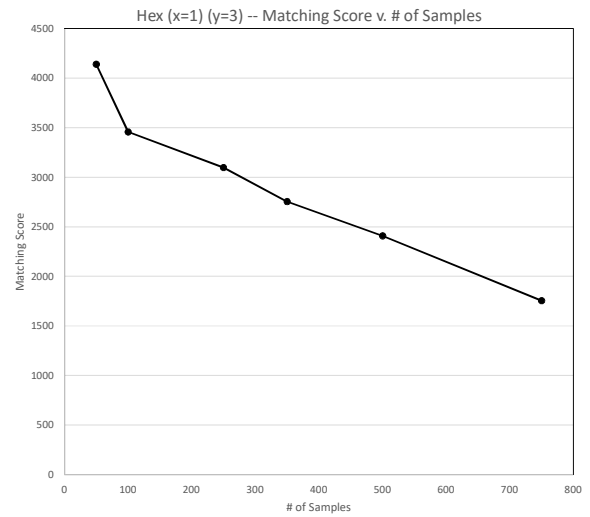
Appendix D: Hexagonal geometry with 5 control points, structural score results







Appendix A

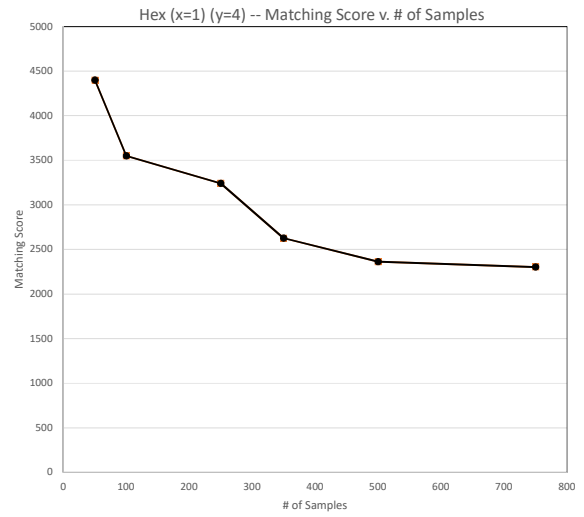
# hexagons (x)	# hexagons (y)	# of samples	# of structure nodes	ratio	geometry	matching score
1	2	50	6	0.120		3513
1	2	100	6	0.060		3107
1	2	250	6	0.024		2672
1	2	350	6	0.017		2617
1	2	500	6	0.012		2147
1	2	750	6	0.008		2229

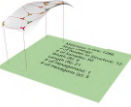

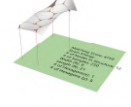


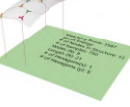


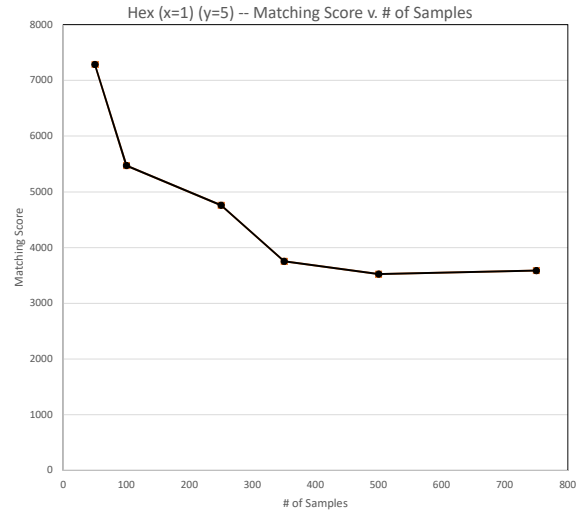
# hexagons (x)	# hexagons (y)	# of samples	# of structure nodes	ratio	geometry	matching score
1	3	50	8	0.160		4140
1	3	100	8	0.080		3458
1	3	250	8	0.032		3098
1	3	350	8	0.023		2755
1	3	500	8	0.016		2409
1	3	750	8	0.011		1755

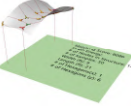


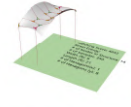




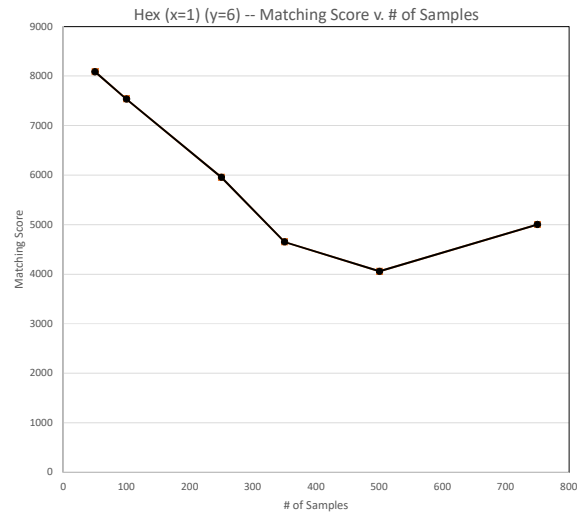
# hexagons (x)	# hexagons (y)	# of samples	# of structure nodes	ratio	geometry	matching score
1	4	50	10	0.200		4400
1	4	100	10	0.100		3549
1	4	250	10	0.040		3241
1	4	350	10	0.029		2627
1	4	500	10	0.020		2363
1	4	750	10	0.013		2303

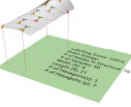

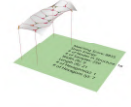





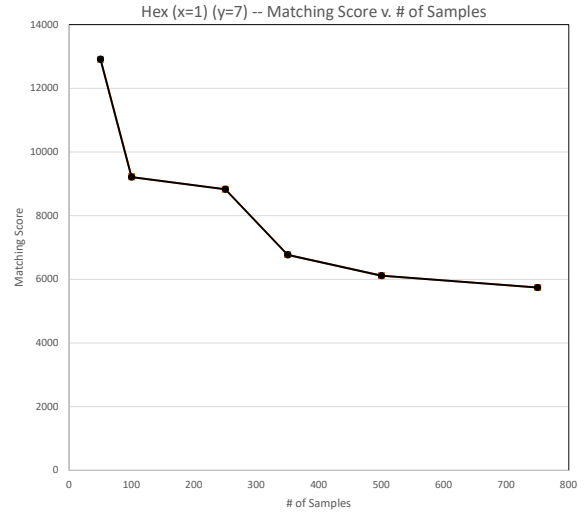
# hexagons (x)	# hexagons (y)	# of samples	# of structure nodes	ratio	geometry	matching score
1	5	50	12	0.240		7286
1	5	100	12	0.120		5473
1	5	250	12	0.048		4759
1	5	350	12	0.034		3753
1	5	500	12	0.024		3525
1	5	750	12	0.016		3587



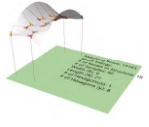


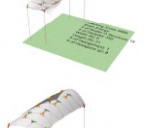
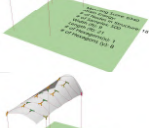

# hexagons (x)	# hexagons (y)	# of samples	# of structure nodes	ratio	geometry	matching score
1	6	50	14	0.280		8086
1	6	100	14	0.140		7536
1	6	250	14	0.056		5956
1	6	350	14	0.040		4652
1	6	500	14	0.028		4058
1	6	750	14	0.019		5004

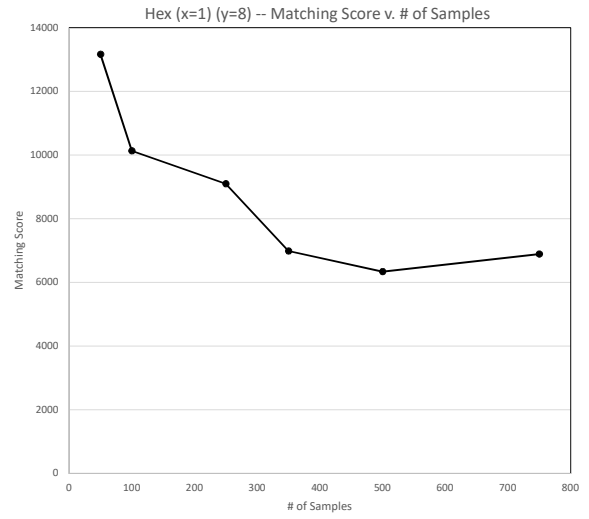


# hexagons (x)	# hexagons (y)	# of samples	# of structure nodes	ratio	geometry	matching score
1	7	50	16	0.320		12914
1	7	100	16	0.160		9215
1	7	250	16	0.064		8834
1	7	350	16	0.046		6774
1	7	500	16	0.032		6119
1	7	750	16	0.021		5744



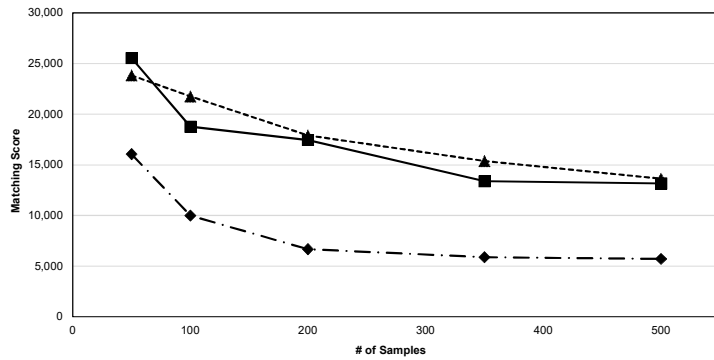
hexagons (x) # hexagons (y) # of samples # of structure nodes ratio geometry matching score

# hexagons (x)	# hexagons (y)	# of samples	# of structure nodes	ratio	geometry	matching score
1	8	50	18	0.360		13165
1	8	100	18	0.180		10129
1	8	250	18	0.072		9095
1	8	350	18	0.051		6986
1	8	500	18	0.036		6339
1	8	750	18	0.024		6893

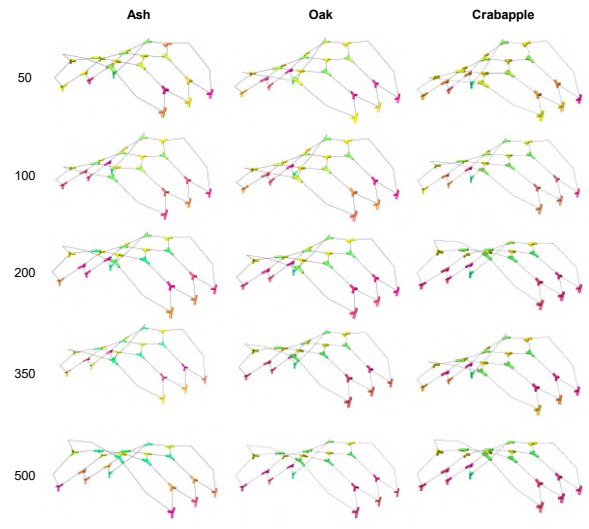


Appendix B

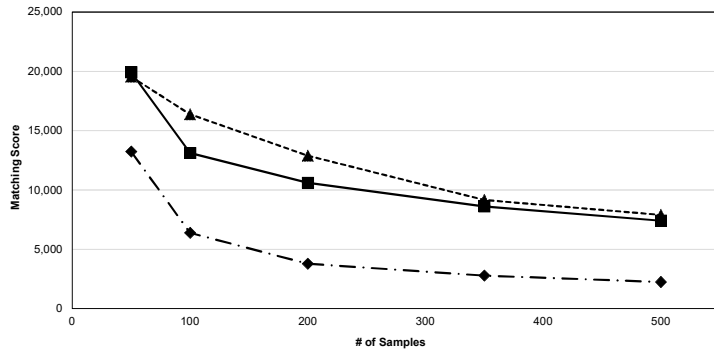
3x3: Hexagonal, 1 Control Curve, 22 Nodes



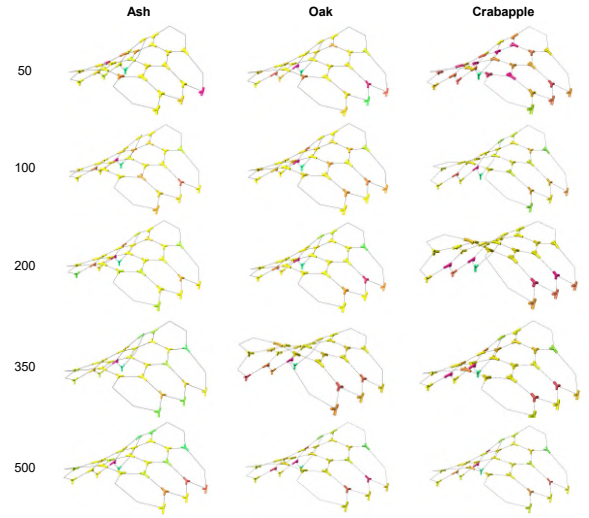
# of samples	Ratio (# structural nodes: # of samples)	Matching Score		
		Ash	Oak	Fruit
50	0.44	16,058	25,543	23,831
100	0.22	9,982	18,779	21,755
200	0.11	6,678	17,447	17,905
350	0.06	5,881	13,383	15,379
500	0.04	5,712	13,161	13,632



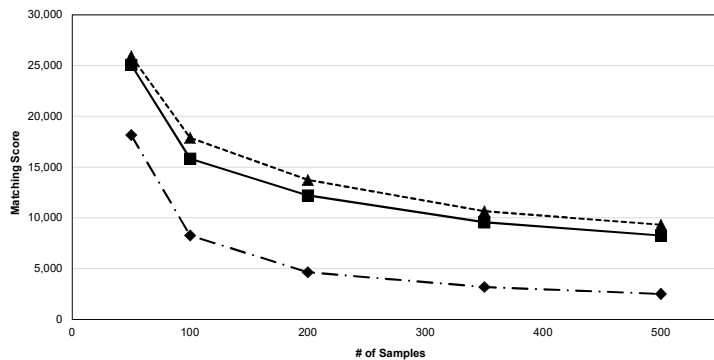
3x4: Hexagonal, 1 Control Curve, 28 Nodes



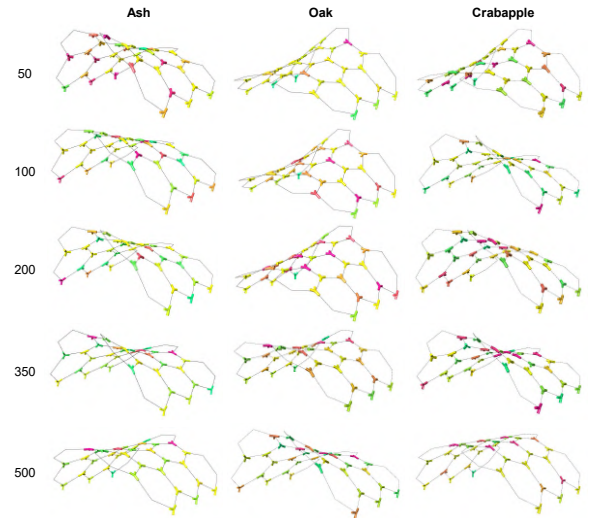
# of samples	Ratio (# structural nodes: # of samples)	Matching Score		
		Ash	Oak	Fruit
50	0.56	13,228	19,923	19,547
100	0.28	6,385	13,111	16,376
200	0.14	3,779	10,601	12,894
350	0.08	2,785	8,619	9,160
500	0.06	2,242	7,409	7,896



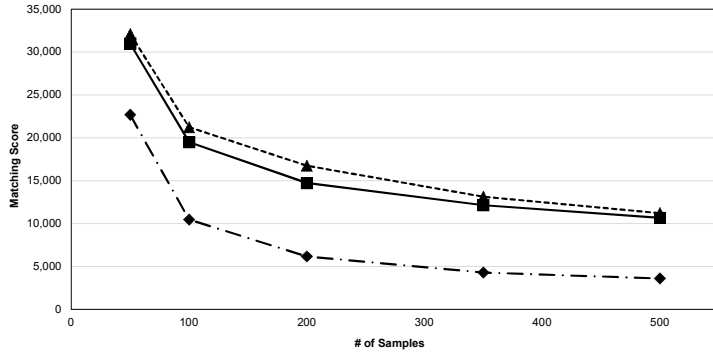
3x5: Hexagonal, 1 Control Curve, 34 Nodes



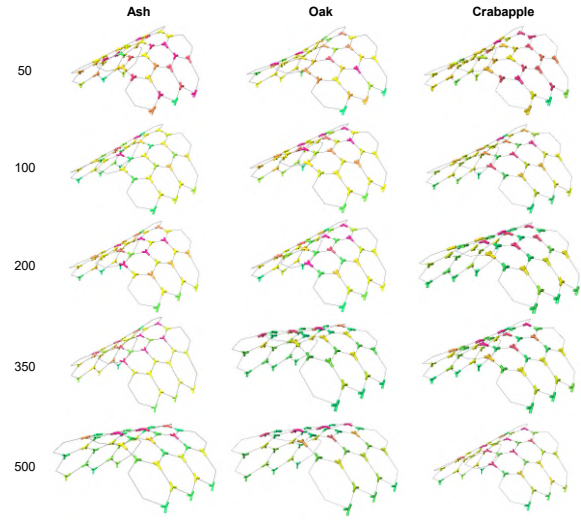
# of samples	Ratio (# structural nodes: # of samples)	Matching Score		
		Ash	Oak	Fruit
50	0.68	18,156	25,090	25,933
100	0.34	8,271	15,836	17,883
200	0.17	4,643	12,217	13,744
350	0.10	3,189	9,572	10,658
500	0.07	2,509	8,264	9,325



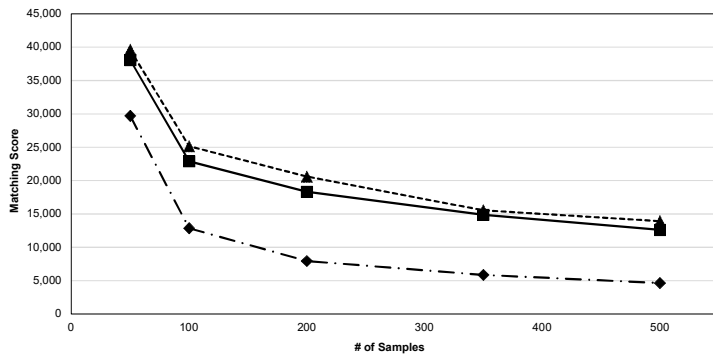
3x6: Hexagonal, 1 Control Curve, 40 Nodes



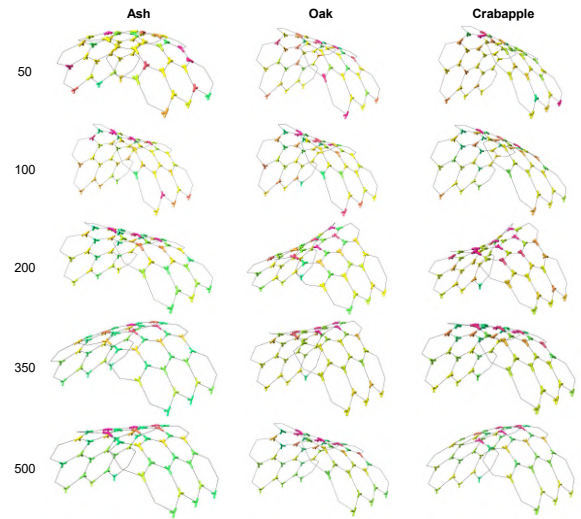
# of samples	Ratio (# structural nodes: # of samples)	Matching Score		
		Ash	Oak	Fruit
50	0.80	22,682	30,991	32,127
100	0.40	10,459	19,510	21,235
200	0.20	6,176	14,727	16,746
350	0.11	4,293	12,153	13,127
500	0.08	3,595	10,683	11,217



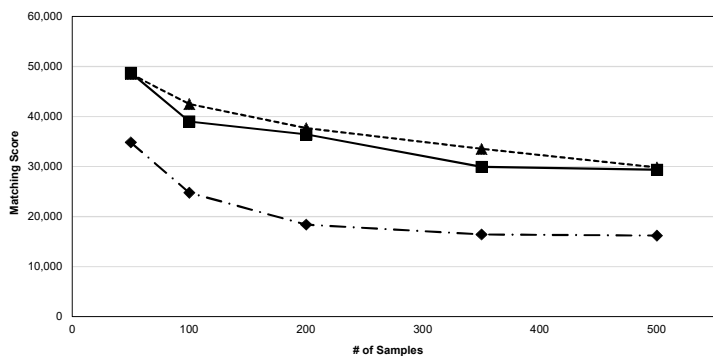
3x7: Hexagonal, 1 Control Curve, 46 Nodes



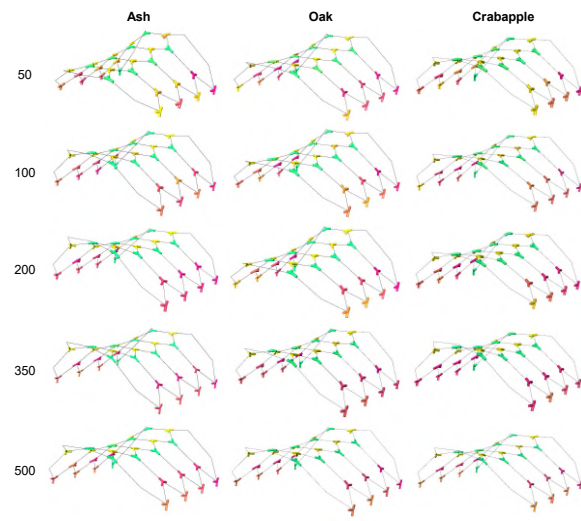
# of samples	Ratio (# structural nodes: # of samples)	Matching Score		
		Ash	Oak	Fruit
50	0.92	29,713	38,094	39,617
100	0.46	12,851	22,894	25,171
200	0.23	7,936	18,320	20,616
350	0.13	5,873	14,883	15,545
500	0.09	4,650	12,625	13,921



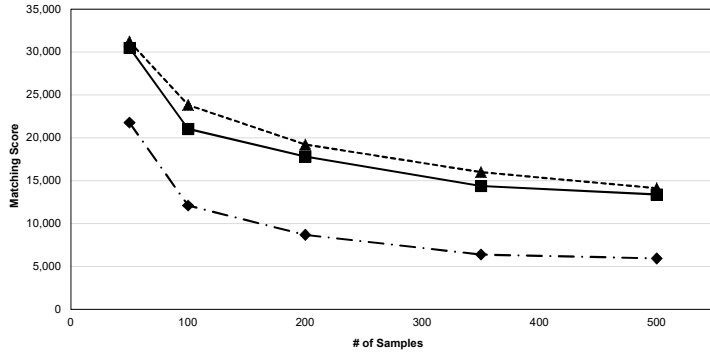
4x3: Hexagonal, 1 Control Curve, 30 Nodes



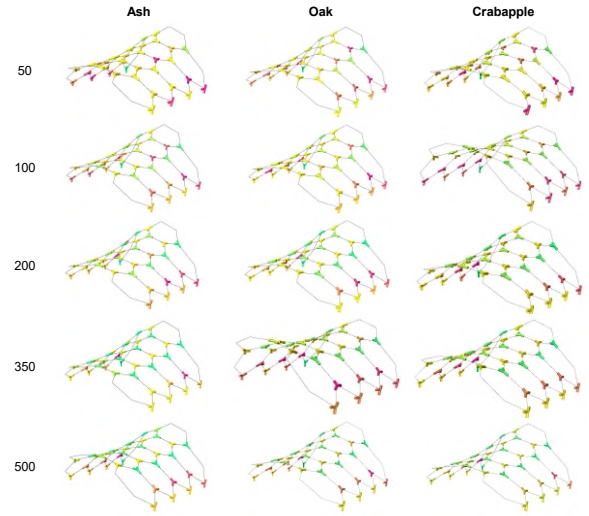
# of samples	Ratio (# structural nodes: # of samples)	Matching Score		
		Ash	Oak	Fruit
50	0.60	34,816	48,745	48,502
100	0.30	24,758	39,006	42,500
200	0.15	18,401	36,426	37,676
350	0.09	16,429	29,966	33,546
500	0.06	16,198	29,358	29,822



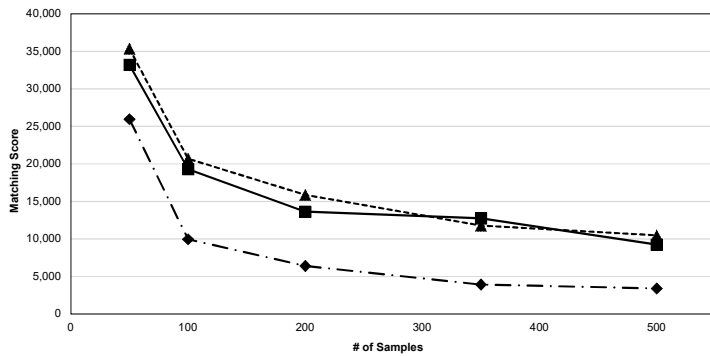
4x4: Hexagonal, 1 Control Curve, 38 Nodes



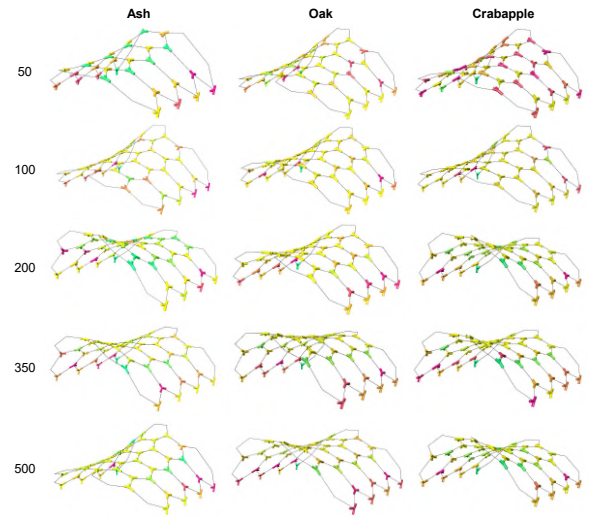
# of samples	Ratio (# structural nodes: # of samples)	Matching Score		
		Ash	Oak	Fruit
50	0.76	21,781	30,490	31,222
100	0.38	12,110	21,047	23,829
200	0.19	8,695	17,818	19,231
350	0.11	6,393	14,376	16,011
500	0.08	5,944	13,399	14,128



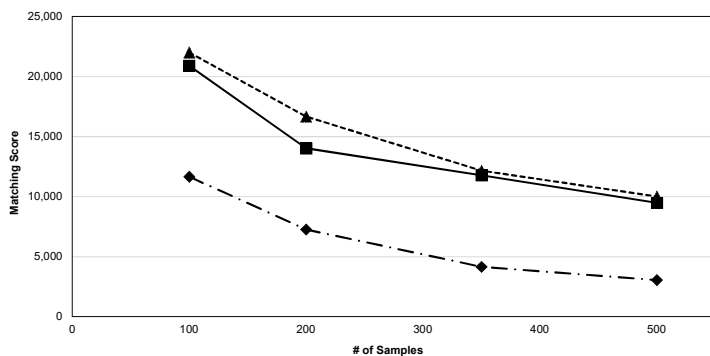
4x5: Hexagonal, 1 Control Curve, 46 Nodes



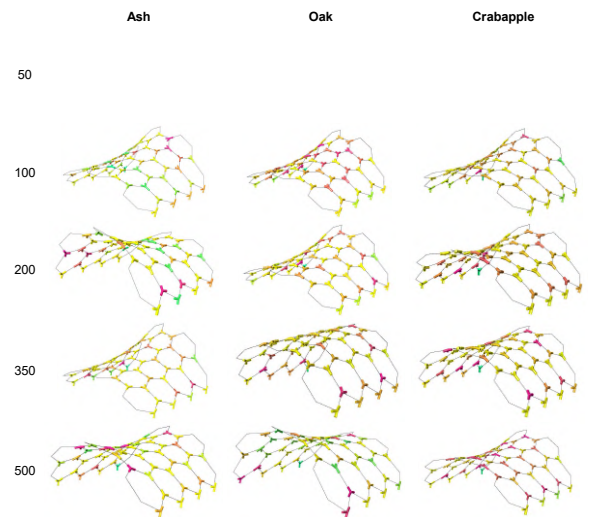
# of samples	Ratio (# structural nodes: # of samples)	Matching Score		
		Ash	Oak	Fruit
50	0.92	25,961	33,222	35,347
100	0.46	9,964	19,303	20,690
200	0.23	6,401	13,639	15,870
350	0.13	3,915	12,752	11,793
500	0.09	3,412	9,245	10,487



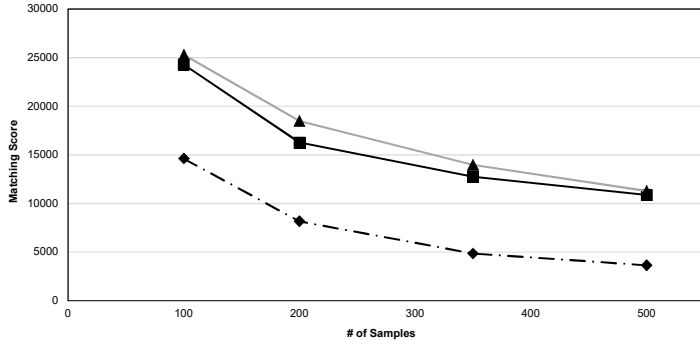
4x6: Hexagonal, 1 Control Curve, 54 Nodes



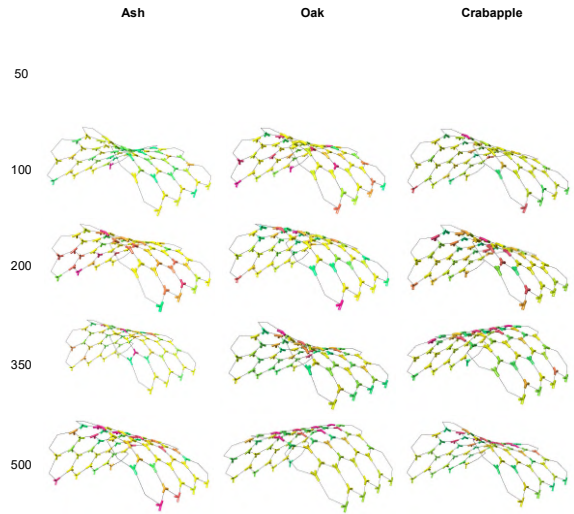
# of samples	Ratio (# structural nodes: # of samples)	Matching Score		
		Ash	Oak	Fruit
100	0.54	11,649	20,901	21,998
200	0.27	7,255	14,022	16,661
350	0.15	4,145	11,778	12,162
500	0.11	3,043	9,476	10,006



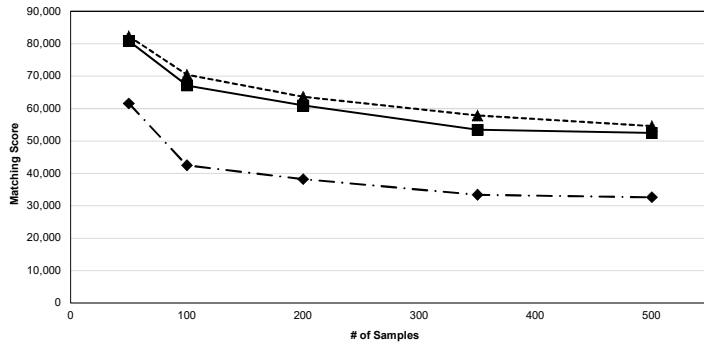
4x7: Hexagonal, 1 Control Curve, 62 Nodes



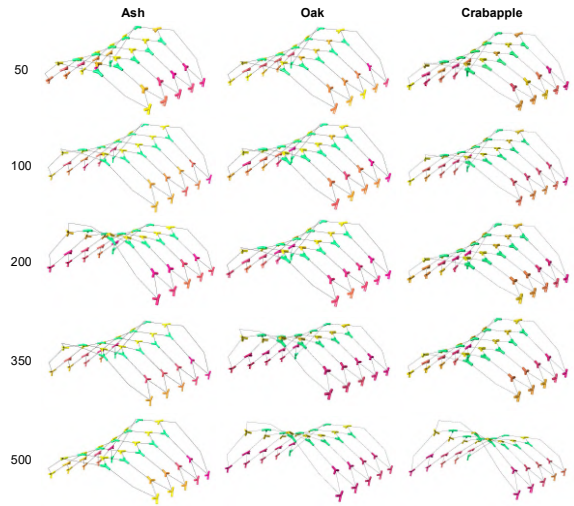
# of samples	Ratio (# structural nodes: # of samples)	Matching Score		
		Ash	Oak	Fruit
50				
100	0.62	14,614	24,288	25,301
200	0.31	8,163	16,271	18,490
350	0.18	4,867	12,779	13,987
500	0.12	3,652	10,877	11,299



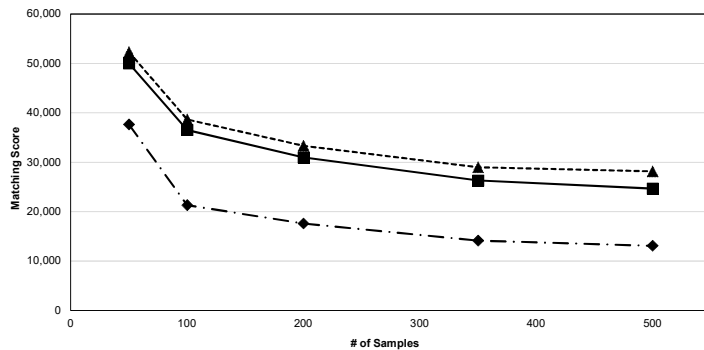
5x3: Hexagonal, 1 Control Curve, 38 Nodes



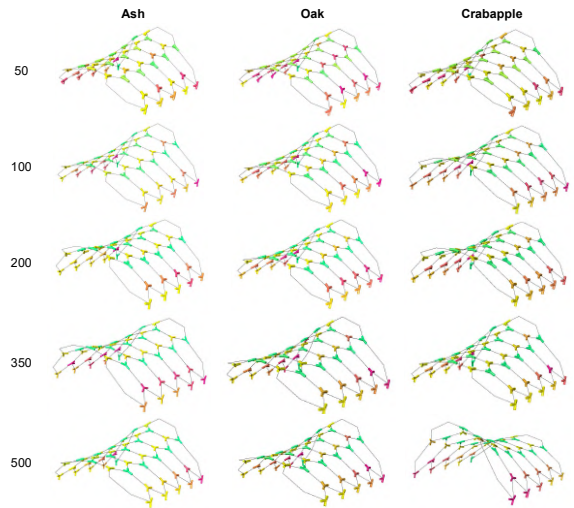
# of samples	Ratio (# structural nodes: # of samples)	Matching Score		
		Ash	Oak	Fruit
50	0.76	61,603	80,866	82,320
100	0.38	42,507	67,131	70,460
200	0.19	38,205	60,955	63,636
350	0.11	33,414	53,483	57,875
500	0.08	32,612	52,489	54,607



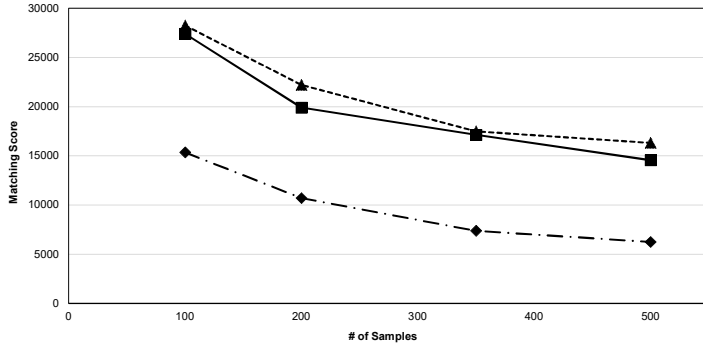
5x4: Hexagonal, 1 Control Curve, 48 Nodes



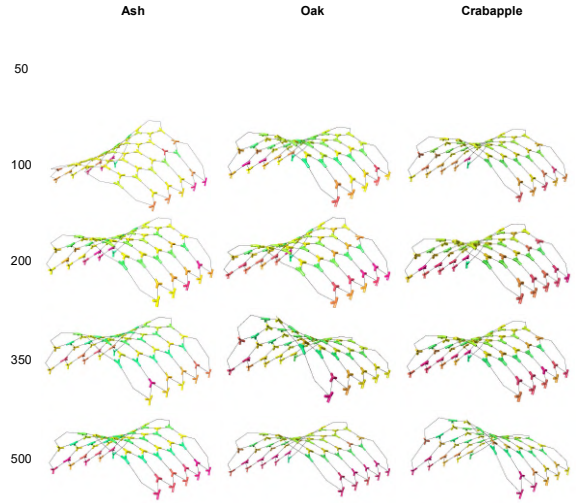
# of samples	Ratio (# structural nodes: # of samples)	Matching Score		
		Ash	Oak	Fruit
50	0.96	37,655	50,008	52,298
100	0.48	21,300	36,516	38,645
200	0.24	17,615	30,985	33,314
350	0.14	14,128	26,341	28,995
500	0.10	13,087	24,672	28,155



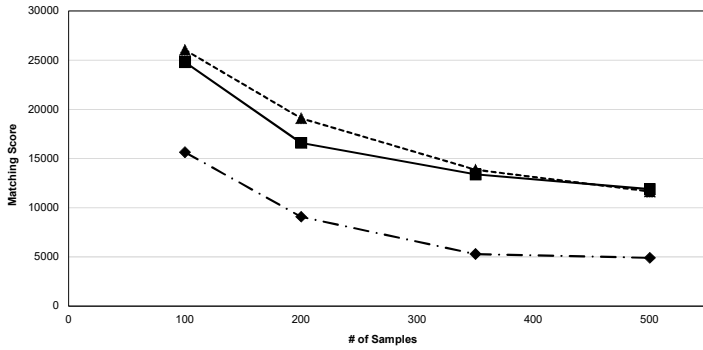
5x5: Hexagonal, 1 Control Curve, 58 Nodes



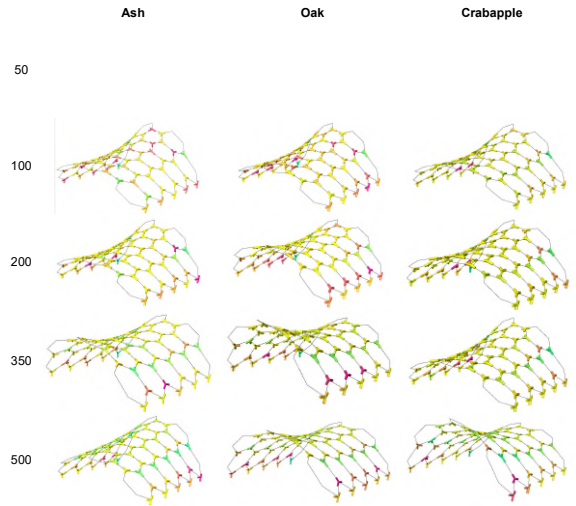
# of samples	Ratio (# structural nodes: # of samples)	Matching Score		
		Ash	Oak	Fruit
50				
100	0.58	15,345	27,409	28,253
200	0.29	10,702	19,911	22,212
350	0.17	7,369	17,140	17,488
500	0.12	6,249	14,555	16,316



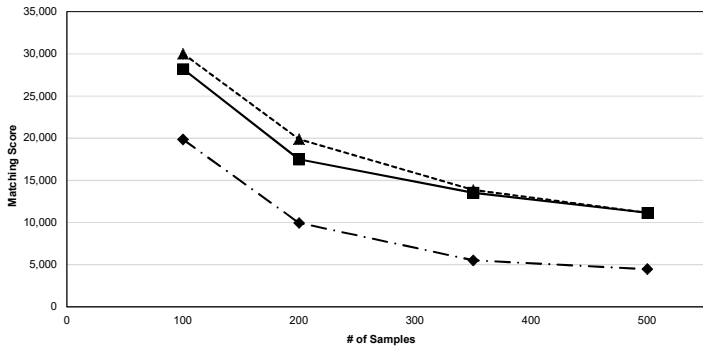
5x6: Hexagonal, 1 Control Curve, 68 Nodes



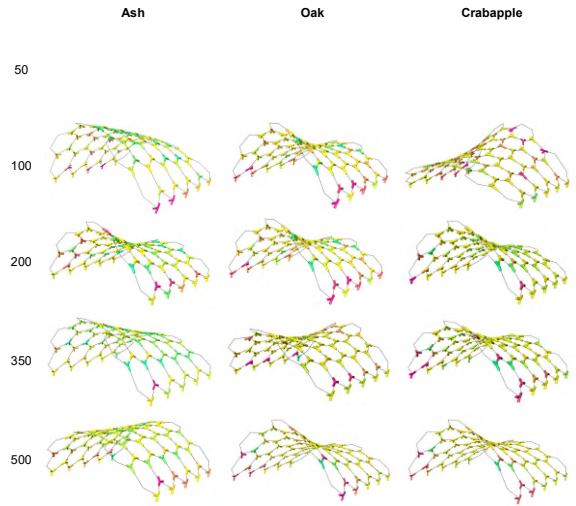
# of samples	Ratio (# structural nodes: # of samples)	Matching Score		
		Ash	Oak	Fruit
50				
100	0.68	15,650	24,798	26,047
200	0.34	9,083	16,586	19,090
350	0.19	5,296	13,403	13,867
500	0.14	4,915	11,895	11,660



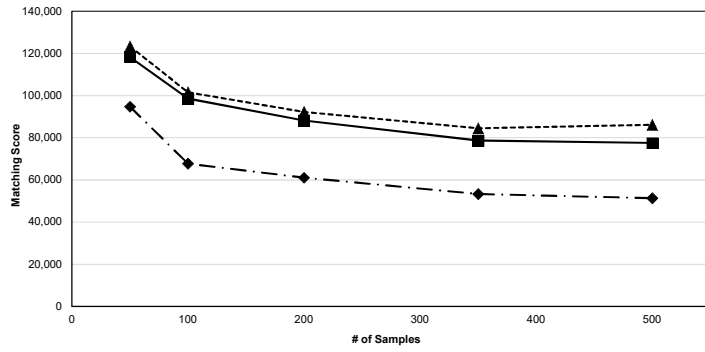
5x7: Hexagonal, 1 Control Curve, 78 Nodes



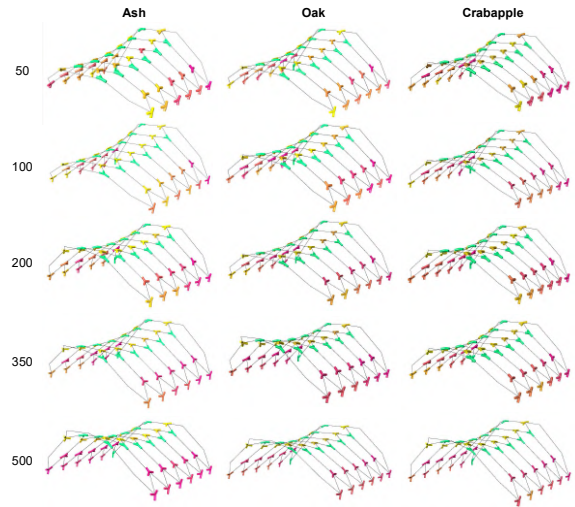
# of samples	Ratio (# structural nodes: # of samples)	Matching Score		
		Ash	Oak	Fruit
50				
100	0.78	19,846	28,217	30,034
200	0.39	9,967	17,507	19,882
350	0.22	5,525	13,539	13,862
500	0.16	4,468	11,149	11,155



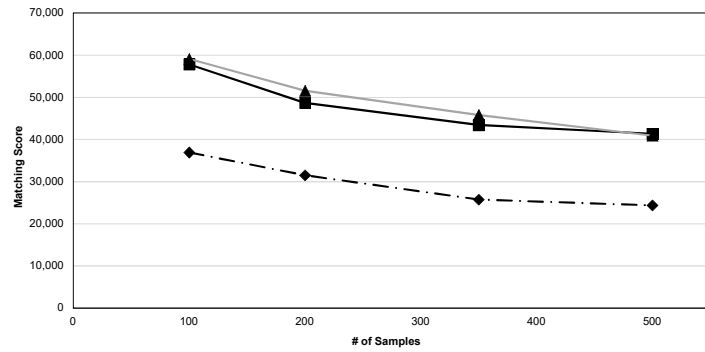
6x3: Hexagonal, 1 Control Curve, 46 Nodes



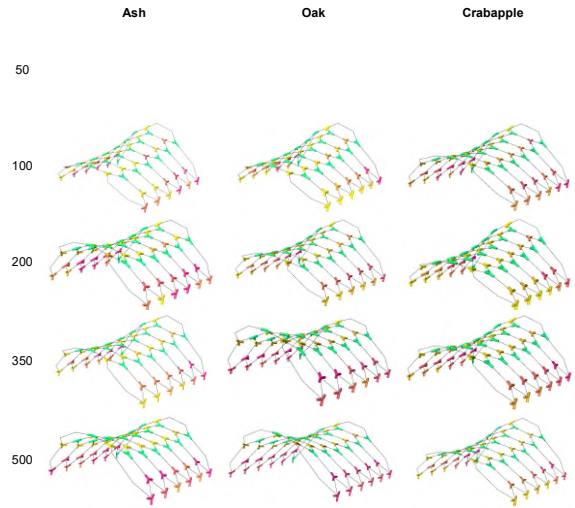
# of samples	Ratio (# structural nodes: # of samples)	Matching Score		
		Ash	Oak	Fruit
50	0.92	94,784	118,347	123,380
100	0.46	67,705	98,582	101,566
200	0.23	61,077	88,188	92,239
350	0.13	53,332	78,688	84,515
500	0.09	51,351	77,536	86,161



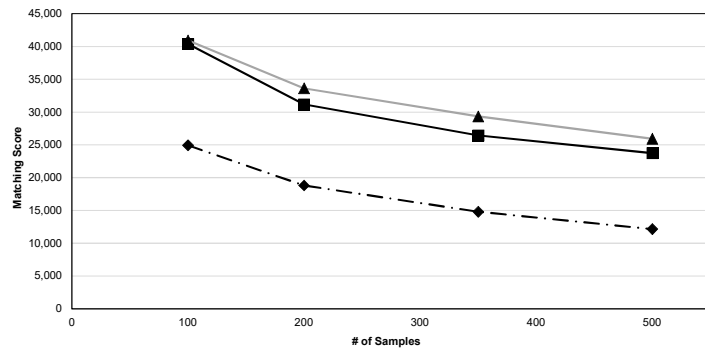
6x4: Hexagonal, 1 Control Curve, 58 Nodes



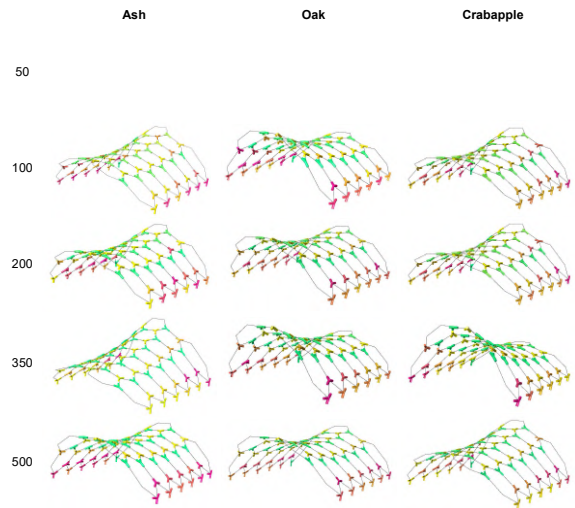
# of samples	Ratio (# structural nodes: # of samples)	Matching Score		
		Ash	Oak	Fruit
50	0.92	94,784	118,347	123,380
100	0.58	36,925	57,838	59,115
200	0.29	31,536	48,697	51,582
350	0.17	25,774	43,461	45,808
500	0.12	24,373	41,356	40,904



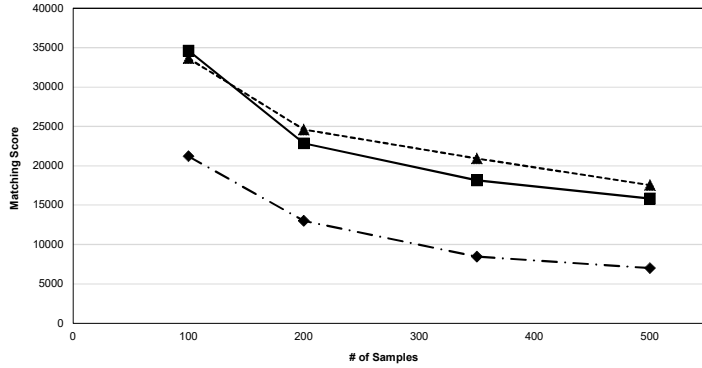
6x5: Hexagonal, 1 Control Curve, 70 Nodes



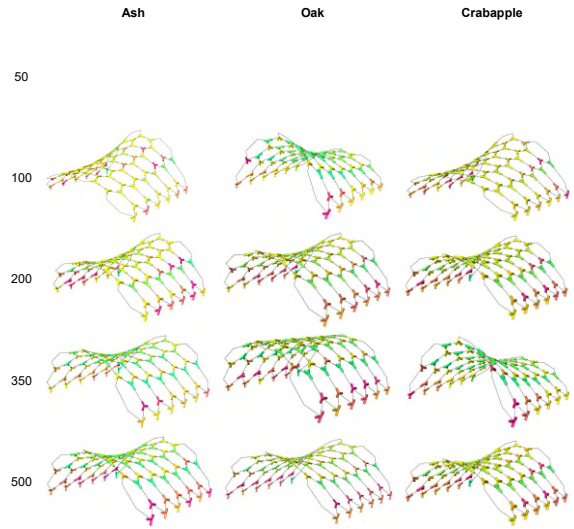
# of samples	Ratio (# structural nodes: # of samples)	Matching Score		
		Ash	Oak	Fruit
50	0.92	94,784	118,347	123,380
100	0.70	24,925	40,412	40,914
200	0.35	18,816	31,160	33,633
350	0.20	14,806	26,443	29,345
500	0.14	12,160	23,745	25,939



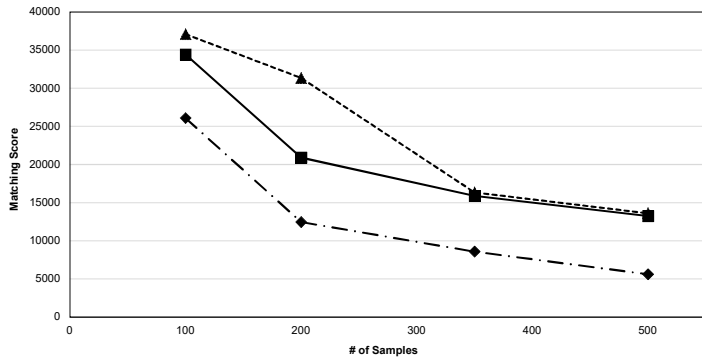
6x6: Hexagonal, 1 Control Curve, 82 Nodes



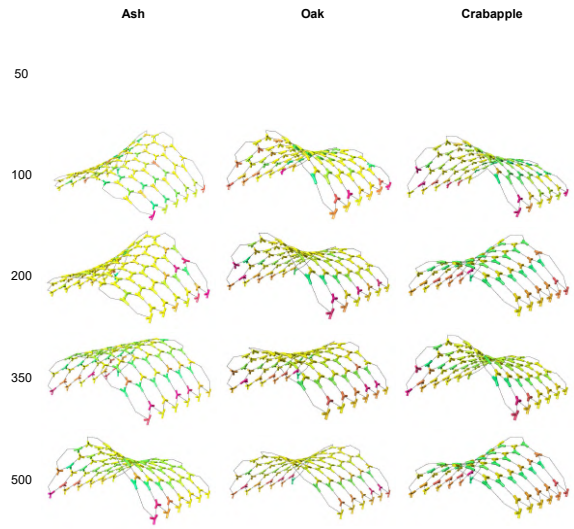
# of samples	Ratio (# structural nodes: # of samples)	Matching Score		
		Ash —◆—	Oak —■—	Fruit —▲—
50				
100	0.82	21,204	34,597	33,641
200	0.41	13,007	22,841	24,612
350	0.23	8,463	18,156	20,924
500	0.16	7,009	15,828	17,545



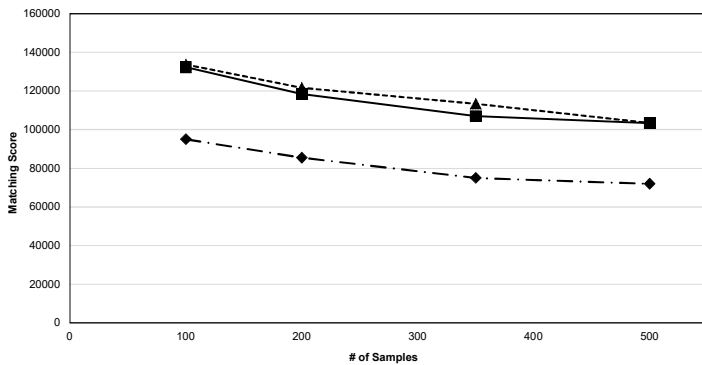
6x7: Hexagonal, 1 Control Curve, 94 Nodes



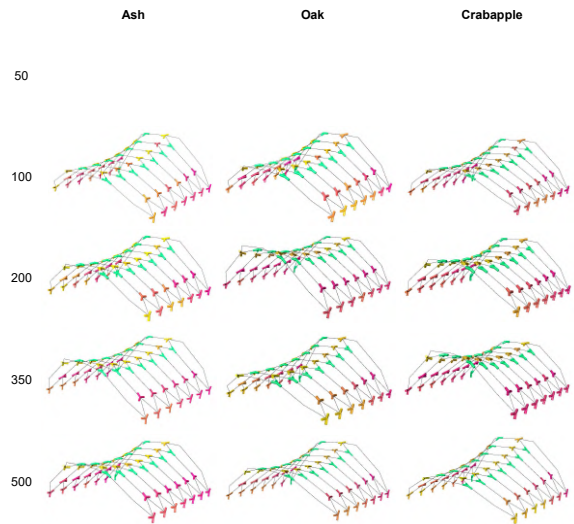
# of samples	Ratio (# structural nodes: # of samples)	Matching Score		
		Ash —◆—	Oak —■—	Fruit —▲—
50				
100	0.94	26,087	34,432	37,091
200	0.47	12,450	20,896	21,357
350	0.27	8,584	15,879	16,351
500	0.19	5,614	13,243	13,607



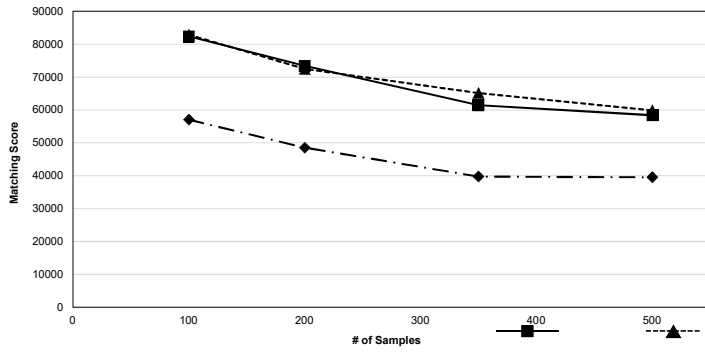
7x3: Hexagonal, 1 Control Curve, 54 Nodes



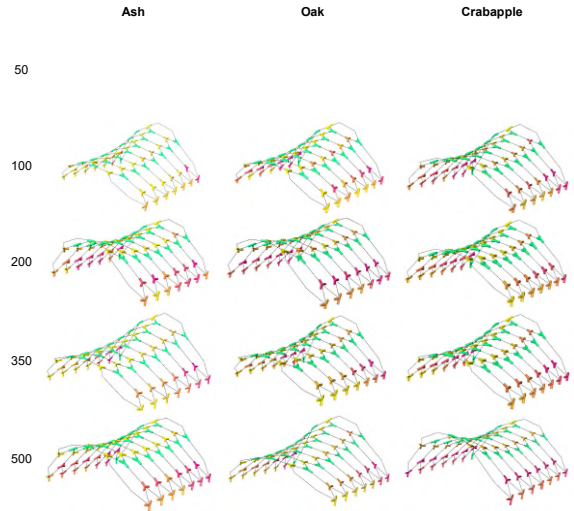
# of samples	Ratio (# structural nodes: # of samples)	Matching Score		
		Ash —◆—	Oak —■—	Fruit —▲—
50				
100	0.54	95,003	132,301	133,709
200	0.27	85,446	118,465	121,652
350	0.15	74,924	106,974	113,377
500	0.11	71,925	103,399	103,455



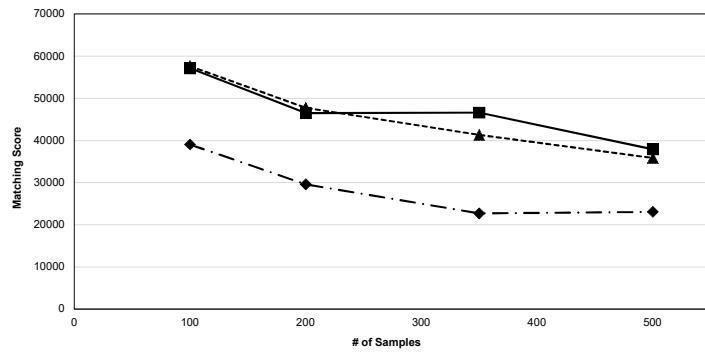
7x4: Hexagonal, 1 Control Curve, 68 Nodes



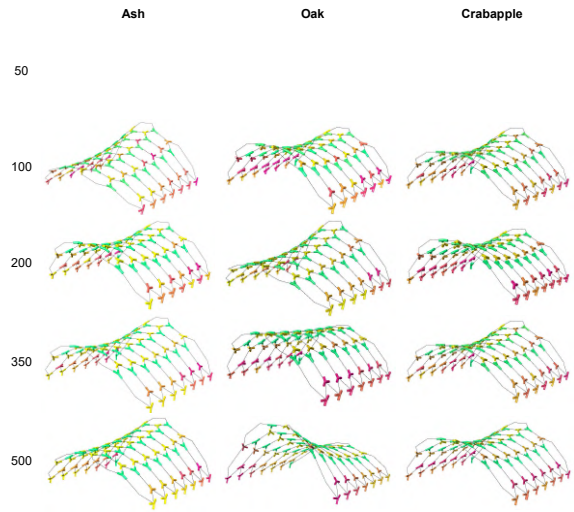
# of samples	Ratio (# structural nodes: # of samples)	Matching Score		
		Ash —◆—	Oak —■—	Fruit —▲—
50				
100	0.68	57,035	82,410	82,908
200	0.34	48,544	73,429	72,509
350	0.19	39,736	61,437	65,154
500	0.14	39,529	58,395	59,881



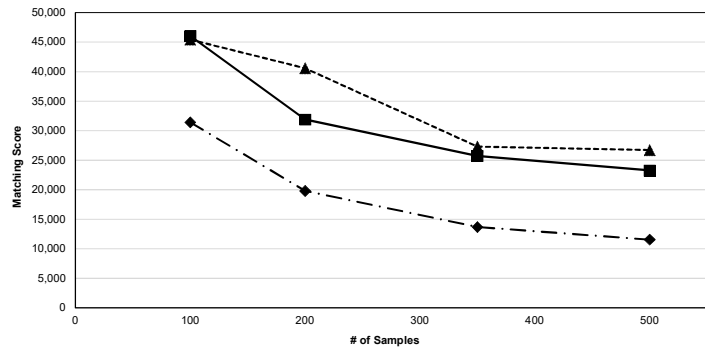
7x5: Hexagonal, 1 Control Curve, 82 Nodes



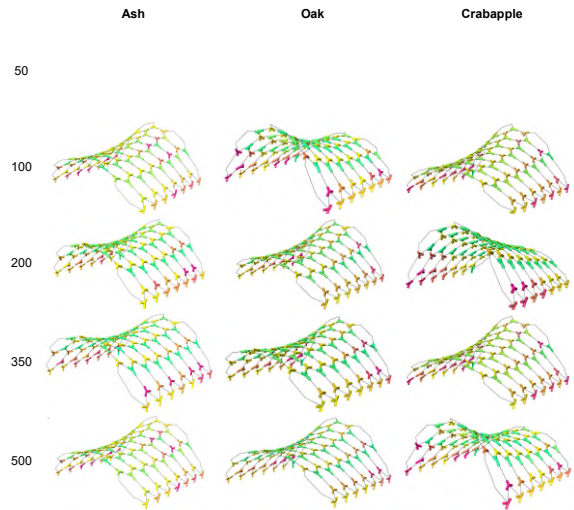
# of samples	Ratio (# structural nodes: # of samples)	Matching Score		
		Ash —◆—	Oak —■—	Fruit —▲—
50				
100	0.82	39,042	57,132	57,617
200	0.41	29,613	46,504	47,752
350	0.23	22,707	46,593	41,307
500	0.16	23,062	37,906	35,853



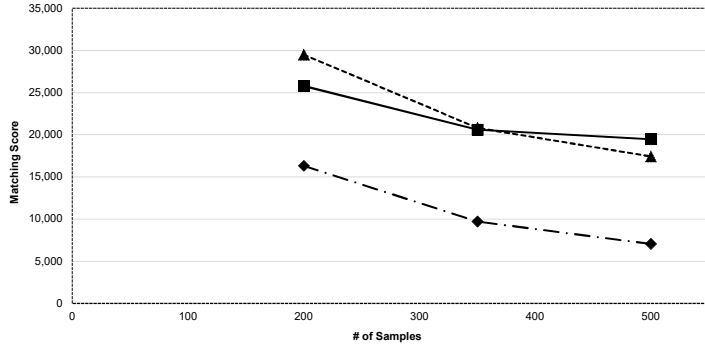
7x6: Hexagonal, 1 Control Curve, 96 Nodes



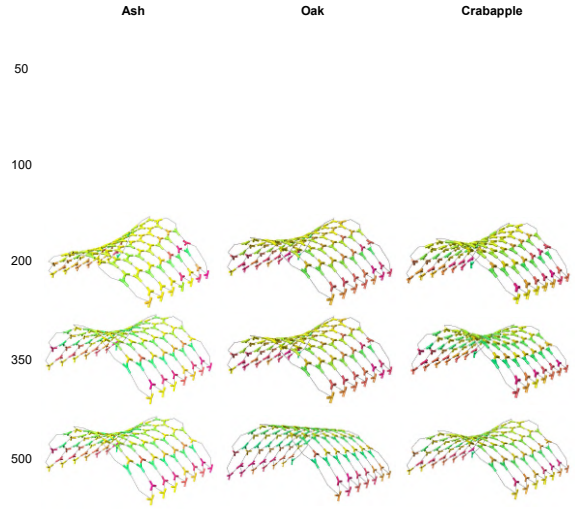
# of samples	Ratio (# structural nodes: # of samples)	Matching Score		
		Ash —◆—	Oak —■—	Fruit —▲—
50				
100	0.96	31,426	46,047	45,439
200	0.48	19,824	31,913	40,583
350	0.27	13,688	25,720	27,323
500	0.19	11,546	23,277	26,725



7x7: Hexagonal, 1 Control Curve, 110 Nodes

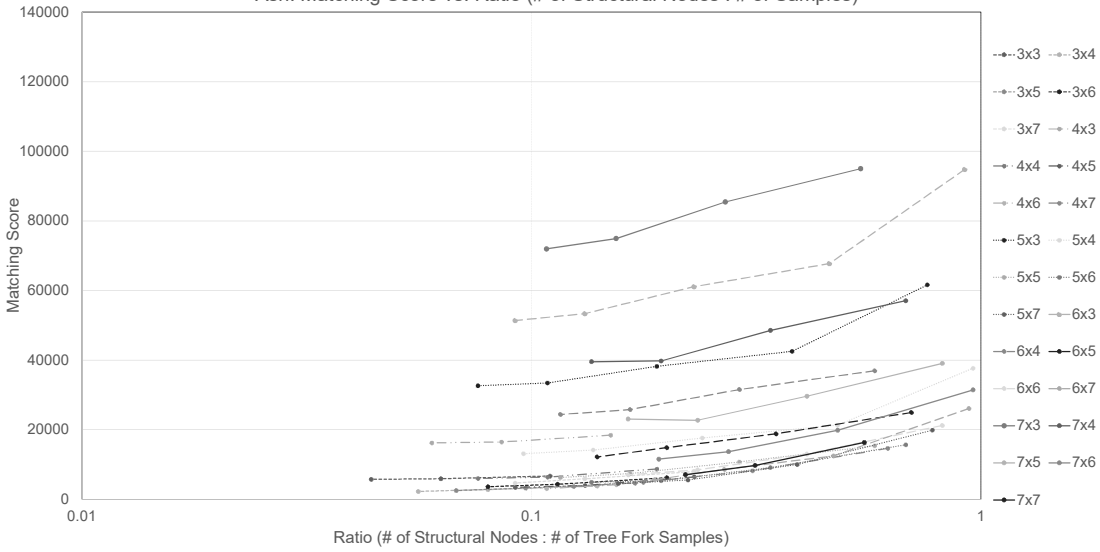


# of samples	Ratio (# structural nodes: # of samples)	Matching Score		
		Ash	Oak	Fruit
50				
100				
200	0.55	16,315	25,784	29,507
350	0.31	9,704	20,597	20,811
500	0.22	7,053	19,473	17,431

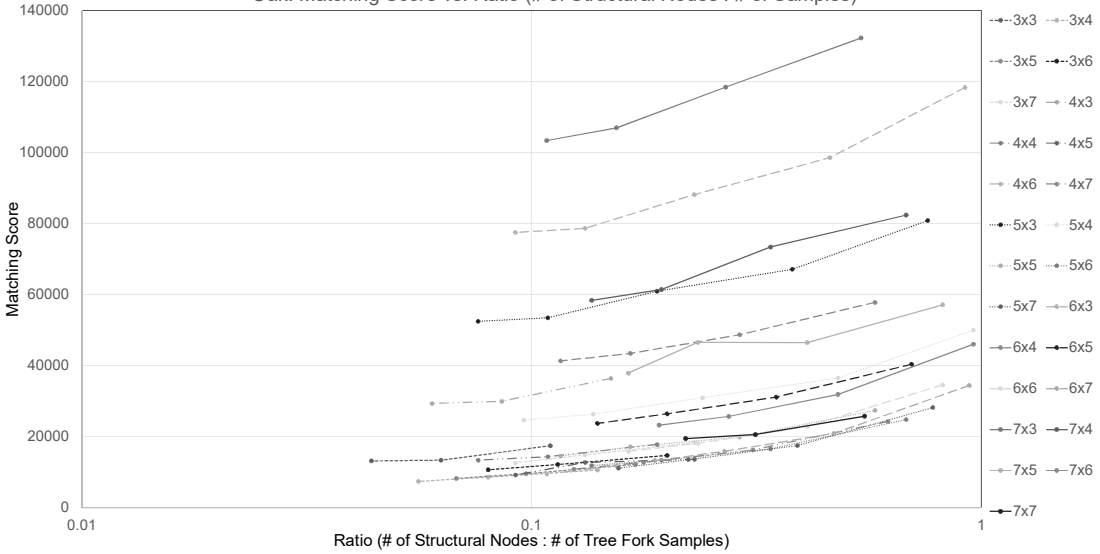


Appendix C

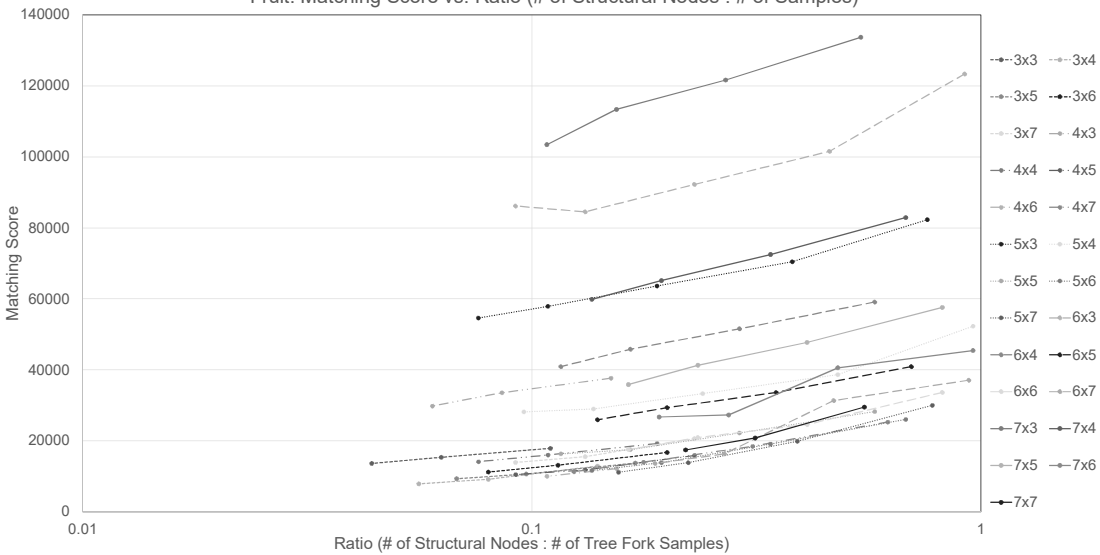
Ash: Matching Score vs. Ratio (# of Structural Nodes : # of Samples)



Oak: Matching Score vs. Ratio (# of Structural Nodes : # of Samples)

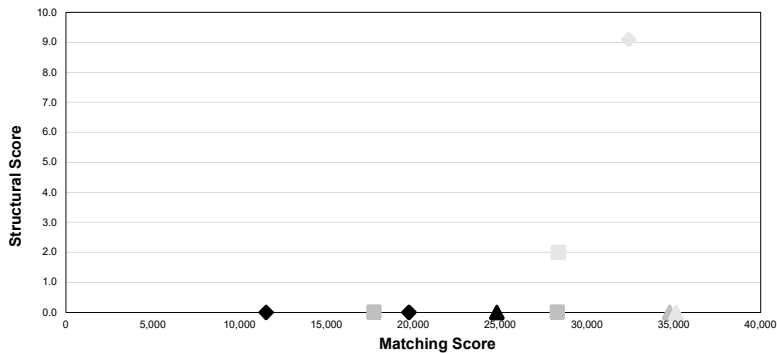


Fruit: Matching Score vs. Ratio (# of Structural Nodes : # of Samples)

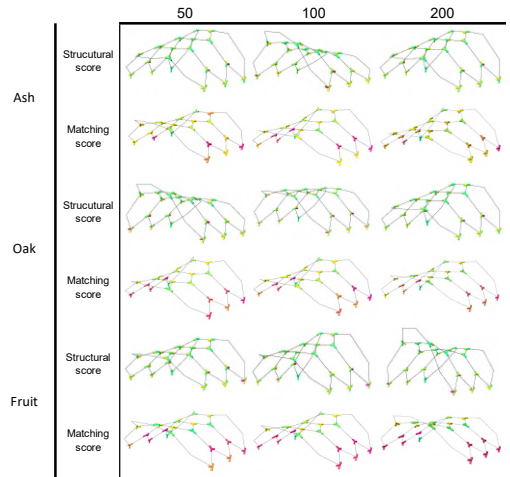


Appendix D

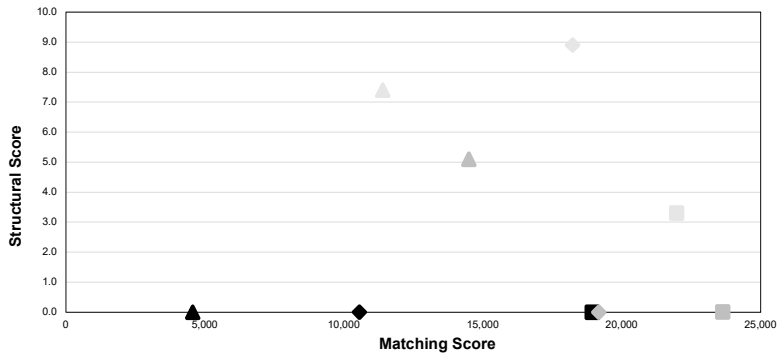
3x3: Hexagonal, 1 Control Curve, 22 Nodes



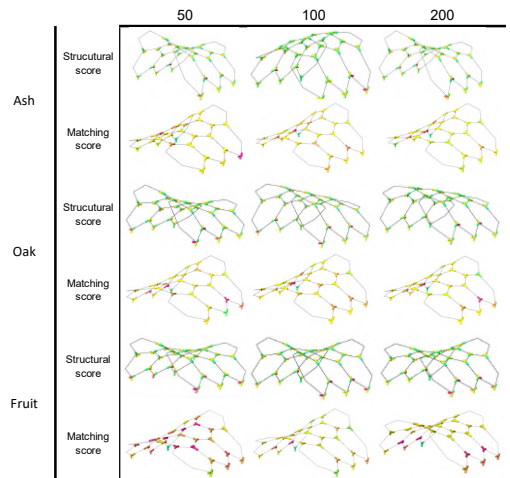
# of samples	Ash			Oak			Fruit		
	Structural Score	Matching Score (n)	Matching Score (o)	Structural Score	Matching Score (n)	Matching Score (o)	Structural Score	Matching Score (n)	Matching Score (o)
50	0.0	24,803	16,058	0.0	34,751	25,543	2.0	28,356	23,831
100	0.0	11,520	9,982	0.0	28,292	18,779	9.1	32,402	21,755
200	0.0	19,742	6,678	0.0	17,742	17,447	0.0	35,111	17,905



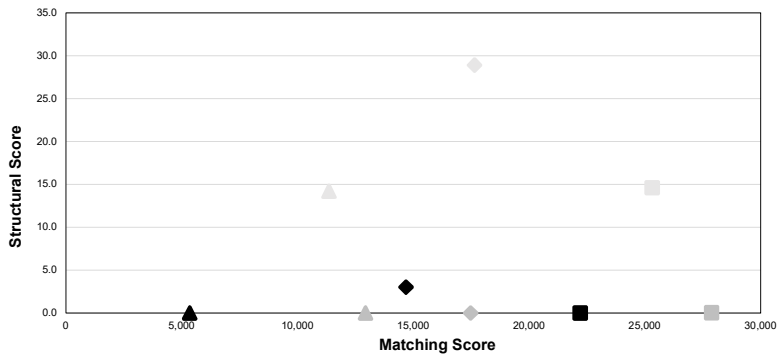
3x4: Hexagonal, 1 Control Curve, 28 Nodes



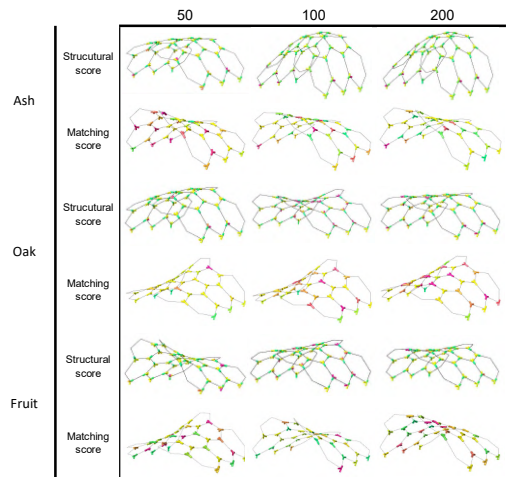
# of samples	Ash			Oak			Fruit		
	Structural Score	Matching Score (n)	Matching Score (o)	Structural Score	Matching Score (n)	Matching Score (o)	Structural Score	Matching Score (n)	Matching Score (o)
50	0.0	18,937	13,228	0.0	23,637	19,923	3.3	21,976	19,547
100	0.0	10,558	6,385	0.0	19,169	13,111	8.9	18,233	16,376
200	0.0	4,559	3,779	5.1	14,493	10,601	7.4	11,390	12,894



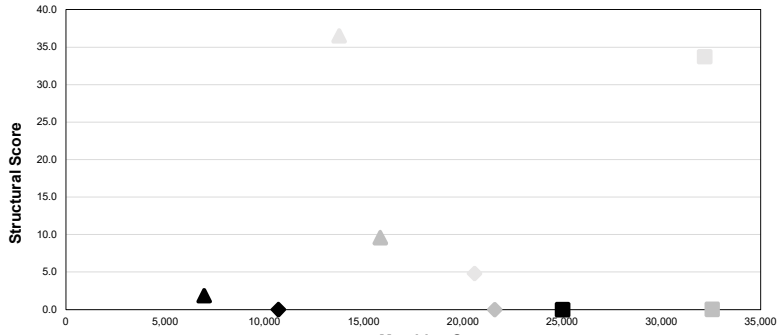
3x5: Hexagonal, 1 Control Curve, 34 Nodes



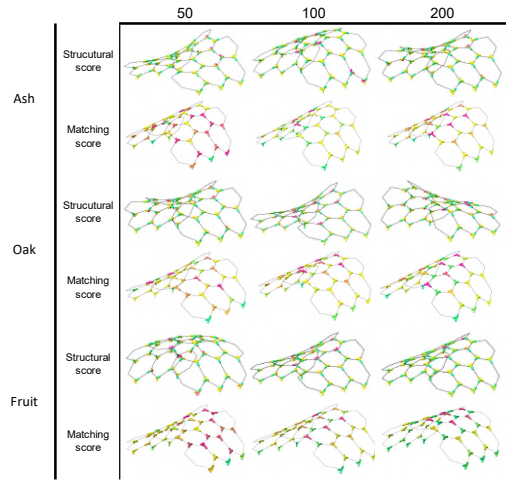
# of samples	Ash			Oak			Fruit		
	Structural Score	Matching Score (n)	Matching Score (o)	Structural Score	Matching Score (n)	Matching Score (o)	Structural Score	Matching Score (n)	Matching Score (o)
50	0.0	22,201	18,156	0.0	27,881	25,090	14.6	25,314	25,933
100	3.0	14,681	8,271	0.0	17,470	15,836	28.9	17,640	17,883
200	0.0	5,331	4,643	0.0	12,932	12,217	14.2	11,344	13,744



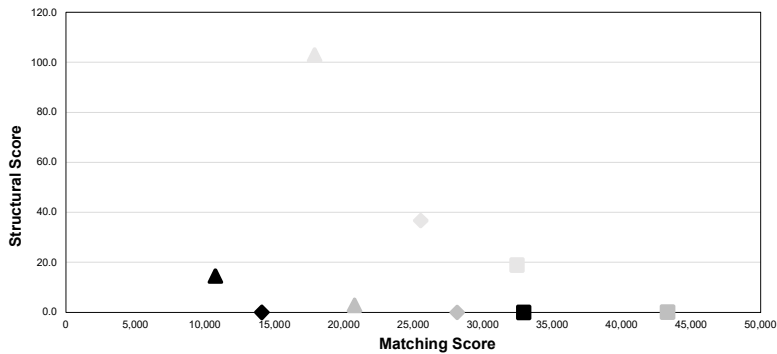
3x6: Hexagonal, 1 Control Curve, 40 Nodes



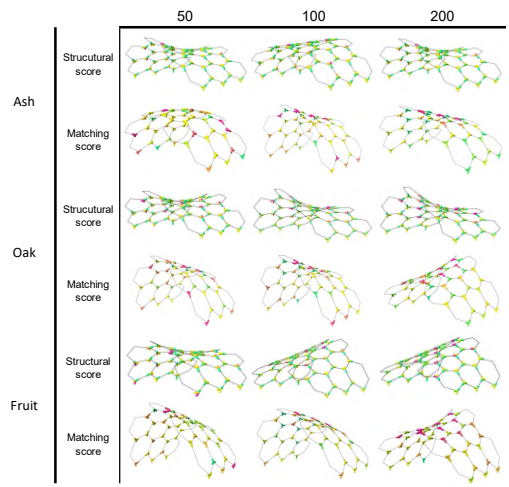
# of samples	Ash			Oak			Fruit		
	Structural Score	Matching Score (n)	Matching Score (o)	Structural Score	Matching Score (n)	Matching Score (o)	Structural Score	Matching Score (n)	Matching Score (o)
50	0.0	25,006	22,682	0.0	32,559	30,991	33.7	32,182	32,127
100	0.0	10,693	10,459	0.0	21,593	19,510	4.8	20,580	21,235
200	1.9	6,950	6,176	9.6	15,827	14,727	36.5	13,753	16,746



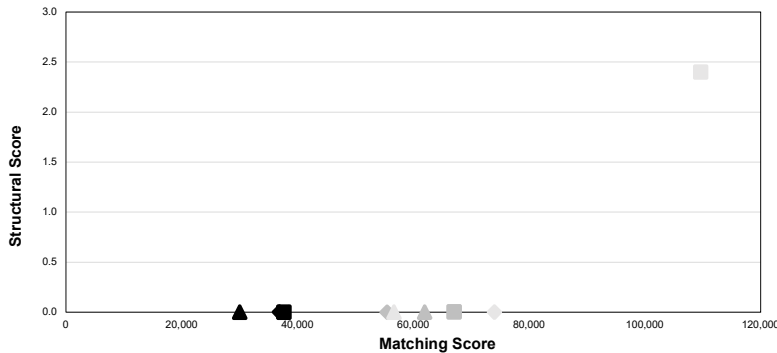
3x7: Hexagonal, 1 Control Curve, 46 Nodes



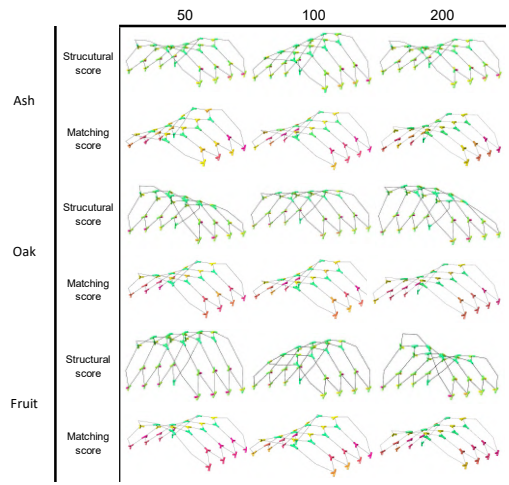
# of samples	Ash			Oak			Fruit		
	Structural Score	Matching Score (n)	Matching Score (o)	Structural Score	Matching Score (n)	Matching Score (o)	Structural Score	Matching Score (n)	Matching Score (o)
50	0.0	32,924	29,713	0.0	43,296	38,094	18.9	32,467	39,617
100	0.0	14,090	12,851	0.0	28,146	22,894	36.7	25,524	25,171
200	14.5	10,744	7,936	2.8	20,755	18,320	103.0	17,885	20,616



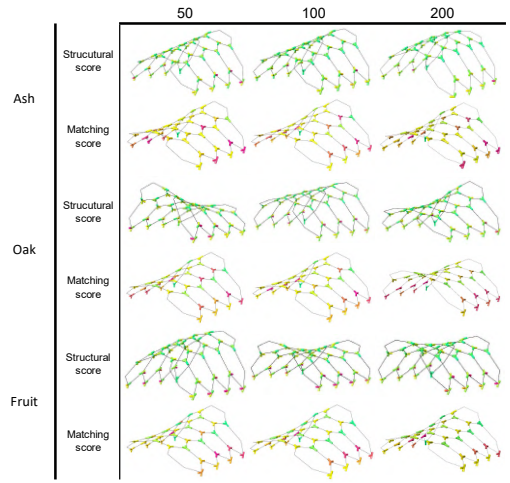
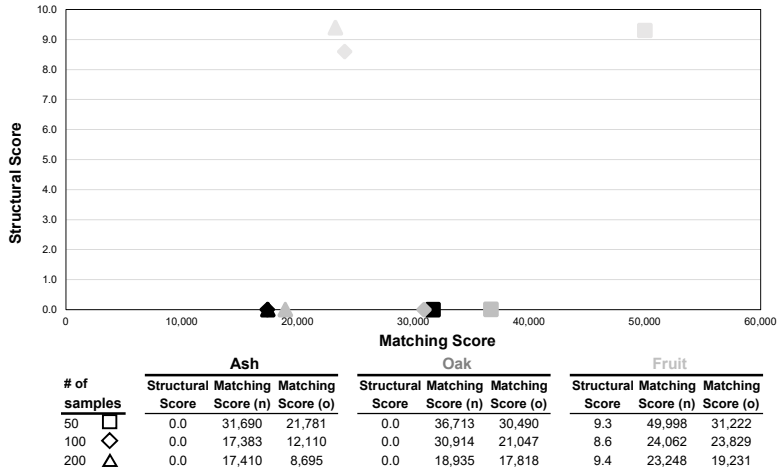
4x3: Hexagonal, 1 Control Curve, 30 Nodes



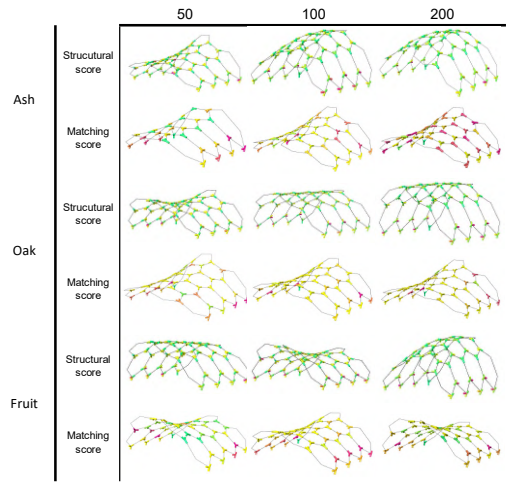
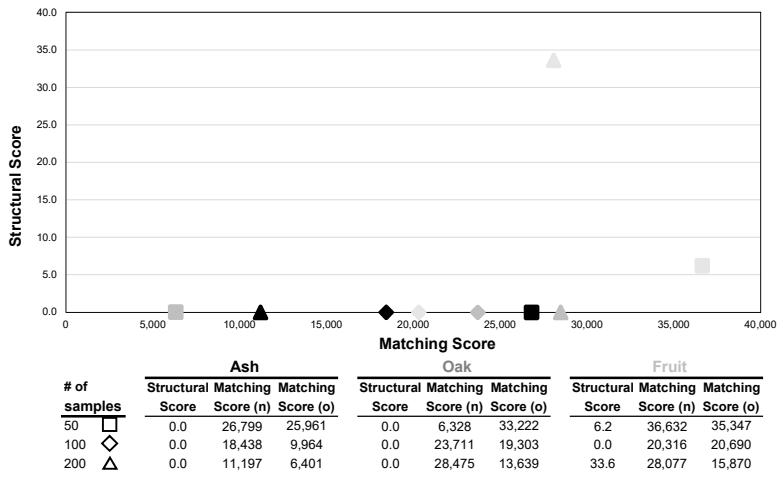
# of samples	Ash			Oak			Fruit		
	Structural Score	Matching Score (n)	Matching Score (o)	Structural Score	Matching Score (n)	Matching Score (o)	Structural Score	Matching Score (n)	Matching Score (o)
50	0.0	37,604	34,816	0.0	67,055	48,745	2.4	109,626	48,502
100	0.0	36,846	24,758	0.0	55,446	39,006	0.0	73,991	42,500
200	0.0	29,968	18,401	0.0	61,914	36,426	0.0	56,638	37,676



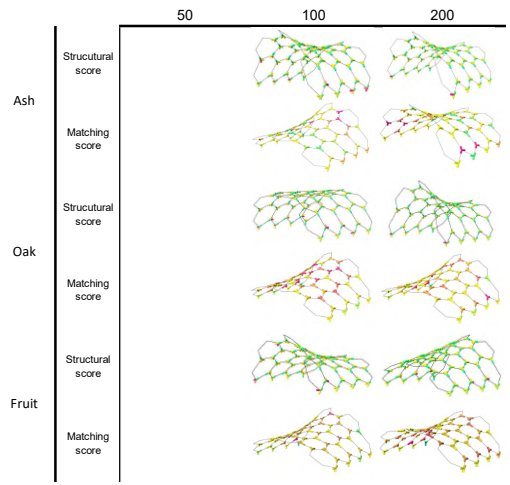
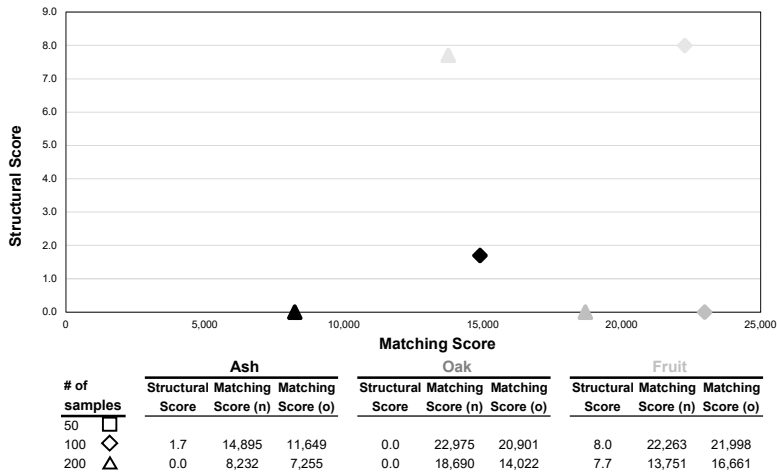
4x4: Hexagonal, 1 Control Curve, 38 Nodes



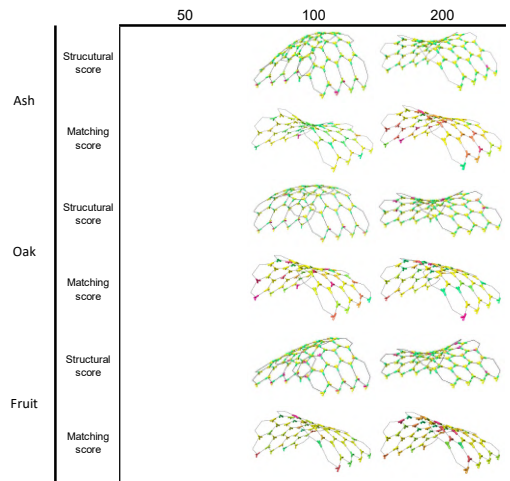
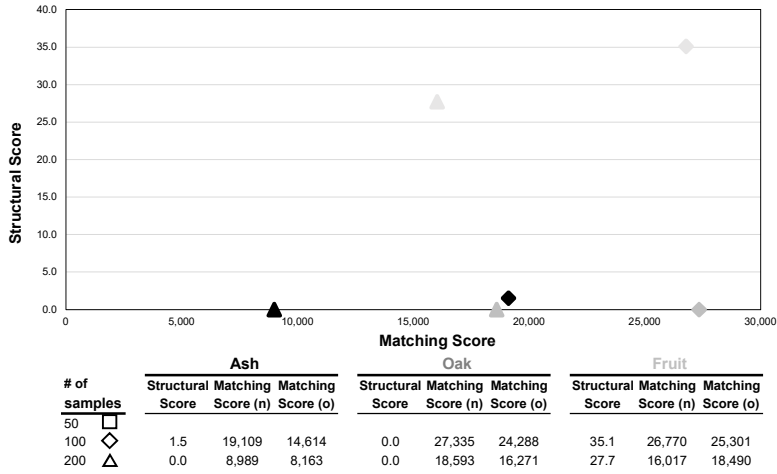
4x5: Hexagonal, 1 Control Curve, 46 Nodes



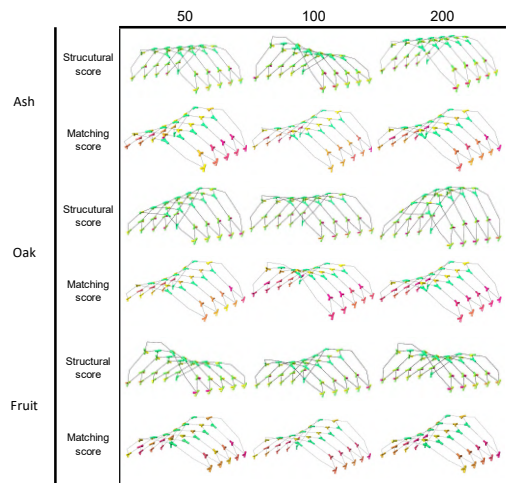
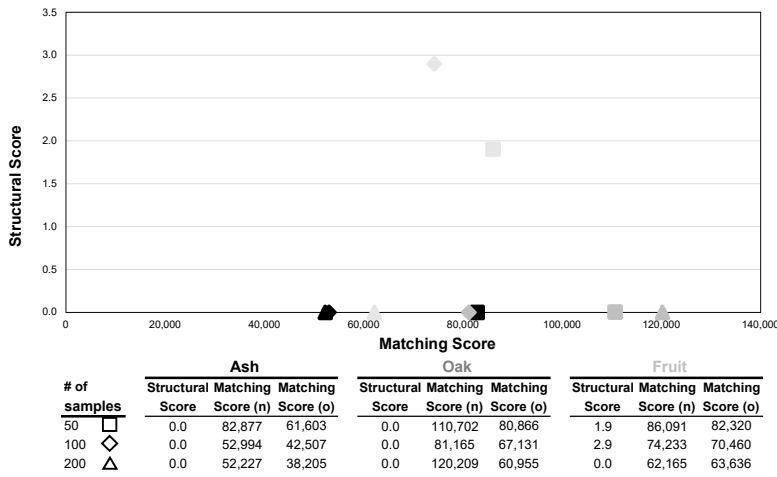
4x6: Hexagonal, 1 Control Curve, 54 Nodes



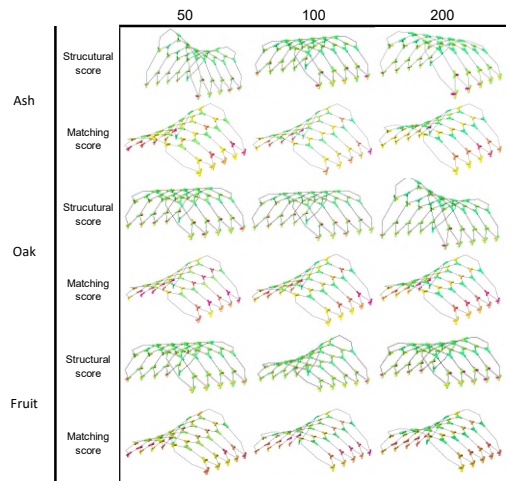
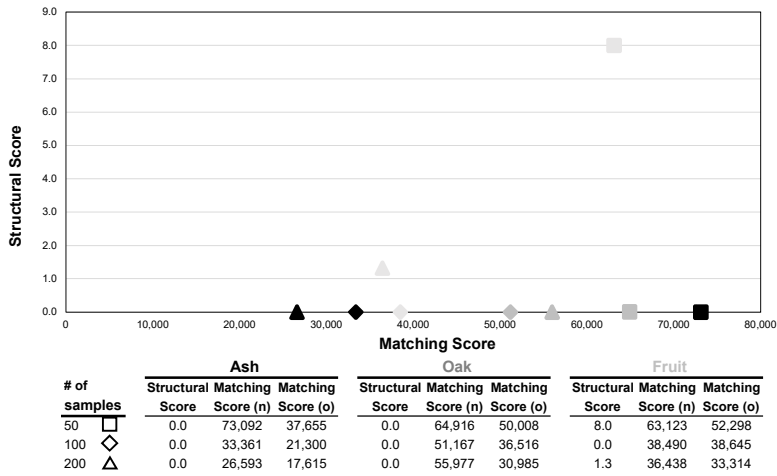
4x7: Hexagonal, 1 Control Curve, 62 Nodes



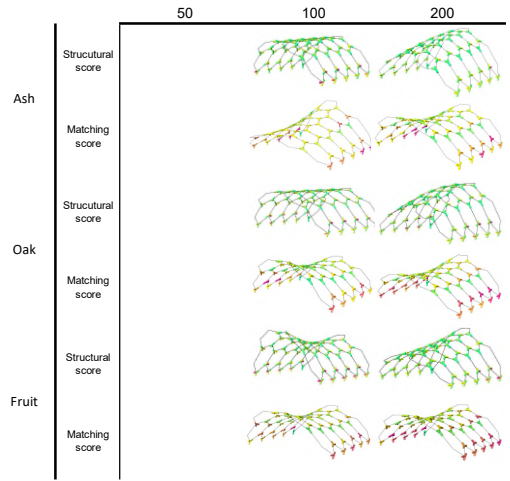
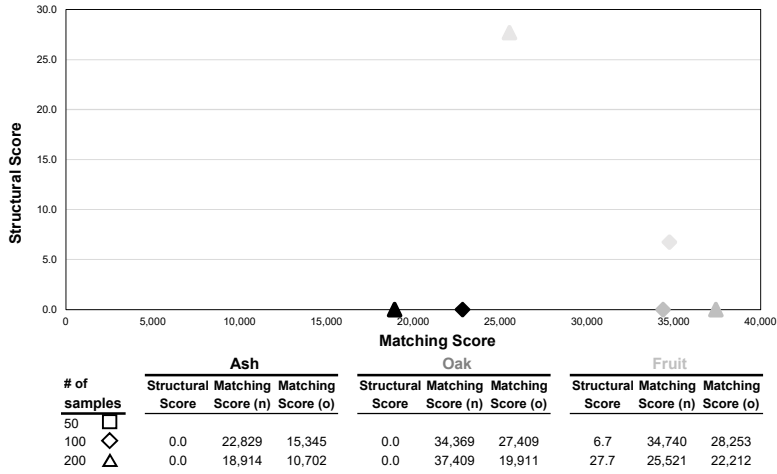
5x3: Hexagonal, 1 Control Curve, 38 Nodes



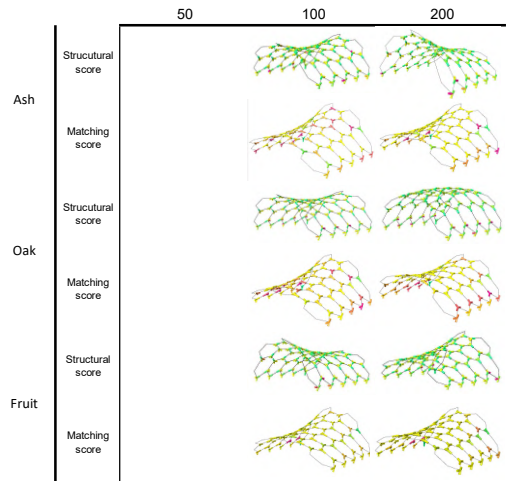
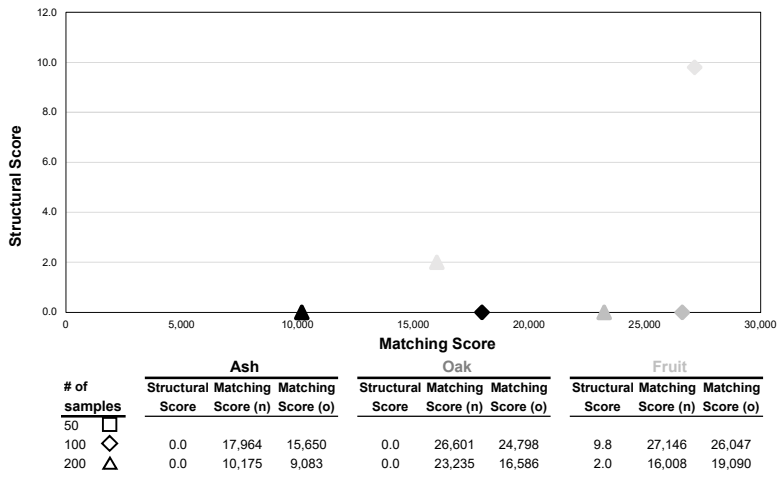
5x4: Hexagonal, 1 Control Curve, 48 Nodes



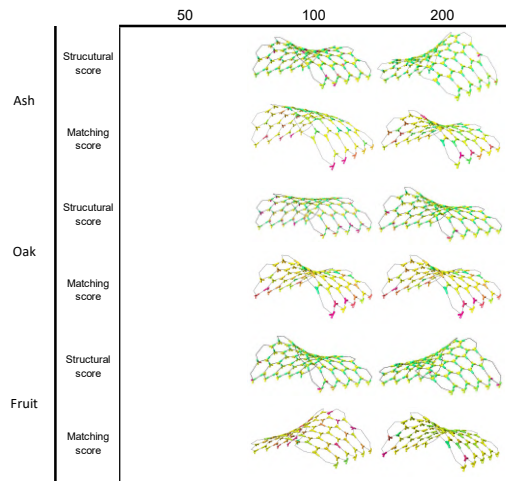
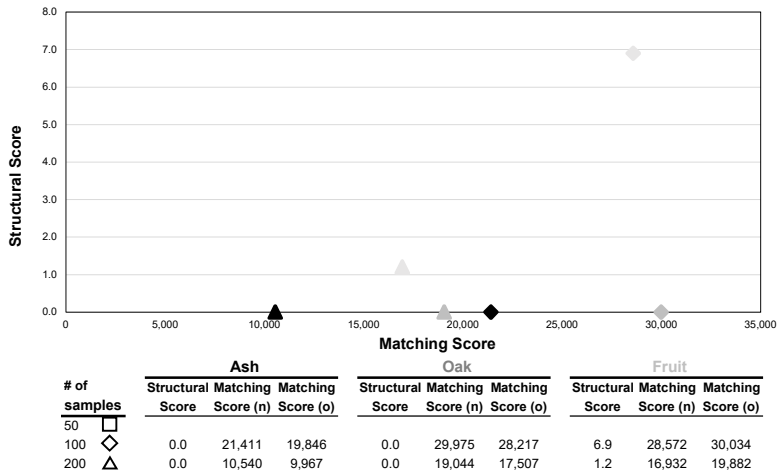
5x5: Hexagonal, 1 Control Curve, 58 Nodes



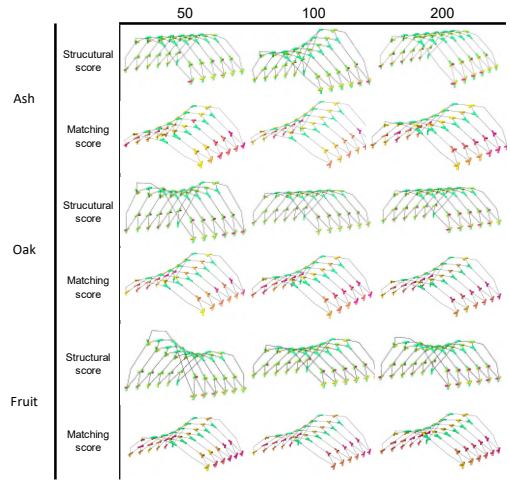
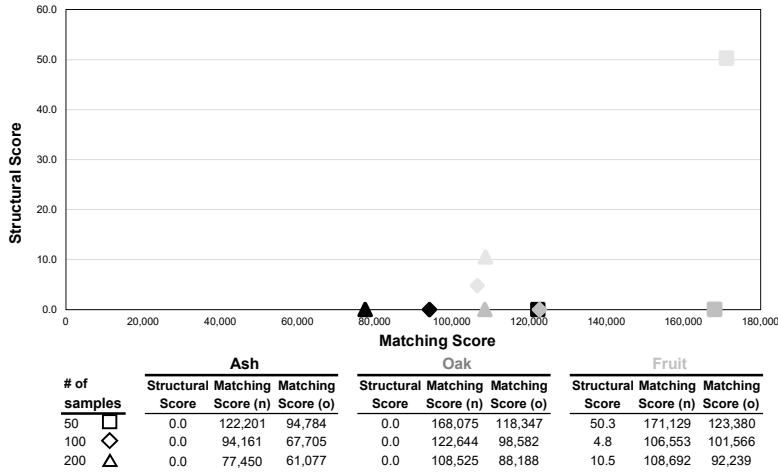
5x6: Hexagonal, 1 Control Curve, 68 Nodes



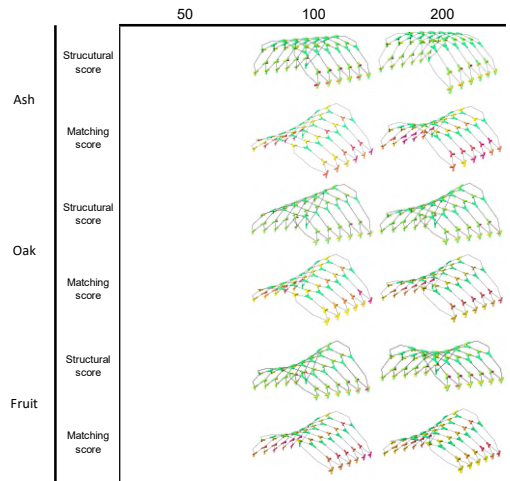
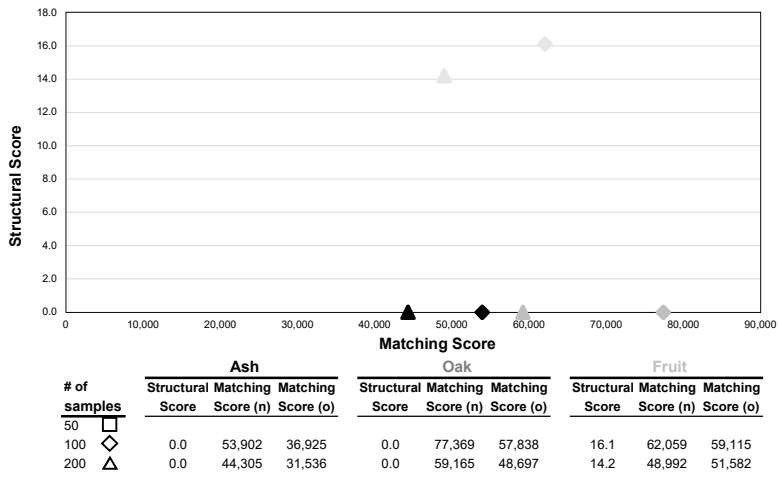
5x7: Hexagonal, 1 Control Curve, 78 Nodes



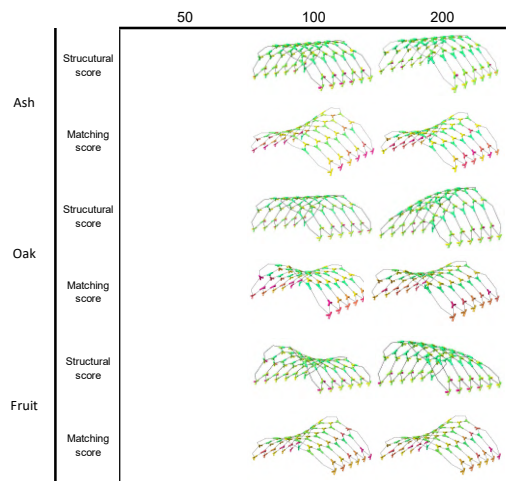
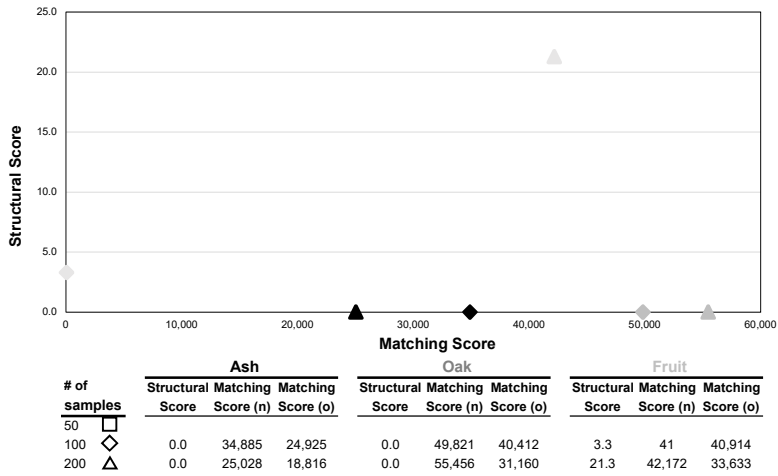
6x3: Hexagonal, 1 Control Curve, 46 Nodes



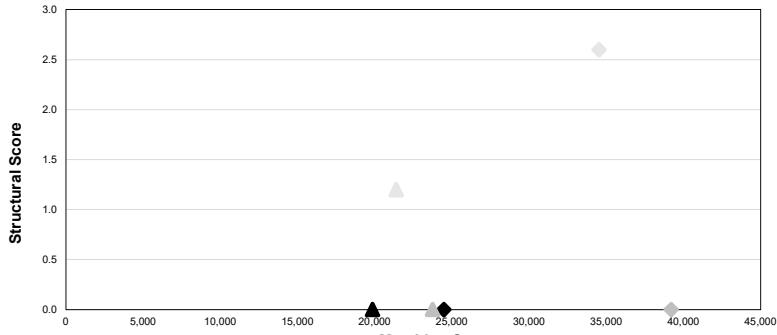
6x4: Hexagonal, 1 Control Curve, 58 Nodes



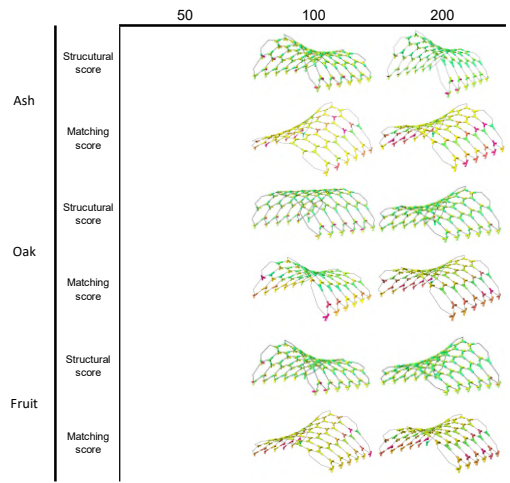
6x5: Hexagonal, 1 Control Curve, 70 Nodes



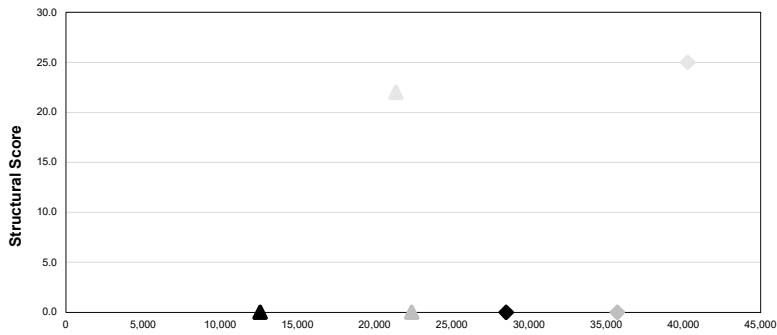
6x6: Hexagonal, 1 Control Curve, 82 Nodes



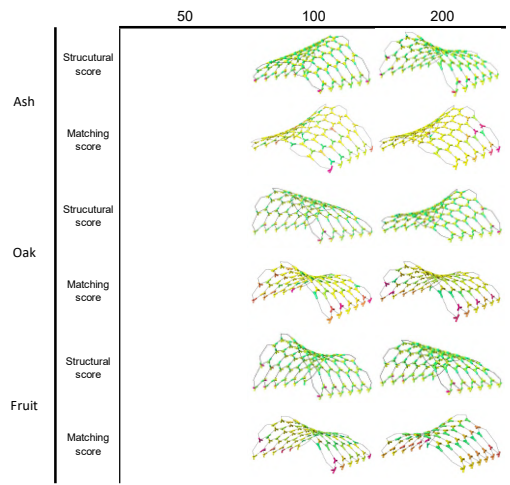
# of samples	Ash			Oak			Fruit		
	Structural Score	Matching Score (n)	Matching Score (o)	Structural Score	Matching Score (n)	Matching Score (o)	Structural Score	Matching Score (n)	Matching Score (o)
50 □	0.0	24,475	21,204	0.0	39,191	34,597	2.6	34,524	33,641
100 ◇	0.0	19,842	13,007	0.0	23,734	22,841	1.2	21,377	24,612
200 △									



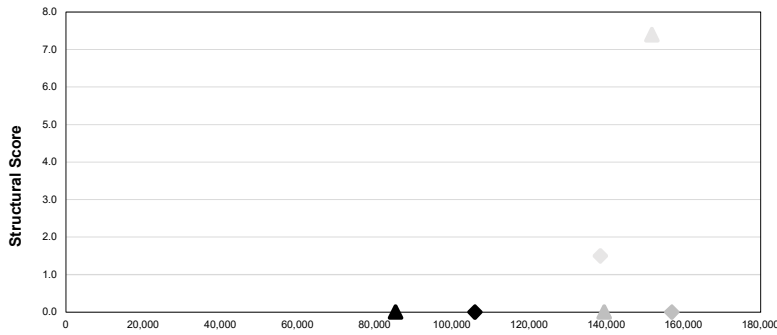
6x7: Hexagonal, 1 Control Curve, 94 Nodes



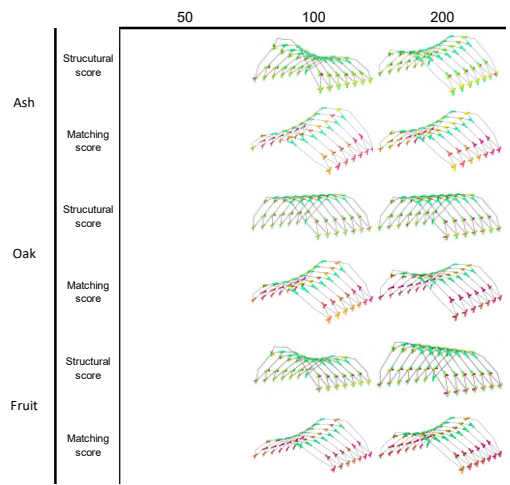
# of samples	Ash			Oak			Fruit		
	Structural Score	Matching Score (n)	Matching Score (o)	Structural Score	Matching Score (n)	Matching Score (o)	Structural Score	Matching Score (n)	Matching Score (o)
50 □	0.0	28,507	26,087	0.0	35,699	34,432	25.0	40,265	37,091
100 ◇	0.0	12,563	12,450	0.0	22,380	20,896	22.0	21,355	31,357
200 △									



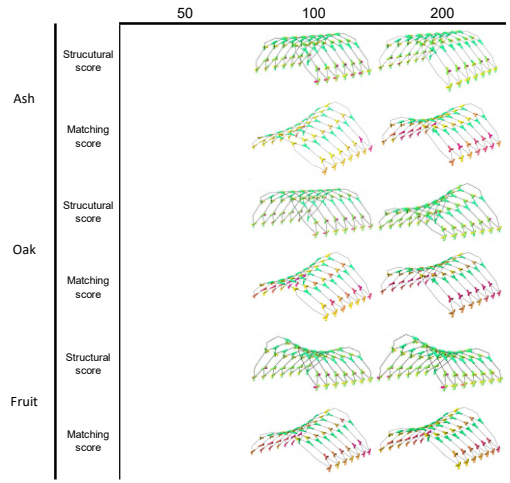
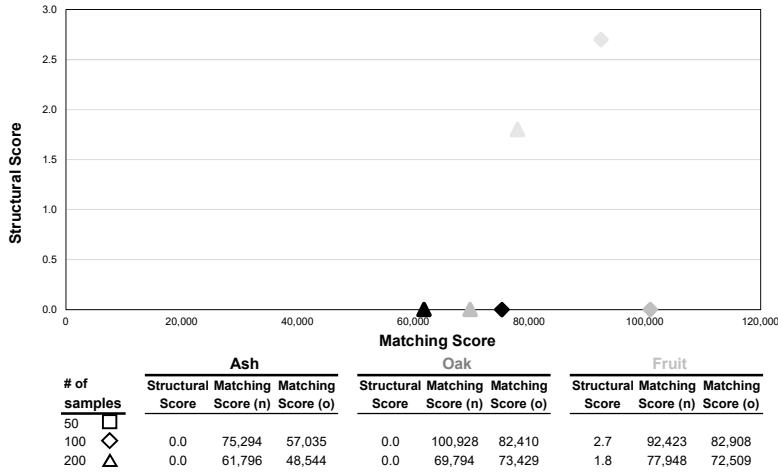
7x3: Hexagonal, 1 Control Curve, 54 Nodes



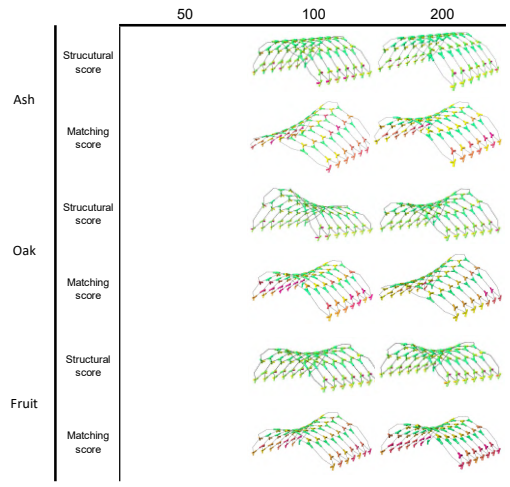
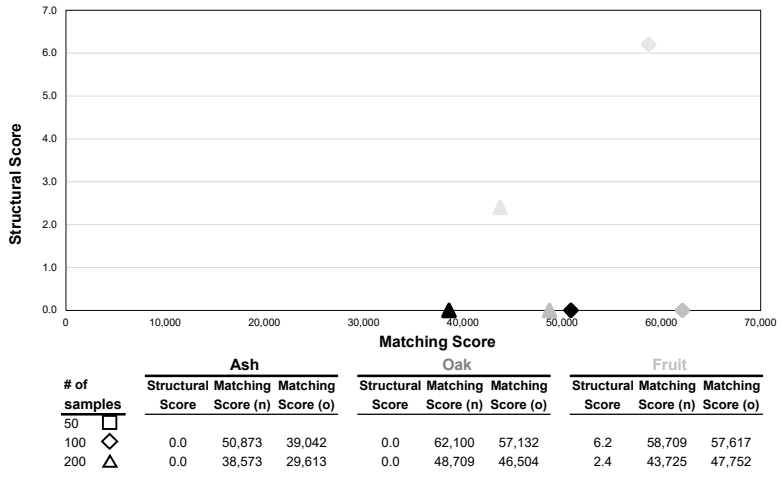
# of samples	Ash			Oak			Fruit		
	Structural Score	Matching Score (n)	Matching Score (o)	Structural Score	Matching Score (n)	Matching Score (o)	Structural Score	Matching Score (n)	Matching Score (o)
50 □	0.0	105,969	95,003	0.0	156,951	132,301	1.5	138,451	133,709
100 ◇	0.0	85,345	85,446	0.0	139,431	118,465	7.4	151,796	121,652
200 △									



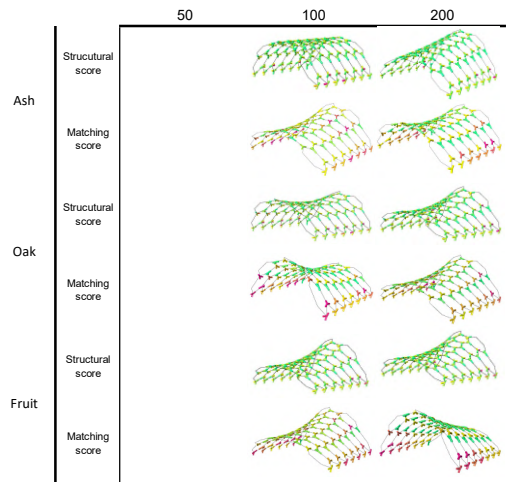
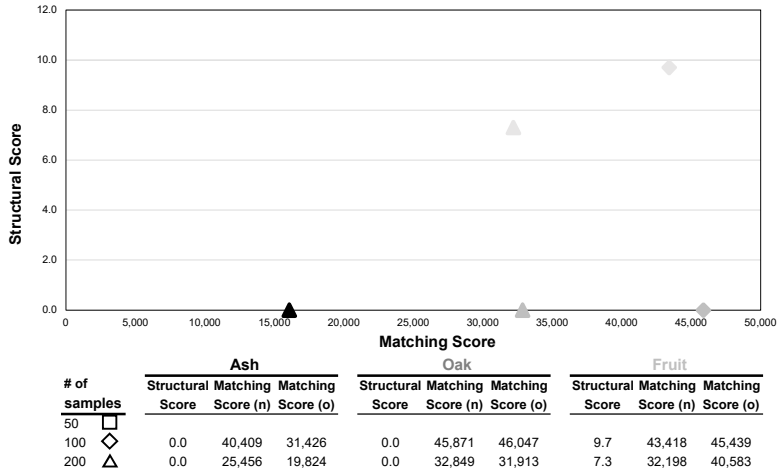
7x4: Hexagonal, 1 Control Curve, 68 Nodes



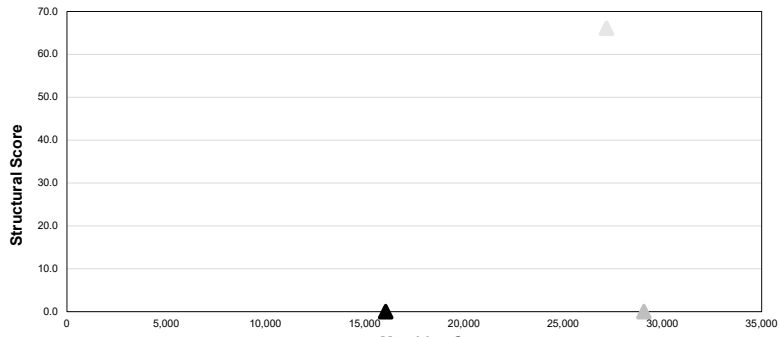
7x5: Hexagonal, 1 Control Curve, 82 Nodes



7x6: Hexagonal, 1 Control Curve, 96 Nodes



7x7: Hexagonal, 1 Control Curve, 110 Nodes



# of samples	Ash			Oak			Fruit		
	Structural Score	Matching Score (n)	Matching Score (o)	Structural Score	Matching Score (n)	Matching Score (o)	Structural Score	Matching Score (n)	Matching Score (o)
50 □									
100 ◇									
200 △	0.0	16,052	16,315	0.0	29,062	25,784	66.1	27,176	29,507

